# On the Effect of Variable Opening Geometries, and Operating Conditions on High Pressure Hydrogen Releases: Ignition Risks

Wissam Nakhle

A Thesis

in

the Department

of

Mechanical and Industrial Engineering

Presented in Partial Fulfillment of the Requirements for the Degree of

Master of Applied Science

In Mechanical Engineering at

Concordia University

Montreal, Quebec, Canada

April, 2013

**CONCORDIA UNIVERSITY**

**School of Graduate Studies**

This is to certify that the thesis prepared

By: **Wissam Nakhle**

Entitled: **Hydrogen Release Ignition Risks**

and submitted in partial fulfillment of the requirements for the degree of

**Master of Applied Science (Mechanical Engineering)**

complies with the regulations of the University and meets the accepted standards with respect to

originality and quality.

Signed by the final Examining Committee:

Chair

**Martin D. Pugh**

Examiner

**Hoi D. Ng**

Examiner

**Simon Li**

Supervisor

**Marius Paraschivoiu**

Approved by

**Muthukumaran Packirisamu**

Chair of Department or Graduate Program Director

2011

**Robin Drew**

Dean of Faculty

Date: 30.04.2013

# ABSTRACT


On the Effect of Variable Opening Geometries, and Operating Conditions on High Pressure Hydrogen Releases: Ignition Risks

Wissam Nakhle

Understanding and predicting the behavior of pressurized hydrogen when released into air is needed for the safe utilization of hydrogen. Analysis based on Computational Fluid Dynamics, can be used to accurately study this flow and anticipate its consequence without performing expensive experimental testing. Simulation of sudden release of highly under-expanded hydrogen jet and detecting auto-ignition is the focus of this work. The present thesis addresses ignition risks associated with the diffusion-expansion of hydrogen into ambient air, through a series of case studies, covering several types of exit geometries: fixed circular, and fixed elliptic openings, as well as expanding circular geometries, under different pressure conditions, to describe the properties that affect ignition and to determine when ignition has occurred. To be more specific this research aims at capturing all the features of the flow required, to examine where and when the probability of ignition exists, and to determine the effect of changing the opening geometry on ignition risks.

**ACKNOWLEDGMENTS**

I would like to thank my supervisor, Professor Marius Paraschivoiu for all his support and help throughout this project.

## Table of Contents

## List of Figures & Tables

- **Figures:**

- **Tables:**

## List of Symbols

- **a** Sound speed
- **C** Concentration of air
- $\mathbf{C_v}$ Constant volume specific heat of real gas
- $\mathbf{C_u}$ Constant volume specific heat of ideal gas
- $\mathbf{C_p}$ Constant pressure specific heat of real gas
- **D** Diameter of the release area
- **P** Pressure
- **R** Specific ideal gas constant
- **T** Temperature
- **t** Time
- ***w*** z-component of velocity
- ***Z*** Distance from the release hole in the z direction
- **Δ*A*** Surface area of the control volume
- **Δ*t*** Time step
- **Δ*x*** Displacement of a node
- **ζ** Compressibility factor
- **γ** Ratio of specific heats
- **ρ** Density
- $\mathbf{u_i}$ Velocity of the ith species
- $\mathbf{u_{d,i}}$ Diffusion Velocity of the ith species
- $\mathbf{Y_i}$ Mass fraction of the ith species
- $\mathbf{w_i}$ Net rate of production of the ith species

# Chapter 1

# Introduction

## 1. Spontaneous Ignition of Pressurized $H_2$ Releases

Hydrogen is a promising form of energy storage; we may produce it through electrolysis, and use it to supply power in many industry sectors, mainly in the automobile industry. Several hydrogen storing, transporting and handling solutions are in progress, to provide better safety standards, owing to the increasing need for replacement fuels.

In fact, hydrogen storage is a challenging field because of the risks associated with high pressure compression tanks, thus the need to develop tools to understand the associated ignition risks. When a high pressure tank suddenly releases hydrogen, ignition risks can be determined from the properties of the interface between hydrogen and the surrounding air, the properties of the leading shockwave and the characteristic geometry that describes the expansion region and the storing tank.

The present thesis addresses ignition risks related to the diffusion-expansion of hydrogen into ambient air, through a series of case studies, covering several forms of exit geometries: fixed circular, and fixed elliptic openings, along with expanding circular geometries under different pressure conditions, to describe the properties that affect ignition and to explain when ignition has occurred.

## 1.1 Problem Definition

Among the main advantages of using Computational Fluid Dynamics is its capacity to numerically, and accurately solve the flow pattern from the release time, with much shorter iteration time increments and study intervals.

In this thesis, a FORTRAN code describes the hydrogen flow, and was created to handle complex three-dimensional problems, and to cut computational time with parallel processing methods. Further, a C++ code describes ignition risks, and is designed to use thermo-chemical data and transport properties of the chemical species involved, through external libraries and chemistry solvers.

In fact, two stages model the hydrogen release problem; the FORTRAN in-house code determines the properties of the shockwave and contact surface, and the expansion rate at the head of the jet, and provides input to the 1-D Lagrangian Diffusion-Reaction (LDR) model, modified from the work of M.I. Radulescu, B. Maxwell [1]. The LDR model is then employed to determine the favorable ignition conditions, and indicates that the ignition process occurs when hydroxide anion productions are high and the OH concentration exceeds a predetermined ignition threshold, further discussed.

Fixed circular, fixed elliptic, and expanding circular geometries are compared, and the pressure cases of 10 MPa, 30 MPa and 70 MPa are examined. The ultimate result is a safety tool that describes a three-dimensional hydrogen flow released into air, and determines the associated ignition risks.

## 1.2 Literature Review

In the hydrogen release problem under investigation, describing the flow requires simulating the complex environment, using a rigorous computational domain and a realistic geometry. Further, in order to assess ignition risks and compute thermodynamic properties and production rates of chemical species, a reaction mechanism providing details of reactions involved is required. The numerical results achieved in [4], provide to the present work the capacity to solve high pressure hydrogen release problems using the Abel-Noble real gas equation.

Radulescu et al. [1], consider highly pressurized round hydrogen jets, for various storage pressures to find the critical orifice size, at which ignition occurs. Radulescu and Maxwell [2] further extend studies to add the effect of the expansion process on ignition, by applying a Lagrangian unsteady diffusion-reaction model that makes use of the ideal gas equation of state.

The LDR model, provided by Radulescu and Maxwell accounts for chemical reactions described by the means of 19 elementary reactions, and uses an ideal gas analytical shock tube solution to describe flow properties during the initial diffusion of hydrogen, and to provide initial conditions to the ignition model.

In the present problem, describing the flow requires a real gas equation since the simulation environment is at high pressure, with shock discontinuities and high temperature peaks.

The properties of the shockwave and contact surface, along with the expansion rate at the jet head depend on the characteristic geometry that describes the expansion region and the storing tank. Further, the operating environment and the short time span studied, supports the assumption of negligible viscosity, and Euler equations are used, thus reducing the computational time.

Mohamed et al. [3], simulate hydrogen releases from high pressure reservoirs, they change the 3-D finite-volume Navier-Stokes model to solve Euler equations and simulate a standard shock tube flow under real gas conditions.

Xu et al. [6], conclude that a lower release pressure will reduce ignition risks, and that even though ignition could occur inside the tube, smaller opening dimensions lead to a more pronounced expansion, and reduced ignition risks. Xu et al. [6], show that modeling the opening using long tubes increase ignition probabilities; for a storage pressure of 7MPa, a 2 cm tube will not ignite, while increasing the tube length to 6 cm shows that ignition will occur. Viscous effects in longer tubes can no longer be neglected, since they allow for a better and longer mixing of hydrogen and air, leading to much higher temperature peaks, and a more probable ignition.

In fact, the exit geometry is an open-ended shock-tube that realistically models the opening, the short tube length and relatively small dimensions used compared to the overall geometry are characteristics of the exit geometry. In this thesis, modeling the opening using a 2cm tube, provides a realistic simulation approach and avoids false ignition due to the effect of longer tubes on ignition risks.

## 1.3 Proposed Methodology for this Study

In the ignition model provided by Radulescu and Maxwell, the evolution of pressure and its gradient at the contact surface as a function of time, derive from one general curve fit expression. This unique expression relating interface pressure and time is set after several numerical simulations for different storage pressures and opening diameters, in standard circular holes, and variable tube lengths.

The first task is to modify the ignition model, by substituting the original ideal gas analytical shock-tube solution for the temperature and pressure distributions across the hydrogen-air contact surface, with a real gas three-dimensional solution along the interface centerline, pertaining to the hottest point on the contact surface, obtained using the in-house FORTRAN code.

The second task is to adjust the ignition model to account for the pressure and its gradient relative to this specific three-dimensional reservoir release problem, which is determined by curve fitting through a $6^{th}$ order polynomial regression, on a case-by-case basis, namely for every pressure condition and opening dimension.

The FORTRAN parallel code is employed to simulate this hydrogen release problem and to explain the flow pattern. The objective of the in-house code is to determine using CFD, the parameters related to the interface and shockwave properties, which in turn are input variables required by the ignition model to describe ignition risks for hydrogen expanding into air.

## 1.4 In-House Code Features

Cirrus is one of the Concordia University supercomputer clusters, and is used to run parallel codes. Numerical solutions, along with pre-processing operations use parallel processing methods.

In the present work a 2 million nodes mesh, consisting of tetrahedral elements much smaller around the release area, and divided into 32 partitions is used. The mesh is generated using GAMBIT, which allows simulating three-dimensional numerical elements to represent the geometry, connected elements where fluids dynamics equations are applied. The density distribution of the mesh, and the number of elements, are the controlling parameters for a more accurate simulation and resolution of the governing equations. The requirement for an increased number of elements around the release area increases the computational effort. Parallel processing is a modern computational technique that uses Message Passing Interface - MPI to operate in parallel, and several computer processor cores to execute a list of commands. The METIS software and a built-in software package are used to create partitions, which are a physical representation of a slice of the geometry, and the basic computational domain handled by a single processor.

In fact, it is difficult to separate a physical problem, into separate commands operated by separate processors. However, parallel processing has an efficient and increasing use in the field of fluids dynamics, because any geometry could be subdivided into planes between which information and data is communicated.

## 1.5 Ignition Model Features

The properties of the hydrogen-air interface, the properties of the leading shockwave that heats the gas interface, along with the interface pressure and pressure gradient, are input parameters to the ignition model. The ignition model incorporates external libraries to handle integration of the complex chemistry in the reaction terms of the governing equations, namely the Sundials and CVODE integrators developed by Hindmarsh [9].

First the diffusive terms are solved using the Cantera libraries for C++ [8], namely the flow average temperature and concentration distributions, which are then used to compute individual specie concentrations and temperatures.

Next, the reaction terms are solved over the same time step, using a reaction mechanism developed by Li, et al. [5] and the temperature solution previously obtained from the diffusive step, to find the production rate of species that is dependent on the rate-of-progress of each reaction, which in turn has a dependency on temperature.

In the last step, the expansion term is treated as a source term and is evaluated independently, and the interface pressure is updated by using the pressure solution obtained from the previous time step.

Ignition occurs when the shock is strong enough and the storage pressure high enough to heat the air. The possibility of ignition is high in front of the hydrogen-air contact surface, where the flow heated by the shockwave, is the hottest. In the next chapter the hydrogen release problem and the models used to describe it, are further explained.

# Chapter 2

# The Hydrogen Release Problem

## 2. Evolution of the Flow during an Accidental Release

### 2.1 Simulation Models

The CFD code is used to capture the evolution of the flow, and the LDR model, provided by Radulescu and Maxwell, looks at the critical ignition point where OH-compounds productions are the highest, and is used to examine how these parameters control the ignition process. First, a three-dimensional model is solved using the FORTRAN code to determine the initial heating of the contact surface, and to describe the expansion process. Next, a one-dimensional LDR model is used to evaluate the competing effects of the heating provided by the shockwave, and the cooling during the expansion flow, and to assess ignition risks.

#### 2.1.1 CFD Model

The LDR model preliminarily solves an ideal gas analytical shock tube problem, which serves as initial conditions for the hydrogen-air contact surface, namely the hot air temperature in front of the gaseous interface, and the cold hydrogen temperature behind it, along with the interface pressure. Figure (2.1) explains the flow behavior in the shock tube problem, which is essential in understanding shock phenomena in high pressure release problems.

In this thesis, the initial solution is provided to the ignition model, using the CFD model and parallel processing methods previously described. The location of the hottest point along the interface, at which the maximum temperature conditions occur, is at the jet head along the centerline. At that location, the flow is the hottest at any given time during the release, failure for ignition to occur at the hottest point means that spontaneous ignition will most likely not be observed at any other location. The analysis follows the gas interface along the centerline, with its rate of expansion prescribed by the local evolution of pressure. The numerical algorithm and the solution approach used to determine the pressure at the contact surface as hydrogen expands, is a continued effort from previous work done by Paraschivoiu, Khaksarfard [4].

The possibility of ignition is high in front of the hydrogen-air contact surface, where the flow heated by the shockwave is the hottest. After the initial compression, the strong expansion hydrogen experiences may delay or suppress ignition. When the rate of expansion is sufficiently strong, which occurs for releases through sufficiently small holes, ignition can be prevented.

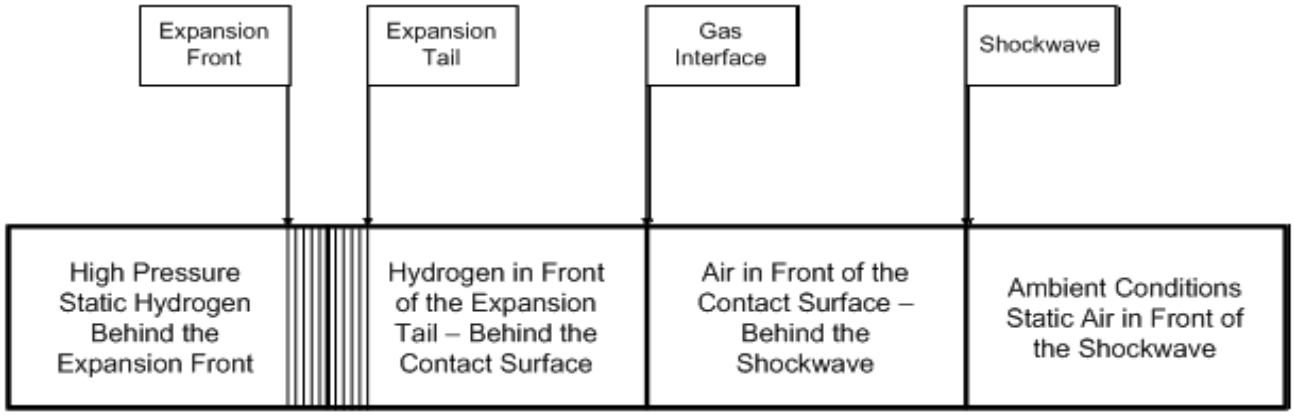


Figure (2.1) - The Shock Tube problem

### 2.1.2 LDR Model

In the LDR model, favorable ignition factors, namely the diffusion of the two gases and the initial heating by the shockwave, compete with the cooling effect of expansion or depressurization, to determine whether ignition has occurred.

The reaction mechanism provided in the LDR model, reacts hydrogen molecules with air, OH compounds are then formed, which when abundant in the mixture, suggest that ignition has occurred. Figure (2.2) shows the steps performed by the ignition model, and the inputs required for the diffusion step, reaction step and expansion step.

Prior to ignition, OH rates are slow, and since chemical reactions have a proportional dependency on temperature, increased temperatures lead to an increase in OH production, and thus more pronounced chemical reactions and higher ignition risks.

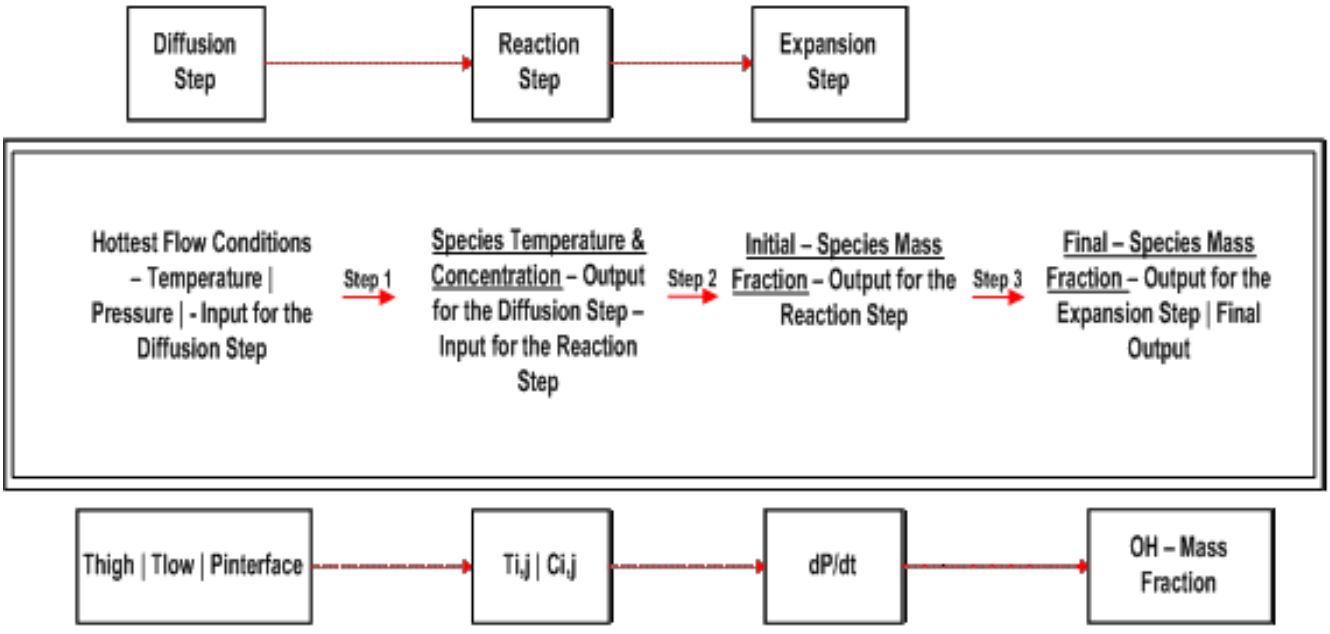


Figure (2.2) - The LDR-model: Input, Output Scheme

## 2.2 Governing Equations

Navier-Stokes equations are the general governing equations for the numerical simulation of viscous fluid flows. These equations can be simplified by removing terms describing viscous actions to yield the Euler equations.

### 2.2.1 Governing Equations - CFD

With a high Reynolds number, Euler equations (2.1) to (2.3) are then used since viscous terms can be neglected. The continuity equation (2.4), which is the rate at which mass changes with time per unit volume, can be written in terms of the material derivative, and is used to guarantee the conservation of physical quantities, such as mass, energy and momentum.

The change in momentum for a fluid particle with a fixed mass and with respect to time, equation (2.5) is related to the net force due to pressure acting on the fluid, to viscous forces, assumed negligible, and to the convective velocity flow field and its unsteady effects.

The conservation of energy for a fluid particle of fixed mass has many forms, equation (2.6) (2.7) can be written in terms of total energy - internal energy, and kinetic energy.

The Abel-Noble equation (2.8) provides a real gas equation that accurately models this high density and high temperature flow, and the advection or transport equation (2.9) provides a rational to describe the concentration distribution of hydrogen and air, as the flow evolves.

- Euler Equations:

$$\frac{\partial U}{\partial t} + \nabla . F = 0 \tag{2.1}$$

$$U = \begin{bmatrix} \rho \\ \rho u \\ \rho v \\ \rho w \\ \rho E \end{bmatrix}, F = \left\| \begin{bmatrix} \rho u \\ \rho u^2 + P \\ \rho uv \\ \rho uw \\ \rho uH \end{bmatrix} \begin{bmatrix} \rho v \\ \rho vu \\ \rho v^2 + P \\ \rho vw \\ \rho vH \end{bmatrix} \begin{bmatrix} \rho w \\ \rho wu \\ \rho wv \\ \rho w^2 + P \\ \rho wH \end{bmatrix} \right\| \tag{2.2}$$

Where:

$$E = i + \frac{1}{2} * (u^2 + v^2 + w^2) \quad , \quad H = E + \frac{P}{\rho} \tag{2.3}$$

- Conservation of mass:

$$\frac{\partial \rho}{\partial t} + \nabla . (\rho v) = 0 \tag{2.4}$$

- Conservation of momentum:

$$\frac{\partial (\rho v)}{\partial t} + \nabla . (v \otimes (\rho v)) + \nabla p = 0 \tag{2.5}$$

- Conservation of total energy:

$$\frac{\partial (E)}{\partial t} + \nabla . (v(E + p)) = 0 \tag{2.6}$$

Where:

$$E = \rho e + \frac{1}{2} \rho |v|^2 \tag{2.7}$$

- Abel-Noble - EOS:

$$p = \frac{\rho RT}{(1 - b\rho)} \quad , \quad b = 0.00775 \ m^3/kg \tag{2.8}$$

- Advection equation:

$$\frac{\partial c}{\partial t} + \nabla . (cv) = 0 \tag{2.9}$$

### 2.2.2 Governing Equations - LDR

The ignition model transforms the governing equations into Lagrangian coordinates in order to keep track of chemical compounds, as the gas expands and occupies more space, this transformation is done by converting spatial coordinates, into a mass-based coordinate system, by integrating the density.

In the LDR model, the continuity of mass of reacting species is related to the production rate and velocity of species, through another transport equation. The transport equations (2.10) (2.11) applied in the ignition model, are solved separately at the end of each time step, to determine the required transport properties for each species: the diffusion velocities of each species and thermal conductivities.

The total velocity of species in this model is the sum of the average velocity and the diffusion velocity. The total diffusion velocity consists of the physical diffusion velocity due to pressure gradients equation (2.14), and gradients in species concentration equation (2.12), the thermal diffusion velocity due to gradients in temperature equation (2.13), and a correction velocity that ensures that the conservation of mass of each chemical species is not violated.

The expansion term in equation (2.14), is treated as a source term and is evaluated by updating the pressure, using the solution obtained from the previous step. The expansion rate reflects the rate of change of pressure with respect to time, as expansion flow develops.

- Diffusion Equations:

- Species Concentration:

$$Y_{i,j}{}^{n+1} = Y_{i,j}{}^{n} - C_n * \left(\frac{\Delta t}{\Delta m^2}\right) \tag{2.10}$$

- Species Temperature:

$$T_{i,j}{}^{n+1} = T_{i,j}{}^{n} - C'_n * \left(\frac{\Delta t}{\Delta m^2}\right) \tag{2.11}$$

$C_n$, and $C'_n$ are functions of $Y_{i,j}{}^{n}$, and $T_{i,j}{}^{n}$ respectively.

- Reaction Equations:

$$\rho * \frac{\partial Y_i}{\partial t} = \omega_i \tag{2.12}$$

$$\rho * C_p * \frac{\partial T}{\partial t} = -\sum_{i=1}^{N} h_i * \omega_i \tag{2.13}$$

$h_i$ is the specific species enthalpy and $\omega_i$ is the specific species production rate.

- Source Term Equation:

$$\rho * C_p * \frac{\partial T}{\partial t} = \frac{\partial P}{\partial t} \tag{2.14}$$

## 2.3 Boundary & Initial Conditions

The full three-dimensional geometry is modeled, and the mesh used has almost 11 million elements and 2 million nodes. The mesh is denser near the exit edge where pressure and flow gradients are higher than in the reservoir and surrounding.

In figure (2.3), the reservoir and the release environment have the same temperature and velocity initially, the fluid is static, and the temperature is 300 K. The reservoir pressure varies by case, and the release environment is at ambient pressure of 101.325 KPa. The initial contact surface is always released from the center of the 2mm extension tube, and the reference zero on the horizontal spatial axis-z is always located at the exit edge of the orifice.

As shown in figure (2.3), the boundary conditions require slip walls since viscosity can be neglected. External body forces, such as gravity, acting on the fluid are negligible, as well as heat fluxes due to radiation.

Three reservoir pressures of 10 MPa, 30 MPa and 70 MPa are examined, boundaries are adiabatic, and the environment in which the tank sits is neglected in terms of heat transfer.

The dimensions are shown in the two-dimensional view, in figure (2.4), the low pressure outside environment is a 20 mm diameter and length cylinder, the reservoir is 100mm in diameter and 50 mm in length, and the opening is a 2 mm long tube with variable dimensions and diameters.

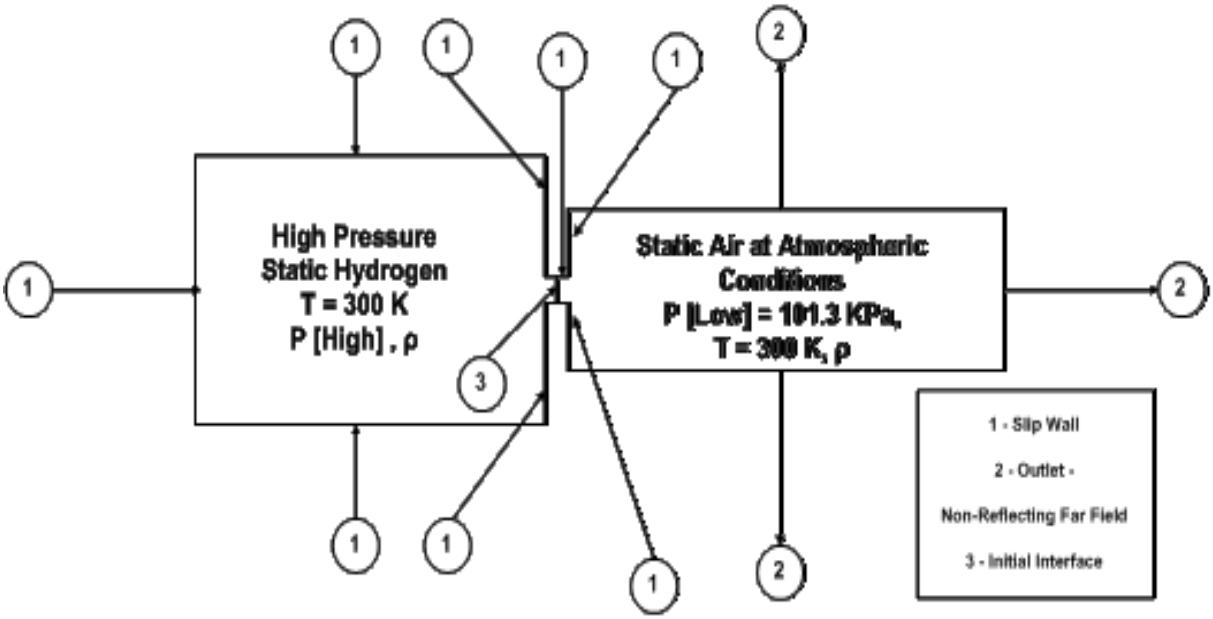


Figure (2.3) - Schematic of Boundary, and Initial Conditions

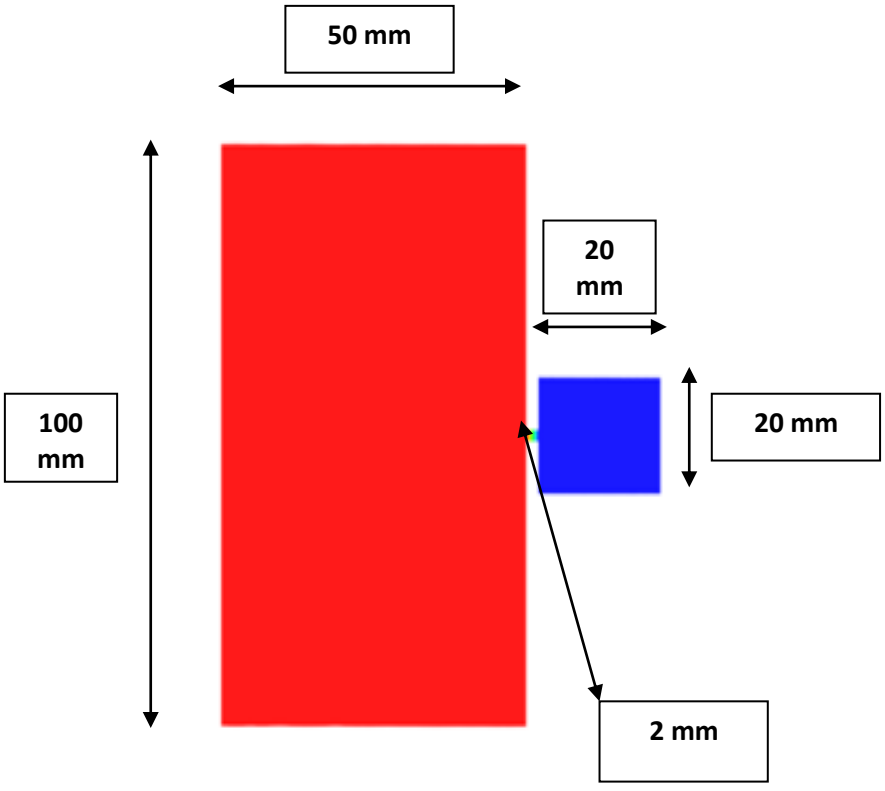


Figure (2.4) - Standard Simulation Geometry, and Dimensions

# Chapter 3

# Numerical Framework and Validation on Fixed Release Orifice

In this chapter, the methodology to predict auto-ignition is developed based on combining the two numerical tools described in chapter 2. This methodology is further validated with the existing literature for fixed circular orifices and fixed elliptic orifices.

As hydrogen expands, Radulescu and Maxwell determine a simple time-dependent relationship describing the pressure at the interface, by curve-fitting the numerical results using a unique power-law function. In this thesis, the relationship describing the evolution of the gas interface pressure is determined on a case-by-case basis through $6^{th}$ order polynomial regression curve fits. The rate at which the pressure at the interface decays, which depend on the flow velocity, and the dimensions of the hole is numerically determined based on CFD. Describing the expansion process is essential, in the case where enough OH-compounds to cause ignition, are produced prior to expansion, the expansion process modeled using the pressure-time profile as an independent source term, can slow down or even suppress ignition.

The first task is to describe the flow, at time of release and then during expansion to determine the diffusion and expansion properties of hydrogen, the second task is to assess ignition risks and explain how the storage pressure, the expansion of the gas, and the hole size contribute to ignition.

## 3.1 Fixed Circular Release Area

The objective in this section is to validate ignition results obtained for standard circular holes using CFD coupled with an LDR ignition model.

### 3.1.1 Release Process Prior to Expansion

The first task is to describe the flow, at time of release. The objective of this task is to determine the key physical parameters that directly affect the ignition process. The cold temperature of hydrogen behind the gas interface, and the hot temperature of air leading the interface, as well as the contact surface pressure, are the physical parameters that directly affect ignition.

Due to different properties of hydrogen and air, the stability of numerical results becomes an important factor. The challenge in hydrogen-air release problems is to accurately capture the contact surface generated between hydrogen and air, and its position as it moves in time. In this section, the release flow as hydrogen diffuses is described in terms of temperature profile for the cold hydrogen and hot air on both sides of the contact surface, along with the gas interface pressure.

Diffusion of hydrogen is an early stage event that occurs within 1μs of the release, temperature and pressure profiles should be accurately captured, to first determine the hottest point at the early stages of diffusion. Governing conditions for the hottest point along the interface are required, and numerically resolved in this section, to provide input, as initial conditions for the ignition model.

It is essential to capture temperature for various times during early diffusion stages and later during expansion, to determine the behavior of temperature before and during expansion. Three different reservoir pressures are simulated for three different circular orifice diameters, having a common tube length of 2 mm.

Figures (3.1.1) - (3.1.3), show temperature along the centerline for initial tank pressures of 70 MPa, 30 MPa, and 10 MPa, and circular holes of 1 mm, 2 mm, and 5 mm. The negative temperature gradient is representative of the cold hydrogen lagging the contact surface, and the steep positive temperature gradient that follows is representative of the hot air leading the contact surface.

Figures (3.1.1) - (3.1.3), also show the location of the interface and the shockwave, and confirm that the maximum temperature is achieved in the early stages of hydrogen diffusion. Figures (3.1.1) - (3.1.3), clearly indicate that temperature profiles in 2 mm long orifices are such that after achieving the highest peak value, a decrease in the hot air temperature is observed, and that this maximum temperature value is observed during the release process prior to expansion.

Results for 2 mm long openings have shown that the highest temperature peak is achieved along the centerline, before the interface reaches the exit edge. In this section, the hottest point at the gas interface is determined, the cold hydrogen and hot air temperature, along with interface pressure are then captured at that point to provide diffusion conditions to the ignition model.

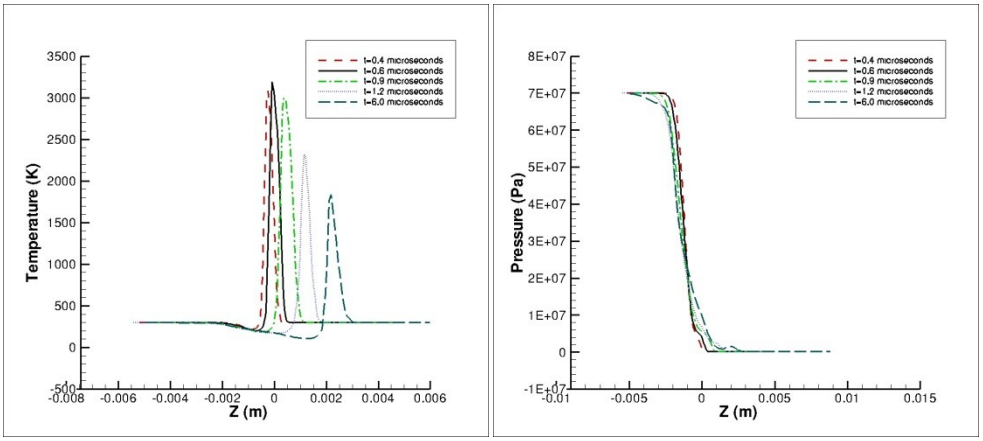


**a) 70 MPa**

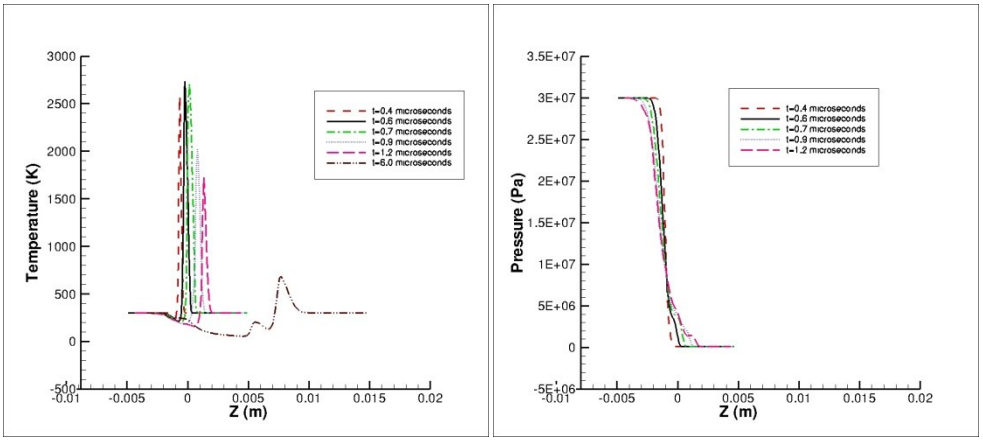


**b) 30 MPa**

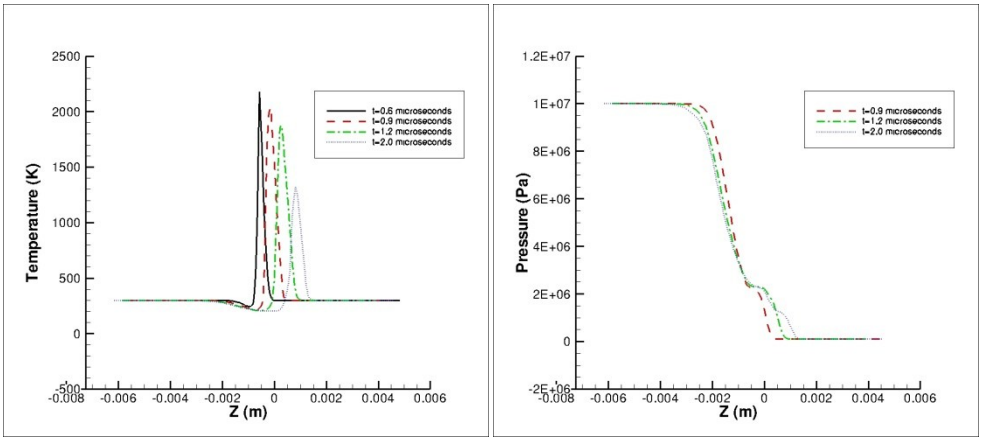


**c) 10 MPa**

Figure (3.1.1) - T (z) (Left), P (z) (Right), 1 mm Case (C), Fixed Circular Geometry

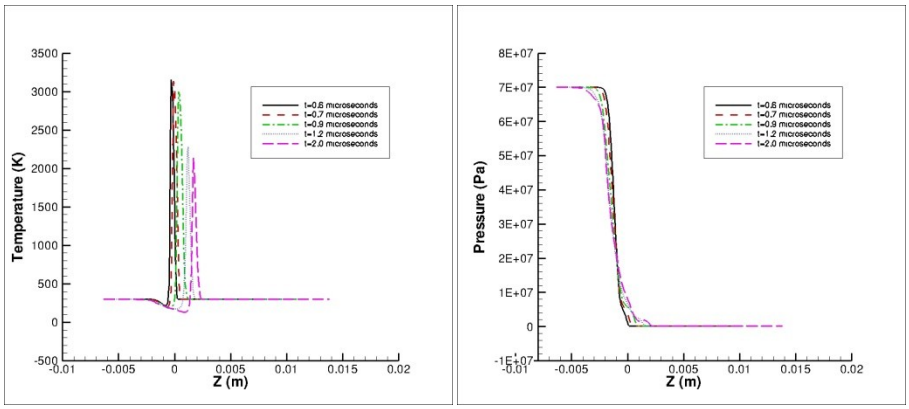


**a) 70 MPa**

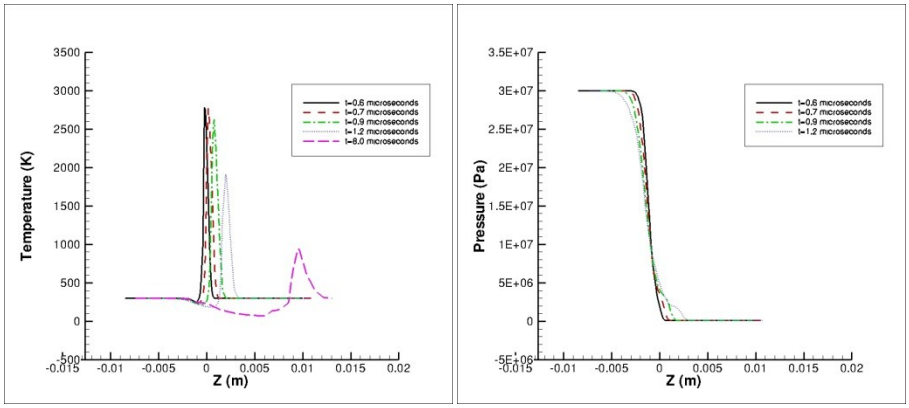


**b) 30 MPa**

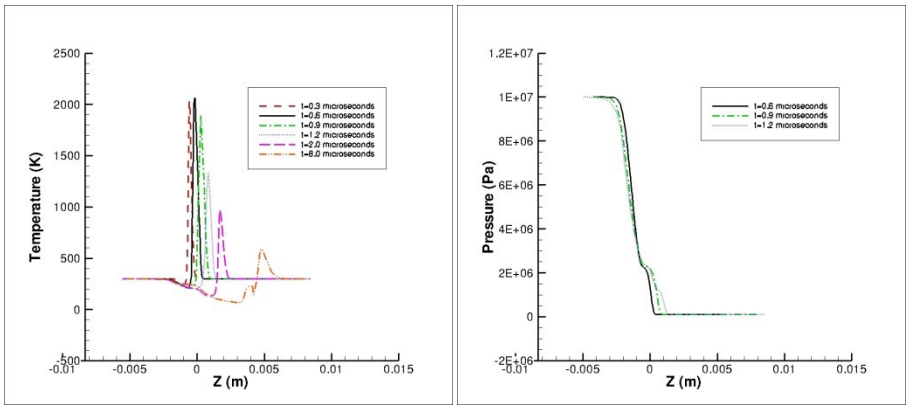


**c) 10 MPa**

Figure (3.1.2) - T (z) (Left), P (z) (Right), 2 mm Case (C), Fixed Circular Geometry

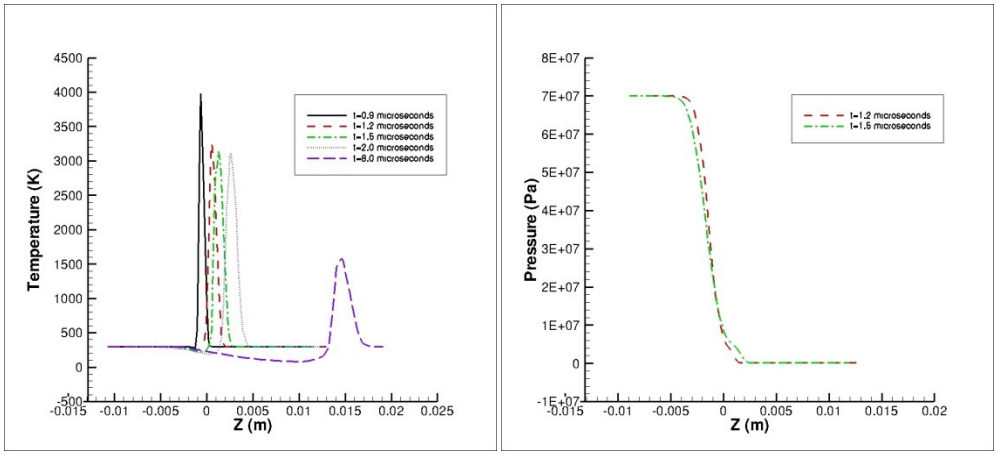


**a) 70 MPa**

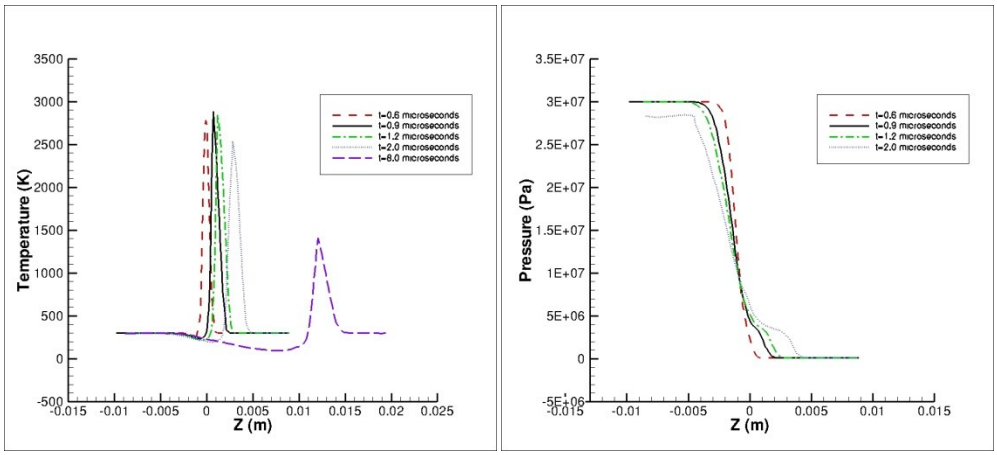


**b) 30 MPa**

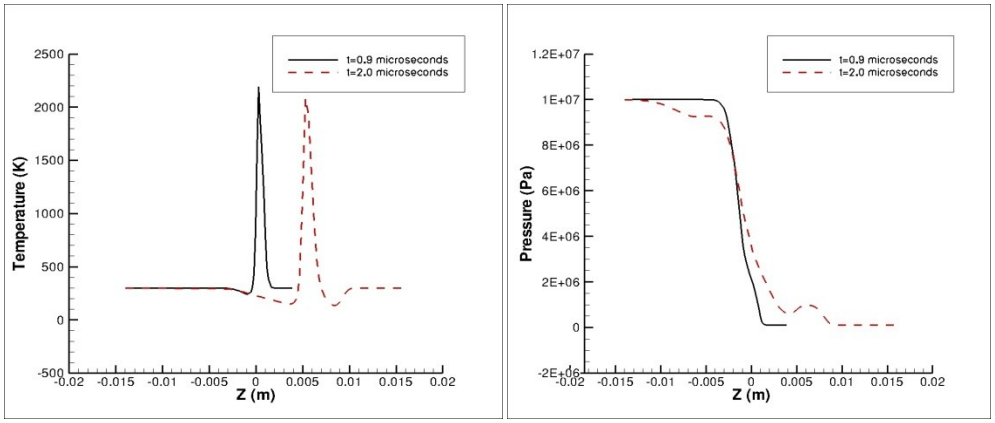


**c) 10 MPa**

Figure (3.1.3) - T (z) (Left), P (z) (Right), 5 mm Case (C), Fixed Circular Geometry

### 3.1.2 The Expansion Flow

In this section, the expansion process is explained, and the pressure decay at the contact surface is prescribed as a source term in the LDR model. The release time is used to refer to the time at which the interface has reached the exit edge, and the decay time is used to refer to the time at which the expansion process starts.

The expansion process is a depressurization of the flow, and is described in terms of the interface pressure, as it starts to decay. Expansion is prescribed in the LDR model by the interface pressure gradient with respect to time, or in other terms the derivative of pressure at the interface with respect to time. The pressure-time gradient for each case is required as a source term to adjust the effect of expansion on the ignition process. In the case where enough OH-compounds to cause ignition, are produced prior to expansion, the expansion process can slow down ignition.

The negative slope of the pressure-time curve is characteristic of the expansion process, and reduces production and reaction rates. The algorithm used to obtain this curve, evaluates the concentration variable and range to capture the interface pressure, since concentration at the contact surface, where both gases meet is divided equally between hydrogen and air.

Using the pressure-time data obtained, a $6^{th}$ order polynomial regression is performed and results in an analytical expression relating time and pressure, which is then derived to obtain the source term. The prescribed source term is obtained by curve fitting the pressure-time profile on a case-by-case basis by using a $6^{th}$ order polynomial.

The interface pressure in figures (3.1.6) and (3.1.8), experiences numerical oscillations; this numerical disturbance observed is affected mainly by the mesh resolution and the time-step used, but also by the accuracy of the algorithm used in capturing the contact surface. The pressure values jump as the contact line move from one element to the next one. A finer mesh and a larger time-step reduce numerical oscillations in capturing the interface pressure. However, for thorough consistency, the mesh used is the same for all cases discussed, and consists of around two million nodes.

In figures (3.1.4) - (3.1.6), pressure at the contact surface is plotted against time, until it has decreased significantly. In figures (3.1.4) - (3.1.6), the pressure peaks to a maximum value before the expansion process starts to depressurize the flow. The behavior of pressure at the interface, during this depressurization is a major factor in avoiding ignition. This behavior is modeled through curve fitting the portion of the pressure curve, when expansion starts taking place, and pressure starts to decay. The pressure at the contact surface experiences a fast rise due to the resulting shockwave, followed by subsequent pressure decay.

The effect of the pressure gradient on OH-compounds productions, show that ignition can be prevented for steeper pressure gradients in the expansion flow, and that even when local ignition has occurred in the release area, steep pressure gradients can limit the flame propagation process, and only localized ignition would be observed. In this section, the derivative of pressure with respect to time is numerically determined by curve fitting the interface pressure, the decay time is recorded, and a summary table of input parameters required for the ignition model is provided.

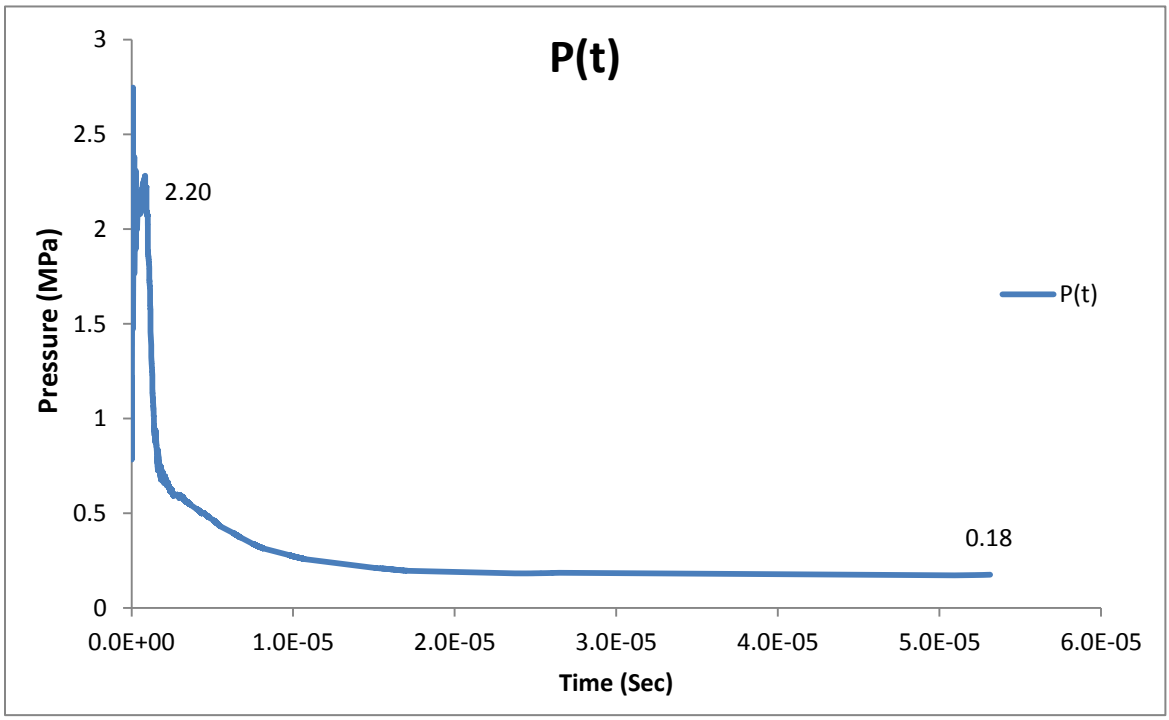


**a) 30 MPa**

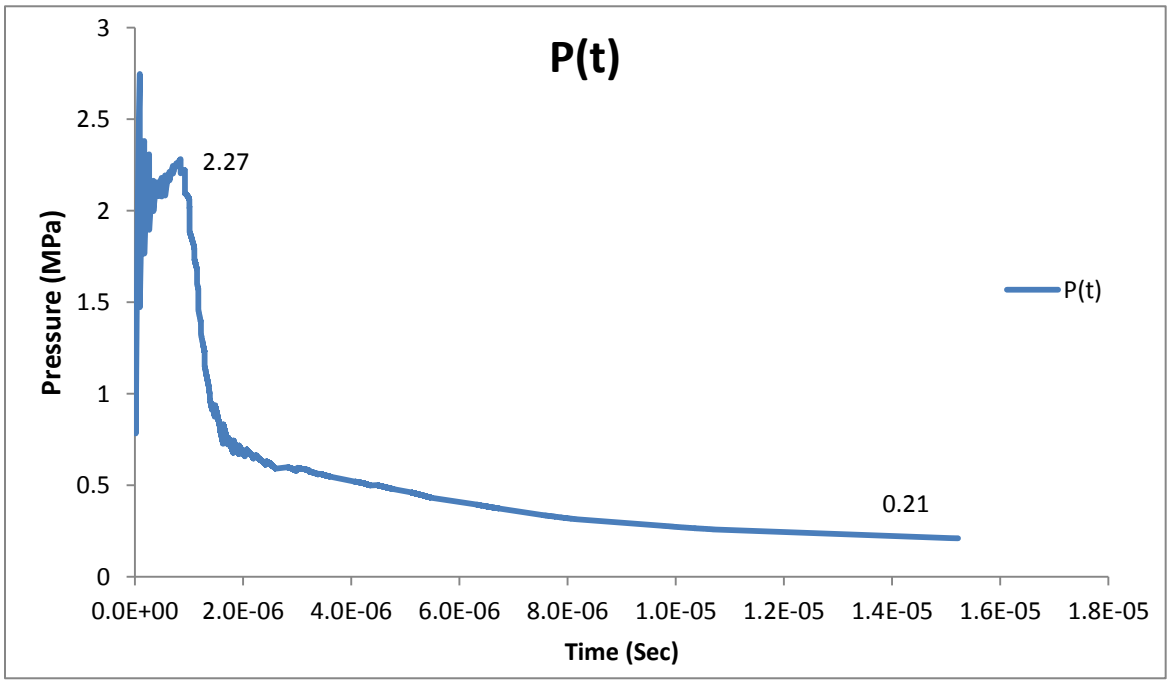


**b) 10 MPa**

Figure (3.1.4) - P (t) curve, 1 mm Case (C), Fixed Circular Geometry

Radulescu and Law have previously determined a unique relation for the pressure-time history at the interface for different jet conditions. However, their analytical curve fit model is only a rough approximation of the release problem under investigation, and their unique expression describing the pressure at the interface, does not accurately describe the expansion process for the current problem.

Figure (3.1.5) compares the pressure-time profile obtained by using the CFD code, to the profile given by the unique curve fit expression (2.15), obtained in the work of Radulescu and Maxwell. In their work, the interface pressure depends on the flow velocity, the size of the hole through which the gas escapes, and takes on a power-law form by curve-fitting the numerical results.

The comparison shows that the LDR-model used in their work, under-estimates the contact surface pressure, for the release problem addressed. One of the reasons is that the curve fitting technique is applied to the complete pressure-time profile, which results in bigger regression errors, compared to curve fitting pressure only in the expansion phase, when pressure starts to drop.

One of the main advantages of the FORTRAN code is that it can accurately capture flow properties at very small time scales. The robustness of the CFD FORTRAN code, allows for a more detailed description of the decay process, the code allows to accurately capturing the interface pressure.

$$\tau = \sqrt{\frac{\rho_{Air_0}}{\rho_{H_{2_0}}}} * \sqrt{\left(\frac{2}{\gamma_{H_2}+1}\right)^{\left(\frac{-1}{\gamma_{H_2}-1}\right)}} * \sqrt{\left(\frac{2}{\gamma_{H_2}+1}\right)} * \frac{1}{r} * t \qquad (2.15)$$

$$P\,(t) = 12.2 * P_{storage} * \tau^{-0.68} \qquad (2.16)$$

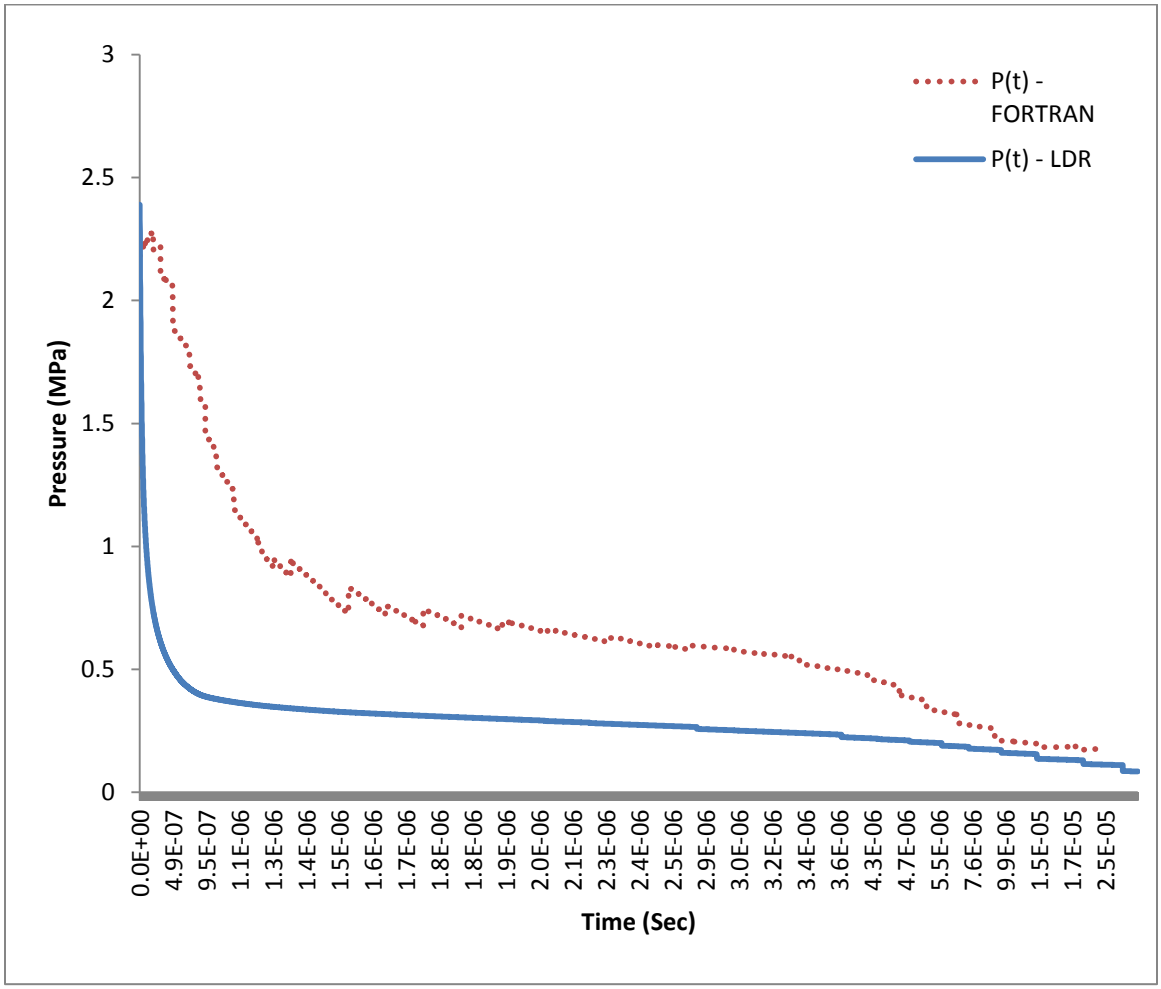


- **30 MPa**

Figure (3.1.5) - Pressure Comparison, 1 mm Case (C), Fixed Circular Geometry - CFD, LDR

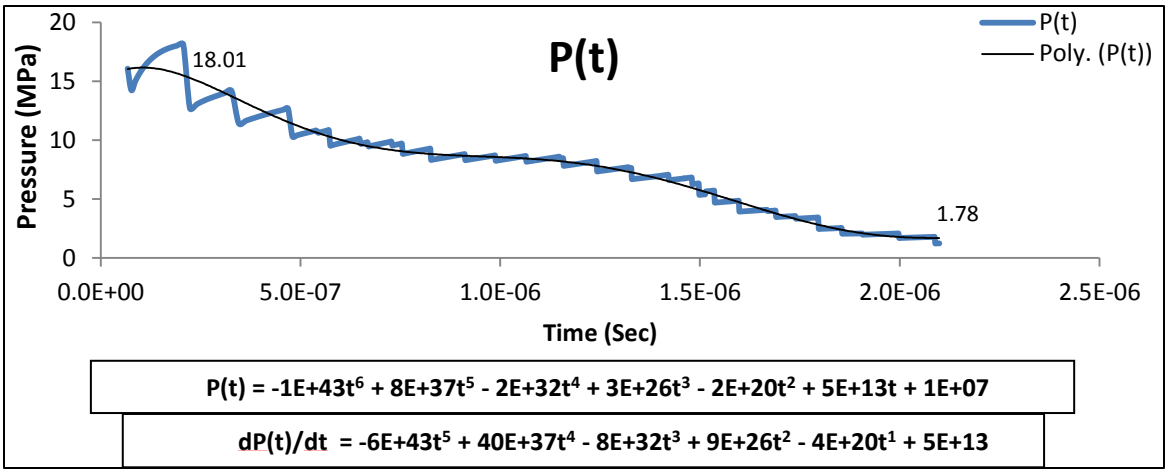


**a) 70 MPa**

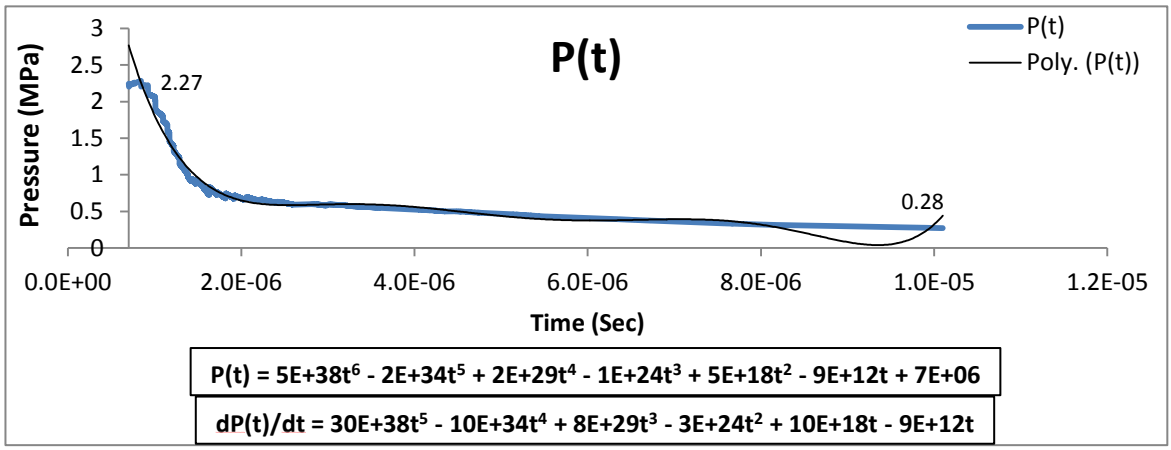


**b) 30 MPa**

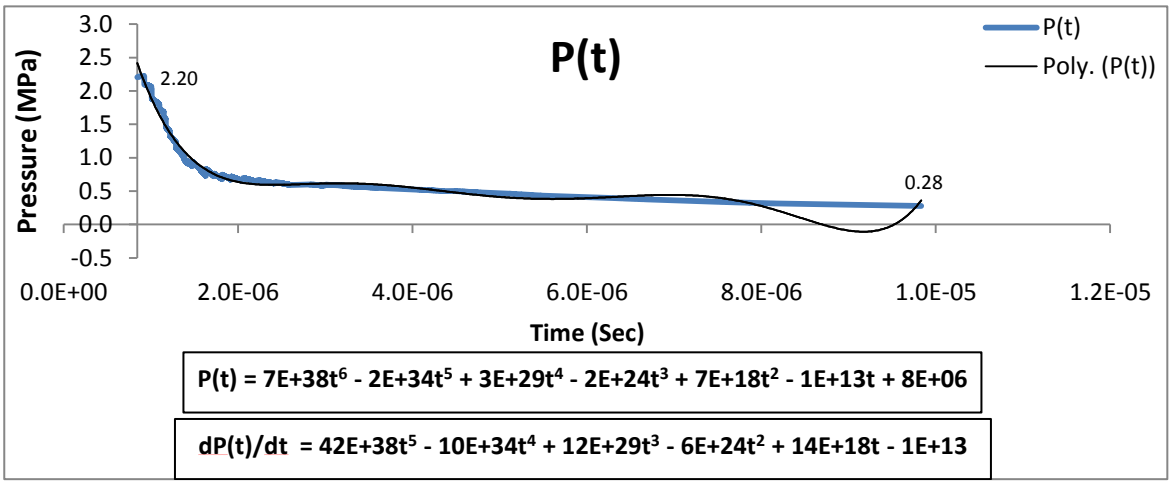


**c) 10 MPa**

Figure (3.1.6) - P (t) & dP(t)/dt, 1mm Case (C), Fixed Circular Geometry

In figure (3.1.7) pressure versus time along the centerline of the contact surface is given for a circular release area diameter of 2mm at 70 MPa. Figure (3.1.7) shows that a better description of the decay process can be obtained by using the CFD code, the resulting curve relies on two-thousand data points to model the pressure behavior. Figures (3.1.8) and (3.1.9) show the behavior of pressure for a fixed circular orifice of 2mm and 5mm, along with the curve fitting technique used.

Pressure is plotted versus time until the end of the expansion process, when the interface pressure drops to ambient pressure whenever possible, or alternatively to conditions asymptotic to the time axis, at which the expansion process can be accurately described and curve fitted. As shown in figure (3.1.7), the gas interface pressure drops significantly, to behave asymptotically to the time axis, signaling the end of the expansion process.

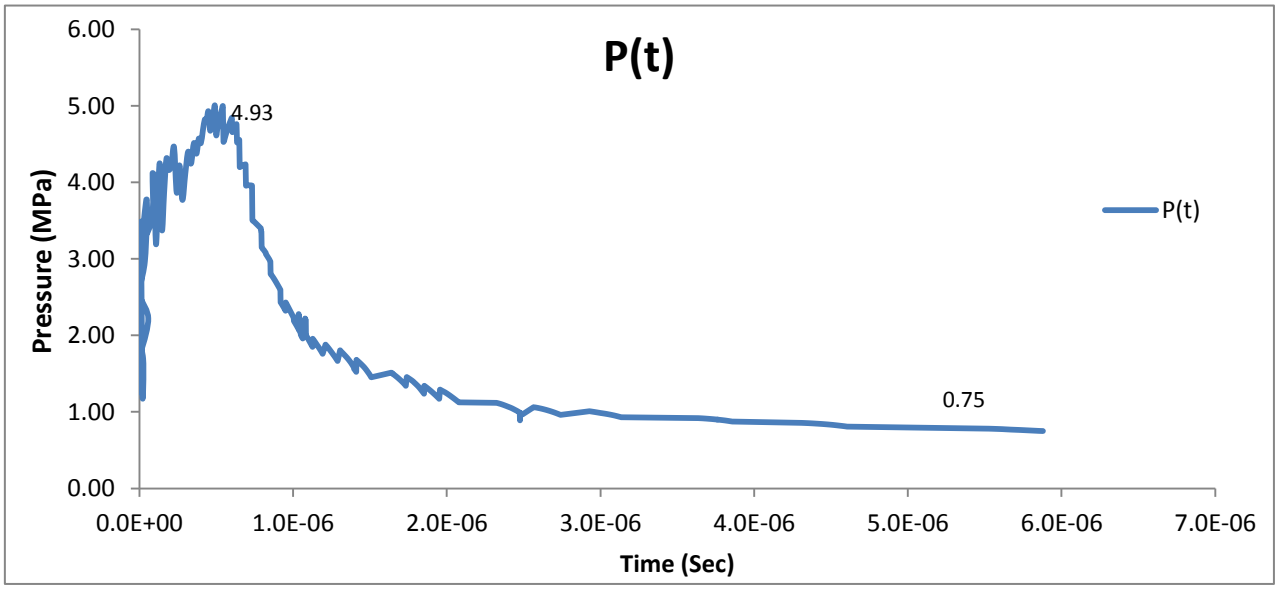


Figure (3.1.7) - P (t) curve, 2 mm Case (C), Fixed Circular Geometry - 70 MPa

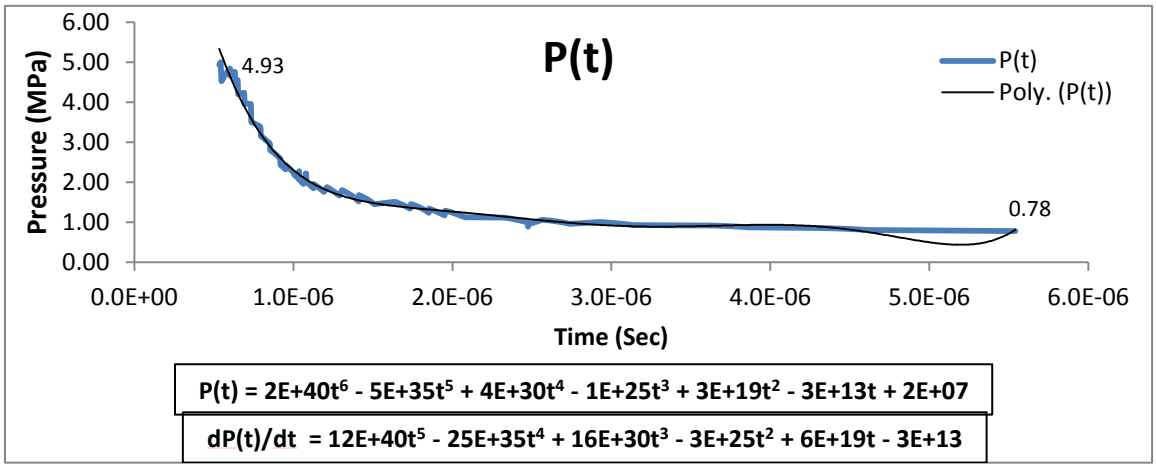


a) 70 MPa

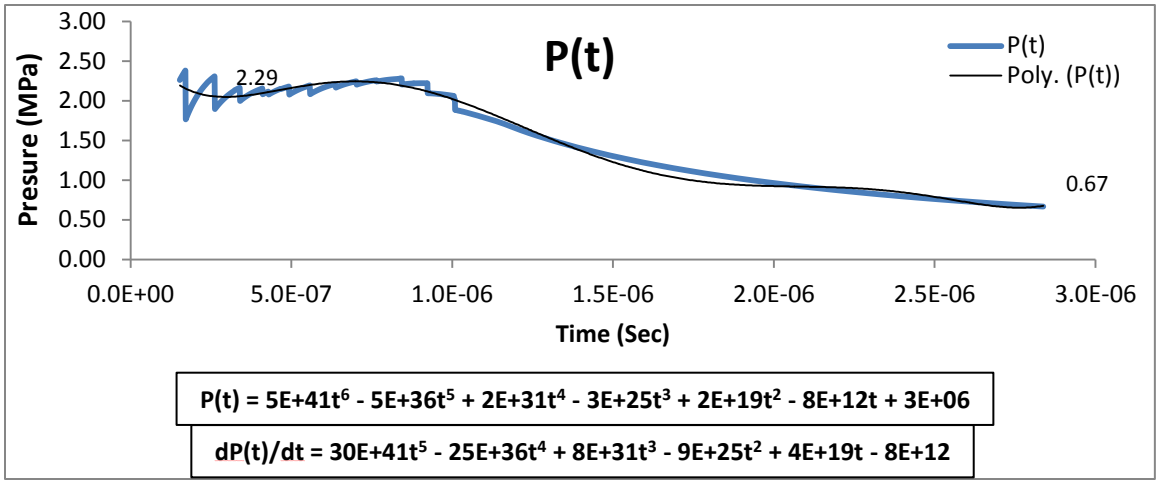


b) 30 MPa

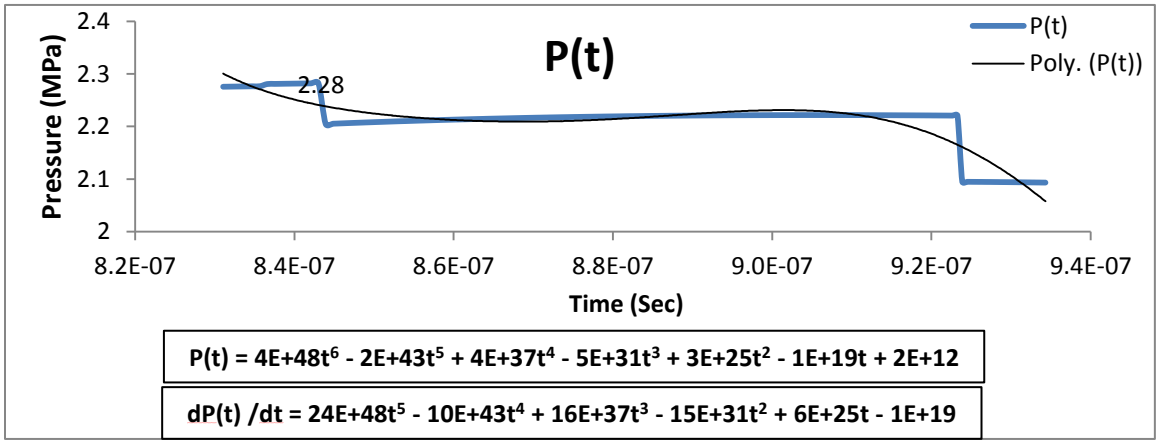


c) 10 MPa

Figure (3.1.8) - P (t) & dP(t)/dt, 2 mm Case (C), Fixed Circular Geometry

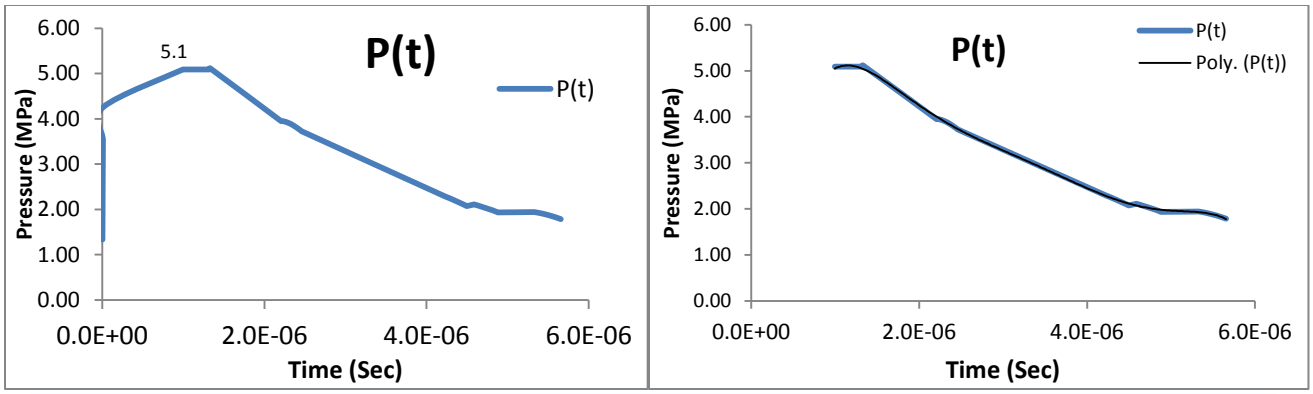


$P(t) = -1E+40t^6 + 3E+35t^5 - 2E+30t^4 + 1E+25t^3 - 2E+19t^2 + 2E+13t - 4E+06$

$dP(t)/dt = -6E+40t^5 + 15E+35t^4 - 8E+30t^3 + 3E+25t^2 - 4E+19t + 2E+13$

**a) 70 MPa**

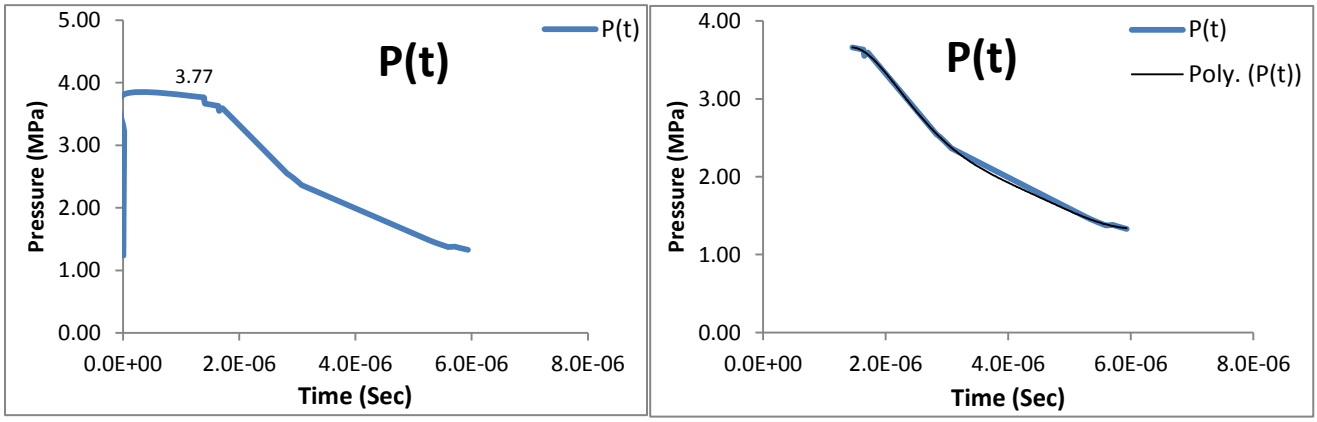


$P(t) = -3E+39t^6 + 8E+34t^5 - 8E+29t^4 + 4E+24t^3 - 1E+19t^2 + 2E+13t - 5E+06$

$dP(t)/dt = -18E+39t^5 + 40E+34t^4 - 32E+29t^3 + 12E+24t^2 - 2E+19t + 2E+13$

**b) 30 MPa**

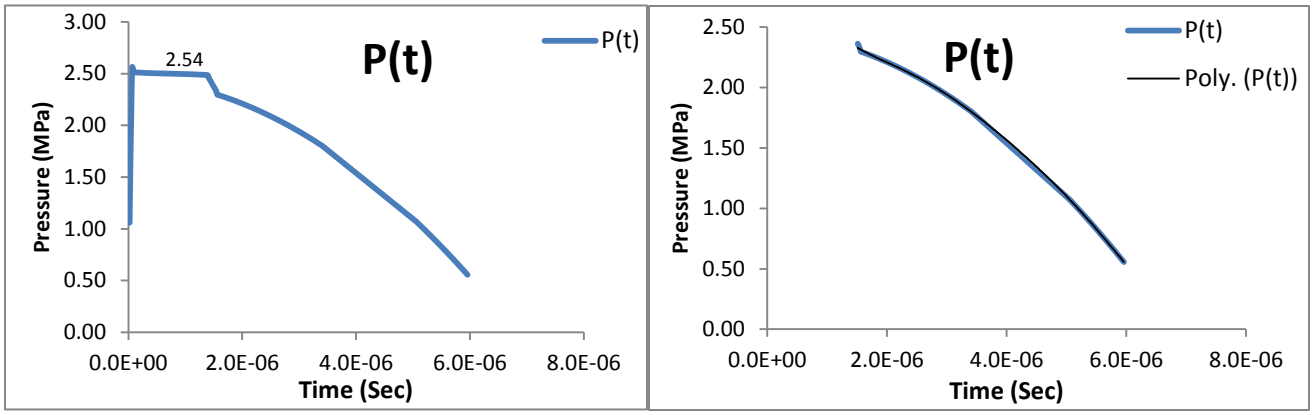


$P(t) = 8E+38t^6 - 2E+34t^5 + 2E+29t^4 - 9E+23t^3 + 2E+18t^2 - 3E+12t + 4E+06$

$dP(t)/dt = 36E+38t^5 - 10E+34t^4 + 8E+29t^3 - 27E+23t^2 + 2E+18t - 3E+12$

**c) 10 MPa**

Figure (3.1.9) - P (t) & dP(t)/dt, 5 mm Case (C), Fixed Circular Geometry

As shown in table (3-1-1), the time gap between the contact surface escaping the orifice and the pressure achieving its maximum before decay is small, and is representative of the lag between the shockwave and the gases interface.

The release and decay times are important parameters, when comparing different geometries, as they describe the effect of the opening shape on both the diffusion and expansion processes.

| Fixed Circular Release Area | | | | |
|---|---|---|---|---|
| **1 mm** | **T[High] [K]** | **T[Low] [K]** | **P [MPa]** | **Release Time [µs]** |
| | | | | 0.6 µs |
| **70 MPa** | 3050 | 180 | 5.75 | **Decay Time [µs]** |
| | | | | 0.65 µs |
| **30 MPa** | 2732 | 192 | 4.51 | **Decay Time [µs]** |
| | | | | 0.7 µs |
| **10 MPa** | 2184 | 215 | 2.38 | **Decay Time [µs]** |
| | | | | 0.8 µs |
| **2 mm** | **T[High] [K]** | **T[Low] [K]** | **P [MPa]** | **Release Time [µs]** |
| | | | | 0.6 µs |
| **70 MPa** | 3127 | 185 | 4.77 | **Decay Time [µs]** |
| | | | | 0.7 µs |
| **30 MPa** | 2750 | 200 | 4.39 | **Decay Time [µs]** |
| | | | | 0.75 µs |
| **10 MPa** | 2270 | 235 | 2.27 | **Decay Time [µs]** |
| | | | | 0.85 µs |
| **5 mm** | **T[High] [K]** | **T[Low] [K]** | **P [MPa]** | **Release Time [µs]** |
| | | | | 0.9 µs |
| **70 MPa** | 3918 | 205 | 4.74 | **Decay Time [µs]** |
| | | | | 1.45 µs |
| **30 MPa** | 2795 | 212 | 4.33 | **Decay Time [µs]** |
| | | | | 1.55 µs |
| **10 MPa** | 2237 | 250 | 2.12 | **Decay Time [µs]** |
| | | | | 1.65 µs |

Table (3-1-1) - Fixed Circular Geometry - Input Parameters

Figure (3.1.10) shows that the evolution of pressure along the hydrogen-air interface depends on the release geometry, increasing the opening diameter, increases the pressure at the interface, but the maximum pressure achieved before expansion starts, is higher for smaller holes. Figure (3.1.10) also confirms that smaller holes have a more pronounced expansion, and a steeper pressure gradient.

The negative slope of the pressure gradient is steeper for smaller holes, which confirms that smaller holes have a more pronounced expansion than larger holes, and supports the fact that smaller holes are less likely to ignite.

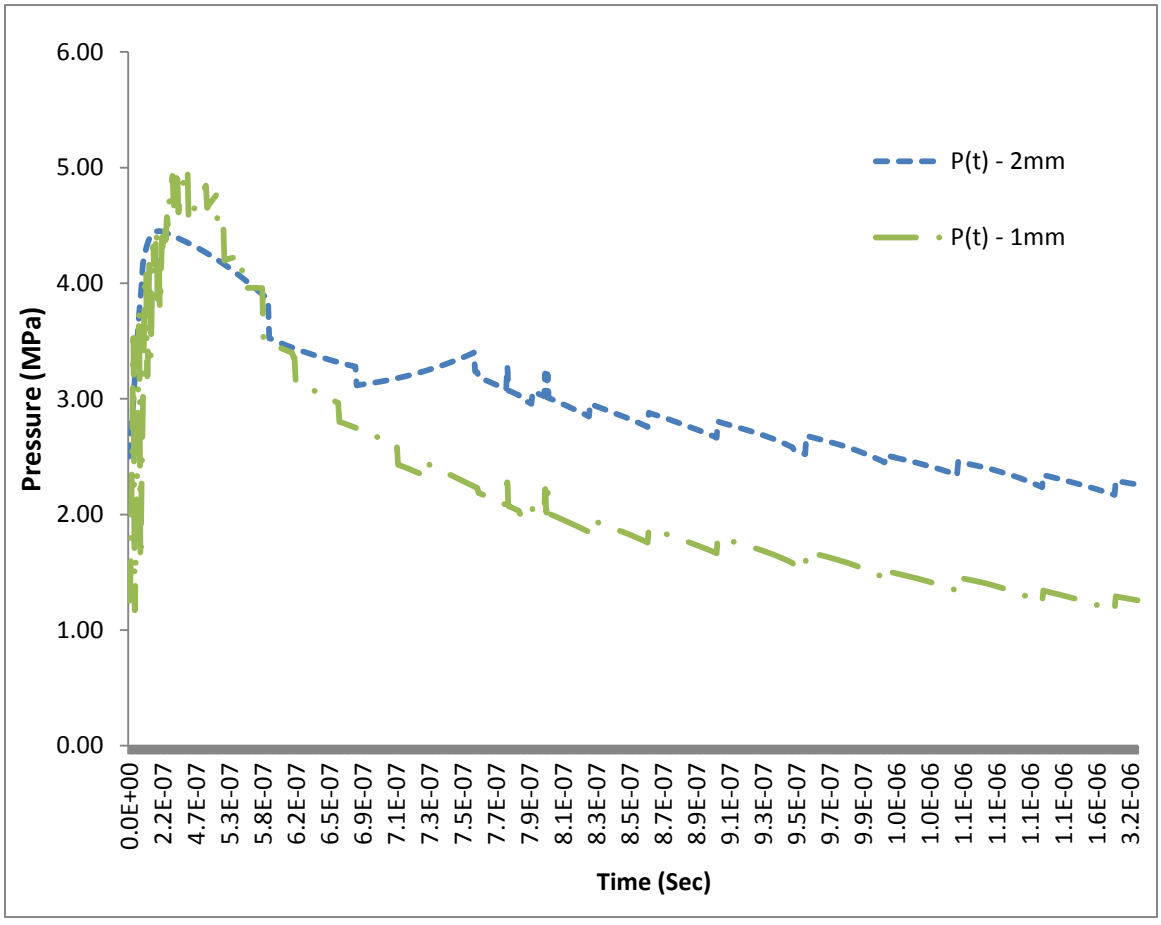


Figure (3.1.10) - P (t) Comparison, 1 mm Case (C) and 2 mm Case (C), Fixed Circular Geometry - 70 MPa

### 3.1.3 Ignition Assessment

There are two competing mechanisms that control ignition in the LDR model, heat addition due to chemical reactions, and cooling due to expansion. OH mass fractions first peak, owing to the diffusion of hydrogen, and the shock-induced heating. Following the maximum OH productions, expansion is accounted for, and starts slowing down chemical reactions, and reducing OH mass fractions. As of the decay time, the ignition model accounts for expansion by using the source term, for the pressure derivative with respect to time, derived in the previous section.

Prior to expansion, the ignition model makes use of a shock tube solution for ideal gases to determine the characteristics of the hottest point, namely temperatures on both sides of the contact surface and the gas interface pressure. Figure (3.1.11) explains the expected analytical behavior of the flow in shock tubes. In analytical solutions, pressure and velocity are constant on both sides of the hydrogen-air interface. Since the interface pressure remains constant as the contact surface and shockwave move, the rate of change of pressure with respect to time prior to expansion is null.

Before the decay time, the pressure gradient is set to zero, which is reflected by a sharp increase in OH mass fractions due to the initial high temperature conditions that trigger pronounced chemical reactions, and explain the sharp mass fractions peaks seen in figure (3.1.12). In other words, the pressure gradient or pressure derivative with respect to time is set to zero and does not contribute to delaying ignition.

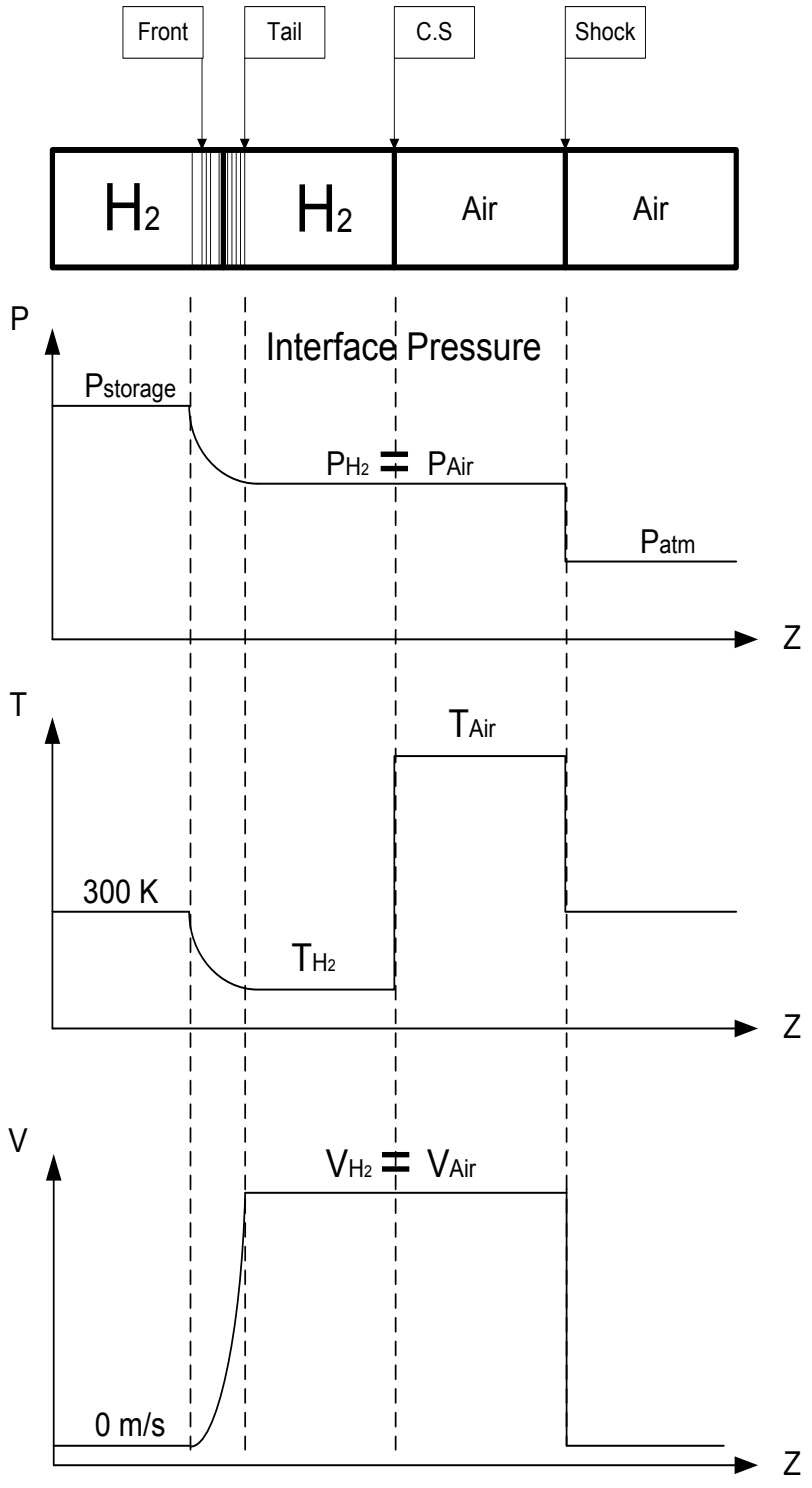


Figure (3.1.11) - Shock Tube Parameters: Pressure, Temperature, and Velocity Profiles

As of the decay time, the negative pressure gradient due to expansion, starts affecting OH mass fractions, which is reflected by their gradual decrease. The negative mass fraction slope correlates to the steepness of the pressure gradient, the steeper the pressure gradient the steeper the mass fraction slope.

Figure (3.1.12) for 1 mm diameter circular openings shows that higher OH peaks are achieved as pressure increases, and that ignition is very sensitive to changes in the operating pressure. Because the size of the opening determines the mixing rate of the gases at the interface, the initial shock-induced heating, and the cooling effect due to expansion, ignition is also very sensitive to changes in the orifice diameter.

The standard ignition production rates set in the work of Radulescu, Maxwell, were found to correlate with their designated problem. Figure (3.1.13), confirms that high storage pressures of 70 MPa will most probably ignite regardless of the exit geometry, based on the ignition limit of 0.001 on OH-mass fraction in their work.

As shown in figure (3.1.13) for high storage pressures, OH-productions reach much higher peaks, above the standard set by Radulescu and Maxwell. The standard ignition production rates set in the work of Radulescu and Maxwell did not correlate with the current release problem. In fact, ignition is a probabilistic event of statistical nature, modeling ignition probabilities is the approach used instead in this thesis, to assess ignition risks.

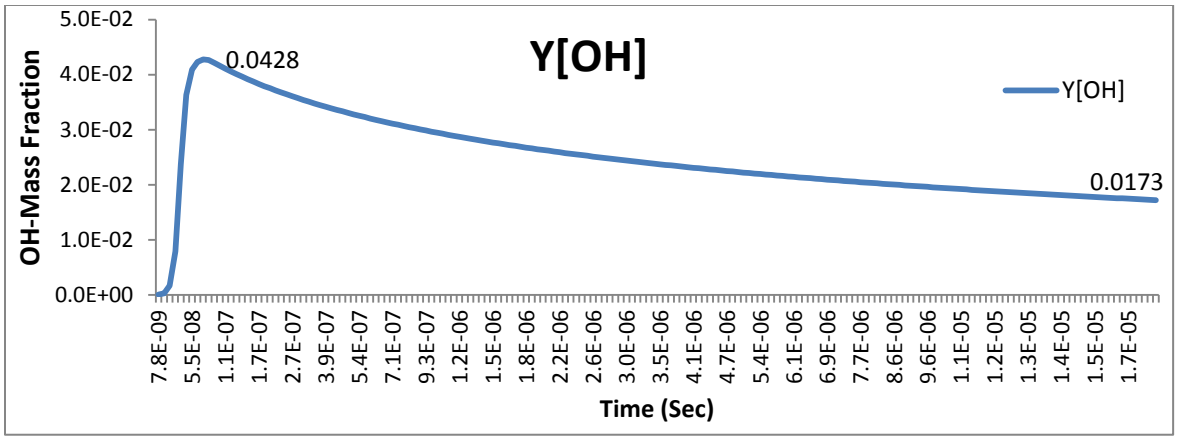


**a) 70 MPa**

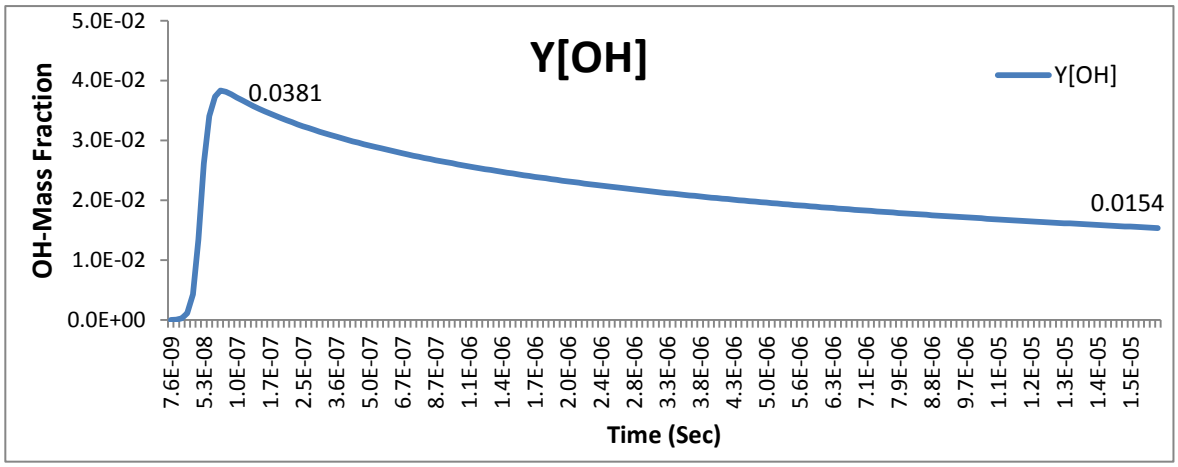


**b) 30 MPa**

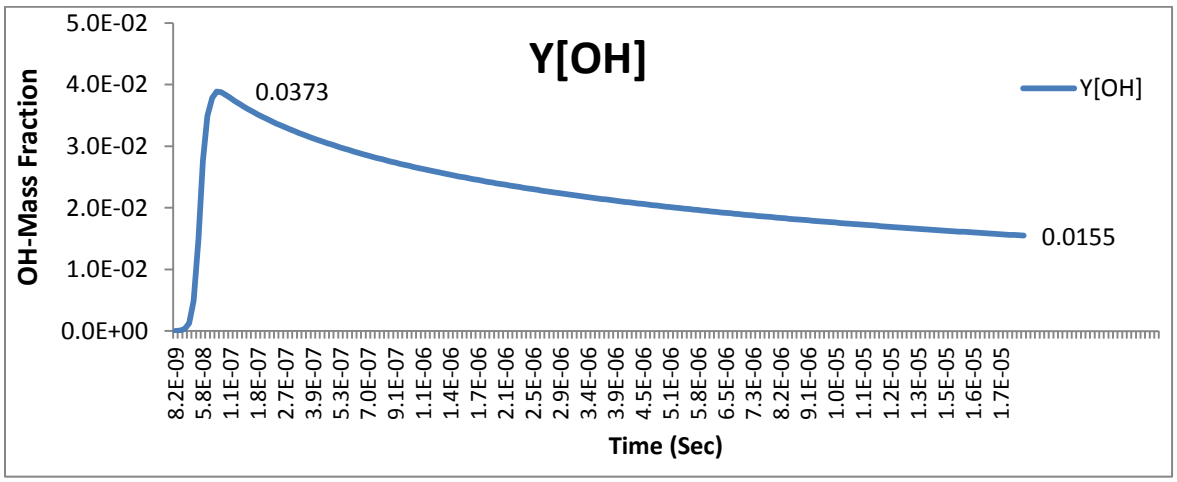


**c) 10 MPa**

Figure (3.1.12) - OH Mass Fraction, 1 mm Case (C), Fixed Circular Geometry

Both the maximum and final OH mass fractions are essential mass fractions to understand and assess ignition risks, as they provide means of accurately modeling ignition probabilities.

Ignition probabilities are determined using the 100% stacked line technique that shows the corresponding data values stacked as a percentage of the total, and allows to see what percentage each value was of the total, instead of comparing total amounts. In other words, the 100% stacked line technique allows visualising the weights of the diffusion process and expansion process in terms of percentage, where higher probabilities mean stronger diffusion and weaker expansion. Figure (3.1.14) is therefore a display of the trend each numerical value contributes over time, and compares ignition probabilities for the three pressure cases discussed.

The plot suggests that ignition is most probable for high pressures of 70 MPa and becomes less probable as storage pressure decreases. Comparing figure (3.1.12), and figure (3.1.15), shows that for smaller openings, ignition is less sensitive to the operating pressure. In fact, as observed in figure (3.1.12) for the 1 mm diameter case, increasing the storage pressure slightly increases OH-productions; whereas for the 2 mm diameter case shown in figure (3.1.15), an increase in storage pressure greatly increases hydroxide mass fraction rates.

Both the maximum and final OH mass fraction values are lower for smaller holes of 1mm diameter, which validates previous conclusions that smaller holes have a less dominant diffusion and a more pronounced expansion.

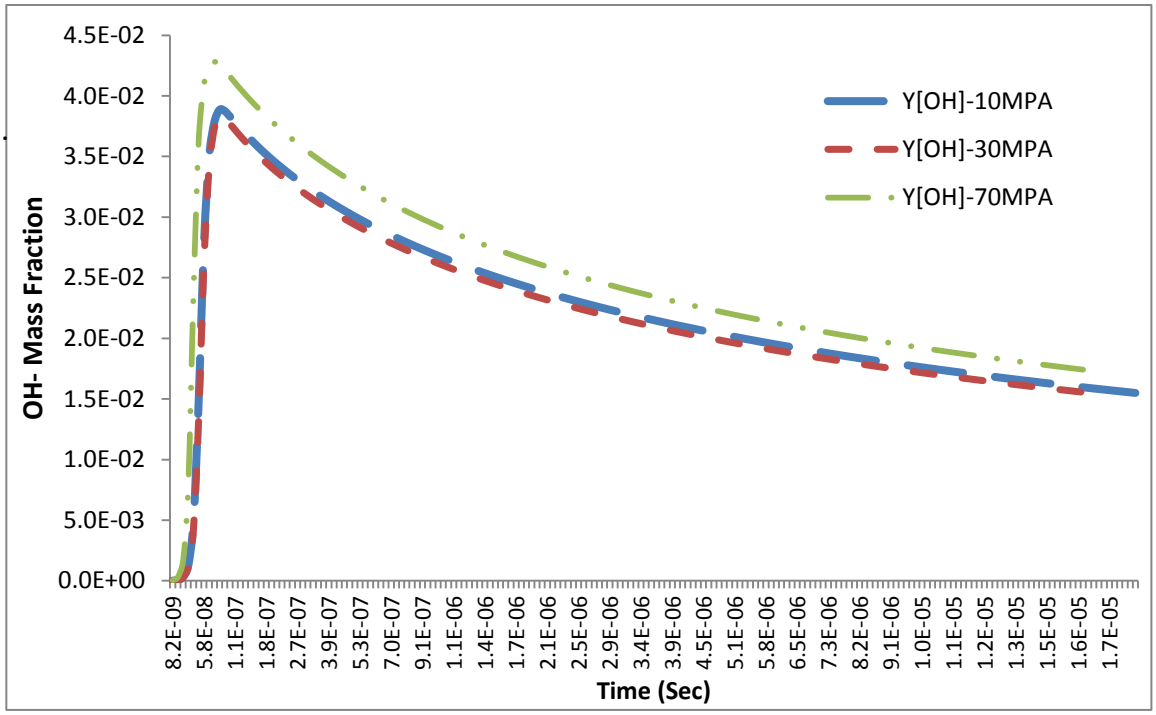


Figure (3.1.13) - OH Mass Fraction, 1 mm Case (C) - 70 MPa, 30 MPa, 10 MPa

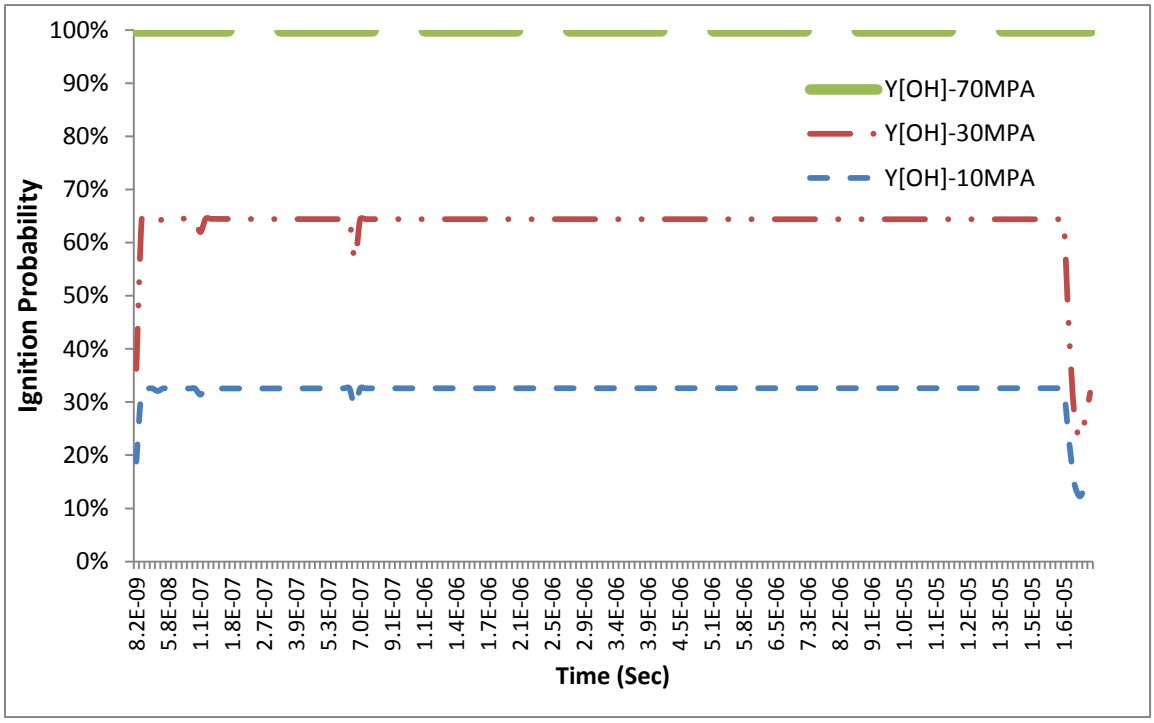


Figure (3.1.14) - Ignition Probability, 1 mm Case (C) - 70 MPa, 30 MPa, 10 MPa

As the hole diameter is increased, the shock-induced heating leads to higher temperature peaks and a stronger diffusion, and a more gradual depressurization indicating a weaker expansion.

Figure (3.1.15) shows that for 2 mm diameter holes, higher temperature peaks induce more OH-productions, which supports the conclusion of a more dominant diffusion in larger holes. Figure (3.1.16) shows the behavior of OH mass fractions for a 2mm diameter circular hole, and clearly indicates higher maximum mass fraction values. The gradual positive OH fraction slope seen for the 2mm case, confirms that larger holes experience a more gradual depressurization and a less pronounced expansion, as clearly shown for the 5 mm diameter case.

Results in figure (3.1.18) for 5 mm diameter circular openings, supports the conclusion of a less pronounced expansion in larger holes. In figure (3.1.18.c), reducing the storage pressure, slightly reduces ignition risks and hydroxide mass fractions, for the 5mm circular case. Comparing figure (3.1.15) for 2mm diameter, and figure (3.1.18) for 5mm diameter, shows a longer positive slope that follows the initial sharp increase in OH-fraction, which implies that the effect of expansion becomes less dominant as the hole diameter is increased.

Smaller holes always have lower ignition probabilities than larger openings, because of their weak diffusion and strong expansion. For high pressure conditions, smaller holes are more suitable to avoid ignition, as they are less likely to ignite than larger holes where the storage pressure becomes critical and ignition risks increase.

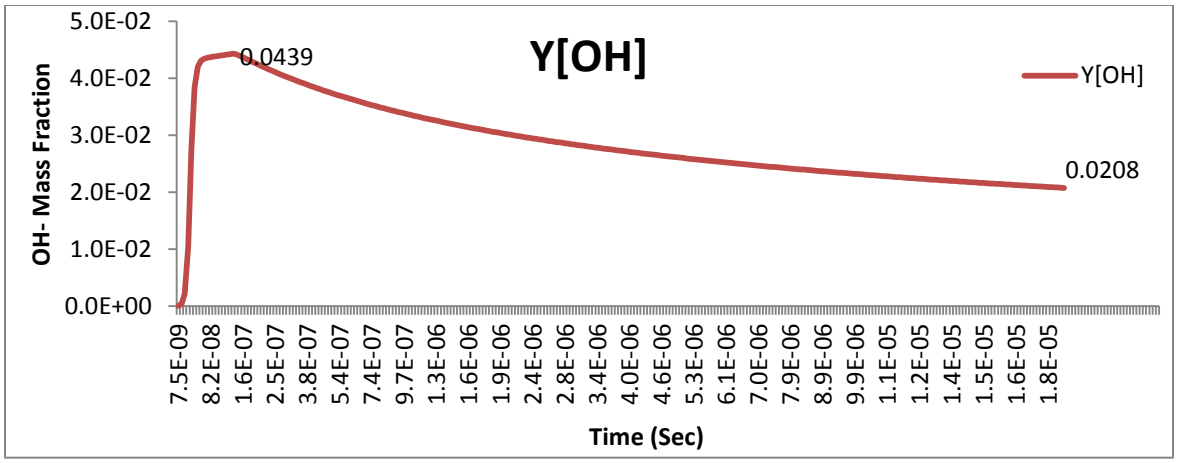


**a) 70 MPa**

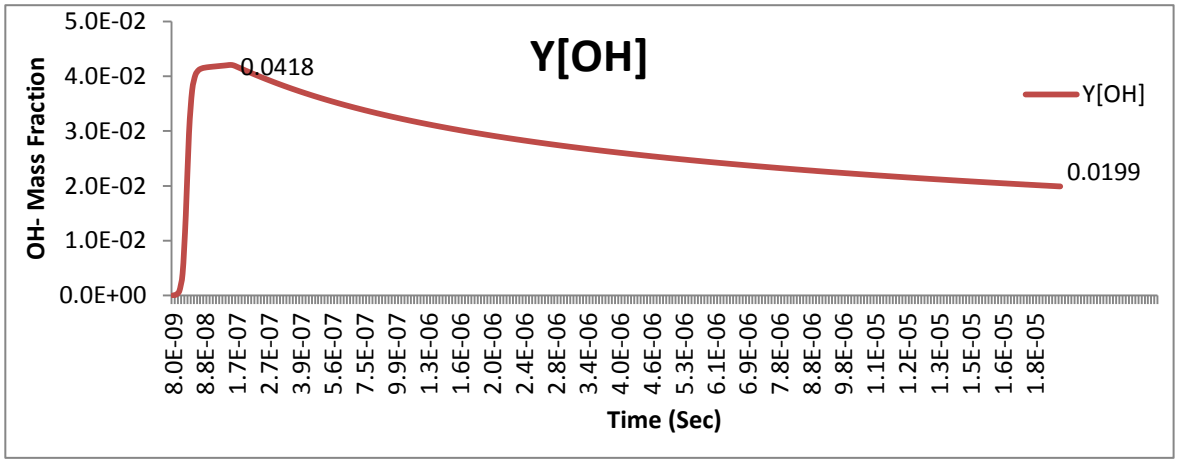


**b) 30 MPa**

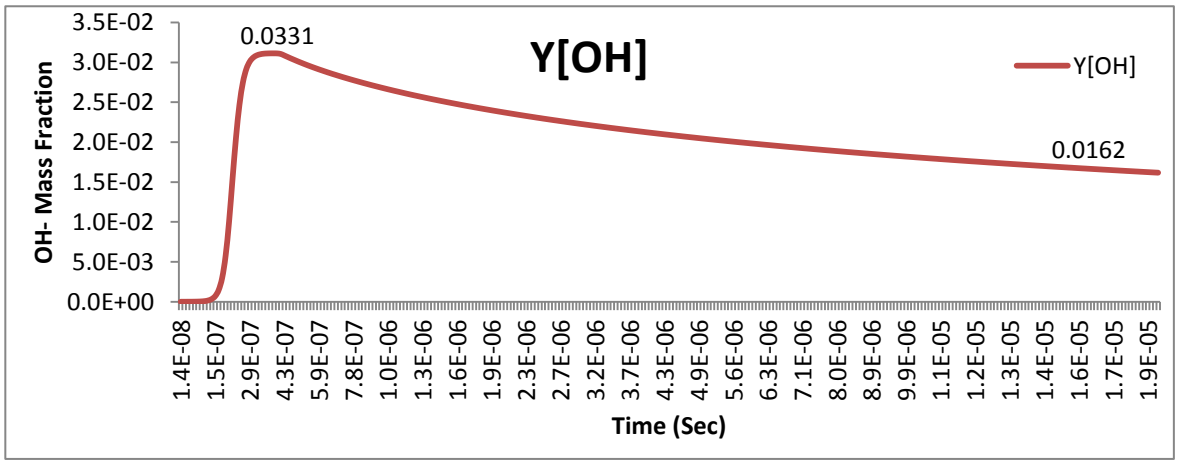


**c) 10 MPa**

Figure (3.1.15) - OH Mass Fraction, 2 mm Case (C), Fixed Circular Geometry

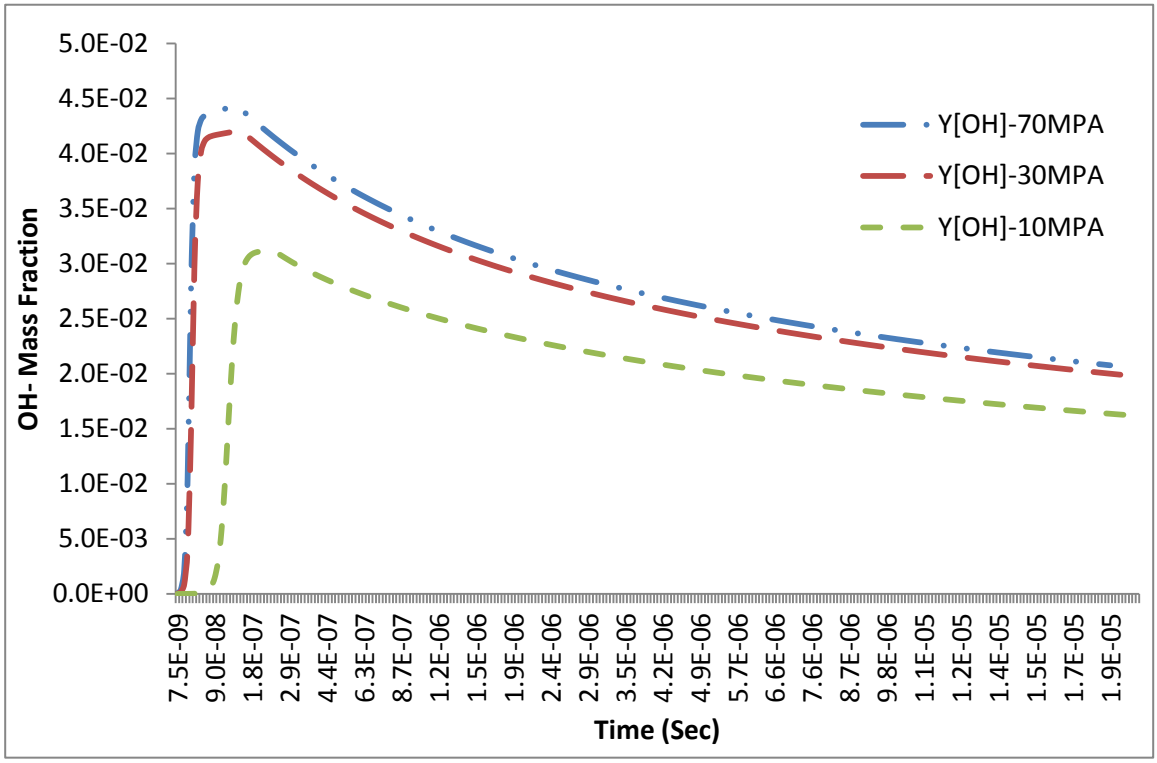


Figure (3.1.16) - OH Mass Fraction, 2 mm Case (C) - 70 MPa, 30 MPa, 10 MPa

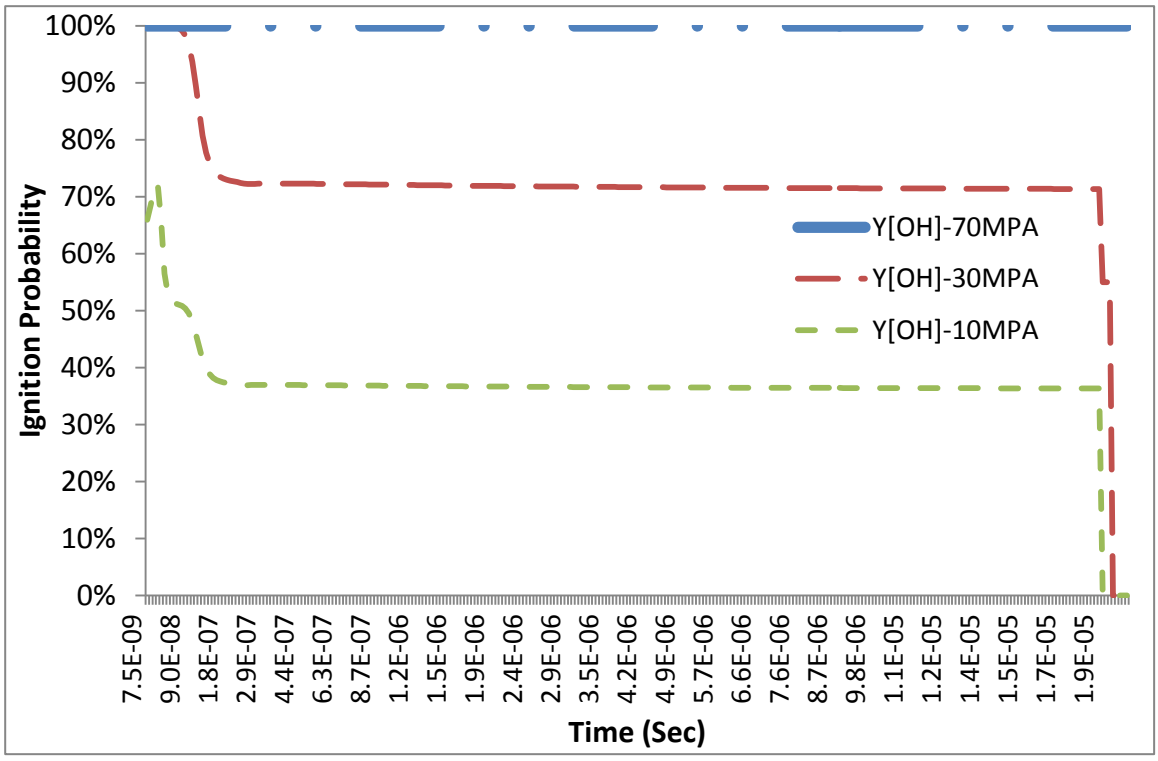


Figure (3.1.17) - Ignition Probability, 2 mm Case (C) - 70 MPa, 30 MPa, 10 MPa

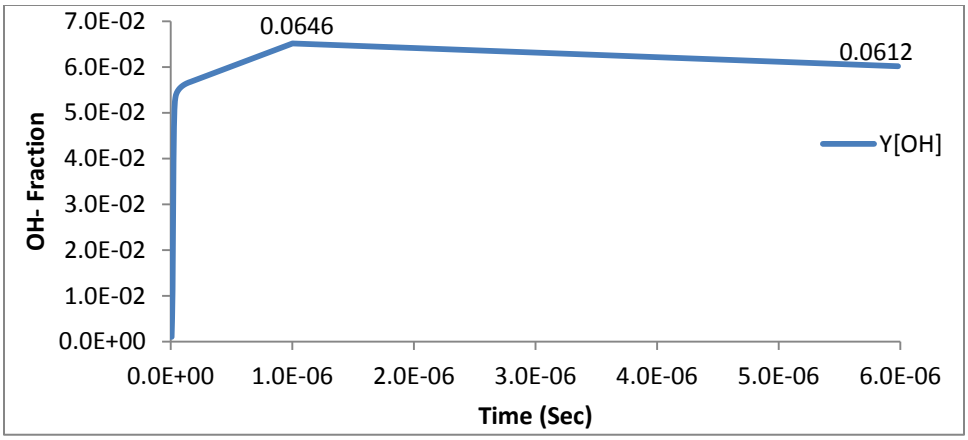


**a) 70 MPa**

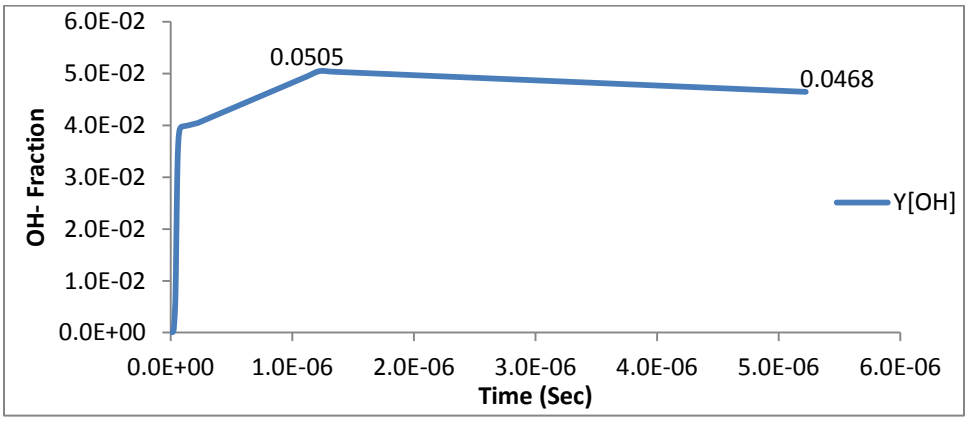


**b) 30 MPa**

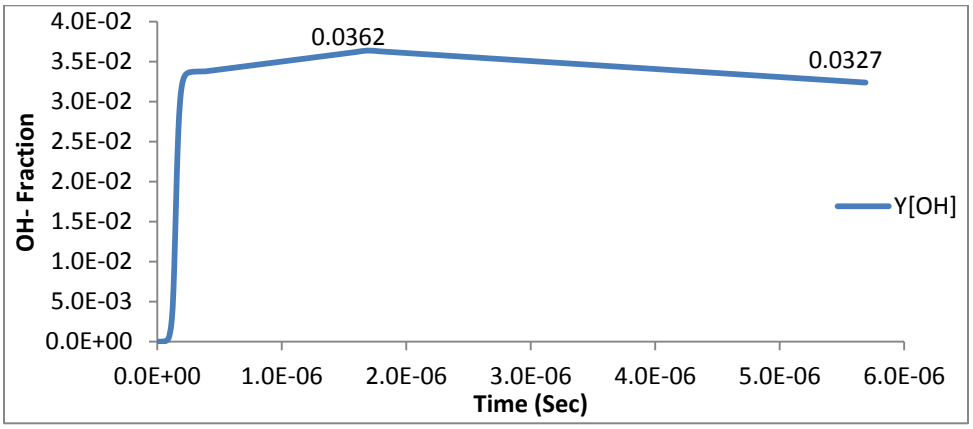


**c) 10 MPa**

Figure (3.1.18) - OH Mass Fraction, 5 mm Case (C), Fixed Circular Geometry

The objective is to determine the correlation between the operating pressure, the release area and ignition risks, and to validate the conclusion that larger holes are more likely to ignite. For larger holes, diffusive properties contribute more to the increasing ignition risks, and pressure decay contributes less to the ignition delay. The larger the hole the less effect expansion has on OH-productions, therefore more OH-compounds are produced for larger holes, as shown in figure (3.1.19).

Figure (3.1.19) shows that as the diameter is increased, diffusive properties become more dominant reflected by higher OH fractions. Figure (3.1.19) also shows that expansion is less dominant in larger holes, reflected by smoother OH mass fraction slopes.

The comparison shown in figure (3.1.20) supports the fact that larger holes have higher ignition probabilities than smaller openings. The comparison in figure (3.1.20) suggests that ignition is more probable in larger holes, which have increasing ignition probabilities, and confirms that expansion in larger holes is sufficiently weak, so that higher ignition risks exist.

For larger openings ignition risks increase, because of their strong diffusion reflected by higher temperature peaks, and their more gradual depressurization, reflected by smoother pressure slopes. Clearly, for larger holes, the energy added due to the shock induced heating is greater than the energy removed due to expansion. Both the maximum and final OH mass fraction values are higher for larger holes of 5mm diameter, which validates the conclusion that larger holes are more likely to ignite.

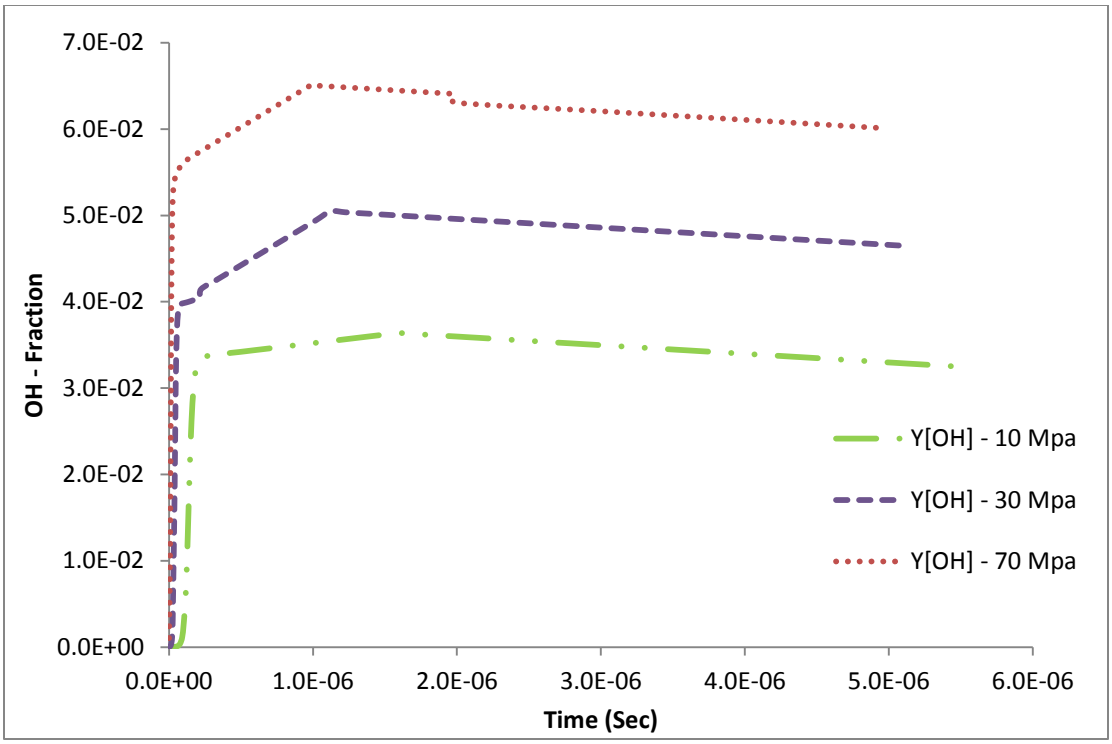


Figure (3.1.19) - OH Mass Fraction, 5 mm Case (C) - 70 MPa, 30 MPa, 10 MPa

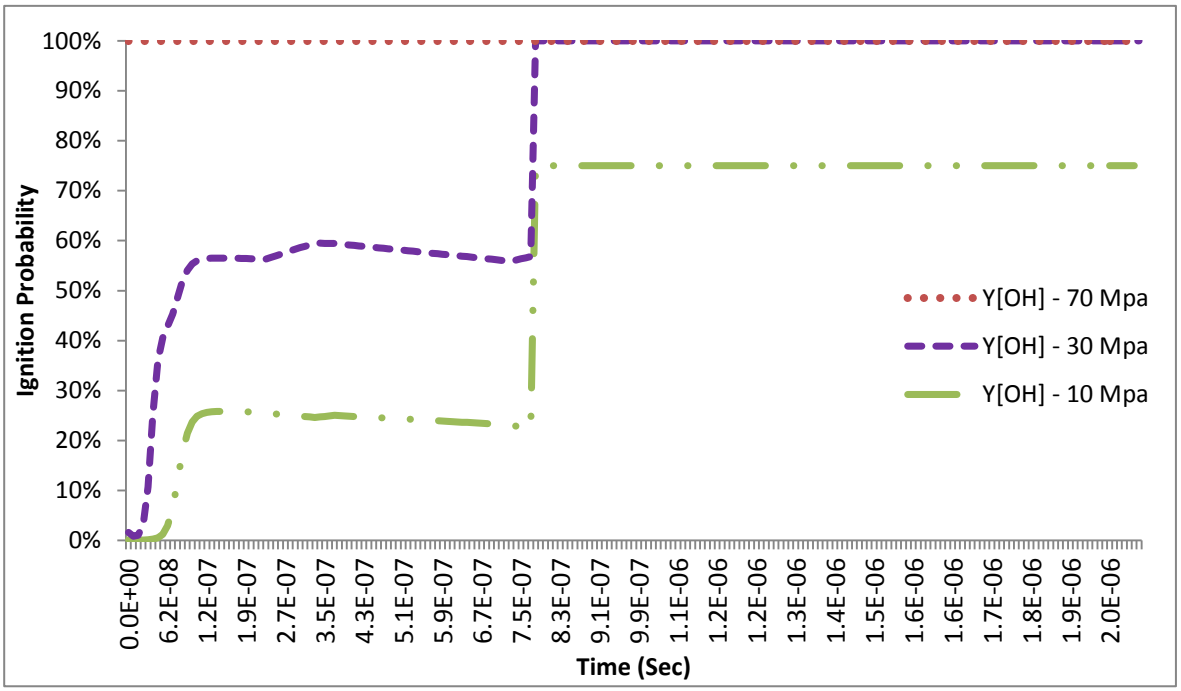


Figure (3.1.20) - Ignition Probability, 5 mm Case (C) - 70 MPa, 30 MPa, 10 MPa

Table (3-1-2) summarizes ignition results for standard circular exit geometries, and compares OH-mass fractions and ignition probabilities for the circular cases of 1mm, 2mm and 5mm diameter holes. Table (3-1-2) clearly shows that the smaller the release area, the smaller the maximum and final OH - mass fraction values, and the lower the ignition probabilities.

The correlation between the operating pressure, the release area and ignition risks, is such that higher storage pressures and larger orifice diameters lead to higher ignition risks.

| **Fixed Circular Release Area** | | | |
|---|---|---|---|
| **1 mm** | **Y[OH] Max** | **Y[OH] Final Value** | **% Ignition** |
| **70 MPa** | 0.042 | 0.0172 | 100 |
| **30 MPa** | 0.038 | 0.0153 | 62 |
| **10 MPa** | 0.037 | 0.0155 | 32 |
| **2 mm** | **Y[OH] Max** | **Y[OH] Final Value** | **% Ignition** |
| **70 MPa** | 0.043 | 0.0207 | 100 |
| **30 MPa** | 0.041 | 0.0199 | 70 |
| **10 MPa** | 0.033 | 0.016 | 38 |
| **5 mm** | **Y[OH] Max** | **Y[OH] Final Value** | **% Ignition** |
| **70 MPa** | 0.0645 | 0.06117 | 100 |
| **30 MPa** | 0.0504 | 0.0467 | 100 |
| **10 MPa** | 0.036 | 0.0326 | 80 |

Table (3-1-2) - Fixed Circular Geometry - Ignition Assessment

## 3.2 Fixed Elliptic Release Area

In this section, two cases are studied for elliptic openings, using the procedure explained in section 3.1 for fixed exit geometries. The hottest point at the gas interface is determined, to provide diffusion conditions, and the contact surface pressure is curved fitted during depressurization, to provide expansion conditions.

The geometry is shown in table (3-2-1), and further compared with standard circular openings. The two elliptic cases are compared to the 1 mm and 2 mm diameter circular cases, by maintaining the same overall areas and tube length, for the two types of openings.

Two scenarios of fixed elliptic openings are discussed, and the pressure cases of 10 MPa, 30 MPa and 70 MPa are examined. The aspect ratio parameter in table (3-2-1) is not investigated in this thesis, and the only conservative criterion is the overall area.

| **Orifice type** | **Major axis, a(mm)** | **Minor axis, b (mm)** | **Aspect ratio, a/b** | **Area, A (mm2)** | **Length, L(mm)** |
|---|---|---|---|---|---|
| **Circular** | 1 | 1 | 1 | 0.79 | 2 |
| **Elliptic** | 2 | 0.5 | 4 | 0.79 | 2 |
| **Orifice type** | **Major axis, a(mm)** | **Minor axis, b (mm)** | **Aspect ratio, a/b** | **Area, A (mm2)** | **Length, L(mm)** |
| **Circular** | 2 | 2 | 1 | 3.14 | 2 |
| **Elliptic** | 4 | 1 | 4 | 3.14 | 2 |

Table (3-2-1) - Fixed Elliptic Geometry

### 3.2.1 Case Study: Elliptic Exit Geometries

The smallest change in the dimensions and shape of the exit geometry can result in ignition or no ignition at all. Studying the effect of the opening shape is essential to understand associated ignition risks.

In figures (3.2.1) through (3.2.12), temperature on both sides of the contacts surface and the interface pressure are determined to provide diffusion conditions. During expansion, the interface pressure curves and pressure gradients curve fitting are presented for the two elliptic cases, using the same procedure followed for circular openings. In figures (3.2.1) - (3.2.4), the hottest point along the interface is determined, then the interface pressure and the hot air and cold hydrogen temperatures, are recorded to provide input for the ignition model.

Figures (3.2.1) - (3.2.3), indicate that temperature peaks are slightly higher for elliptic exit geometries, which suggests a slightly more dominant diffusion, for this type of irregular orifices. Figures (3.2.2) - (3.2.4), show that expansion is slightly delayed in elliptic openings, which suggests a slightly less pronounced expansion compared to circular exits.

As seen in standard circular holes, the temperature profile for fixed elliptic release areas is such that the highest peak is achieved within the release area, prior to the interface reaching the exit edge. After release, during the expansion, the hot air cools down, and the temperature peaks are lower. With both a more dominant diffusion, and a less pronounced expansion, elliptic areas are expected to have higher ignition probabilities than circular areas.

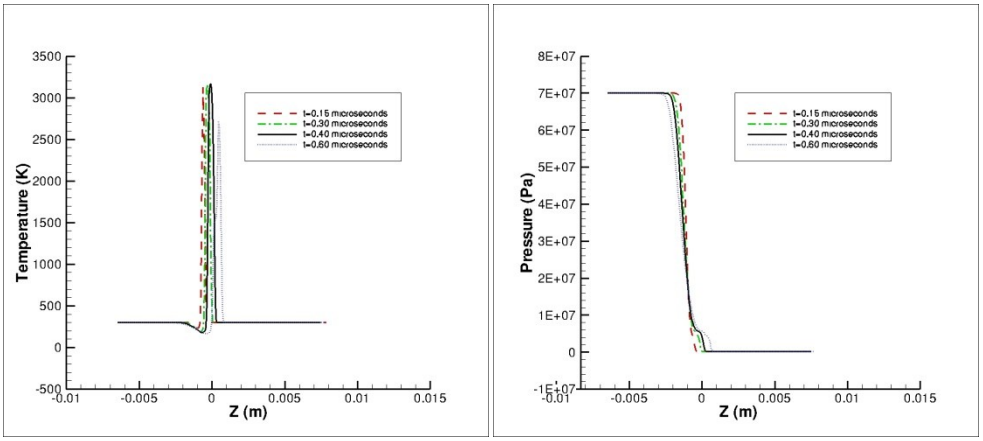


**a) 70 MPa**

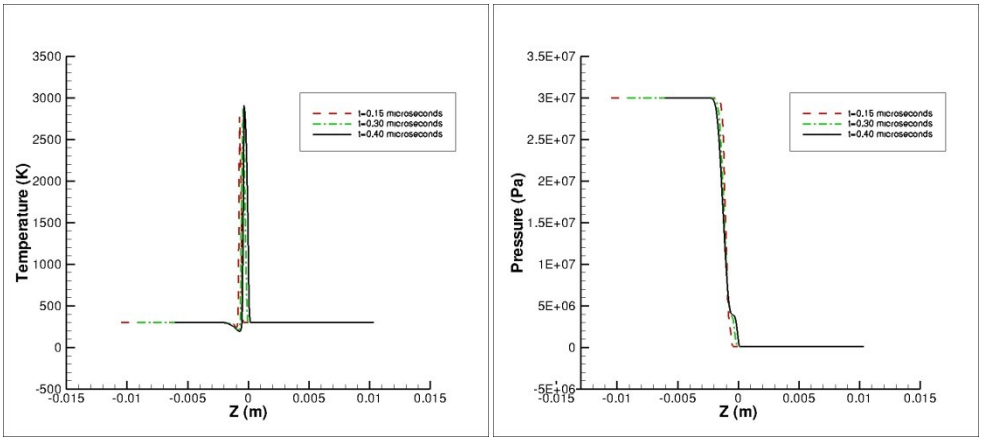


**b) 30 MPa**

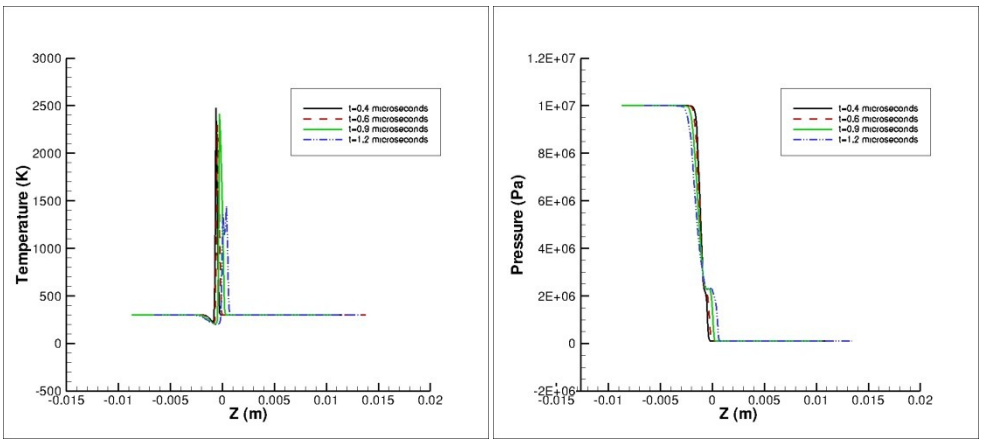


**c) 10 MPa**

Figure (3.2.1) - T (z) (Left), P (z) (Right), 1 mm Case (E), Fixed Elliptic Geometry

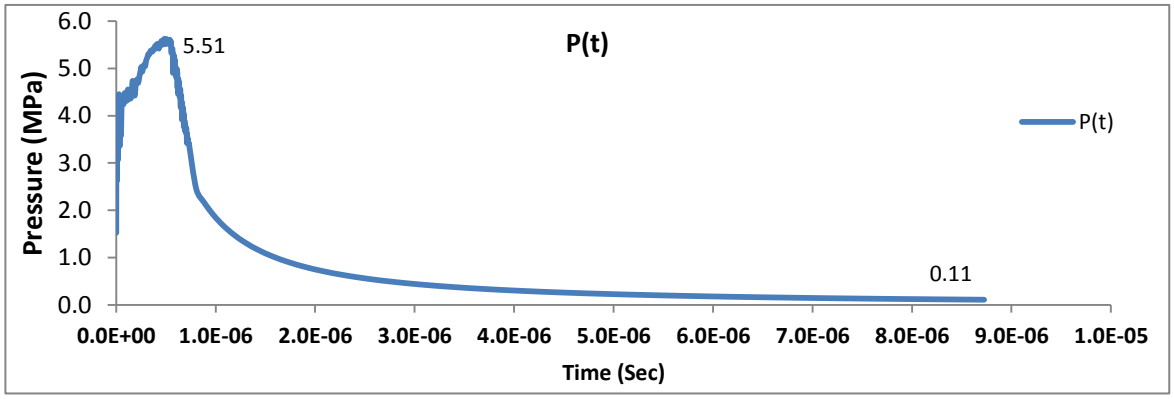


**a) 70 MPa**

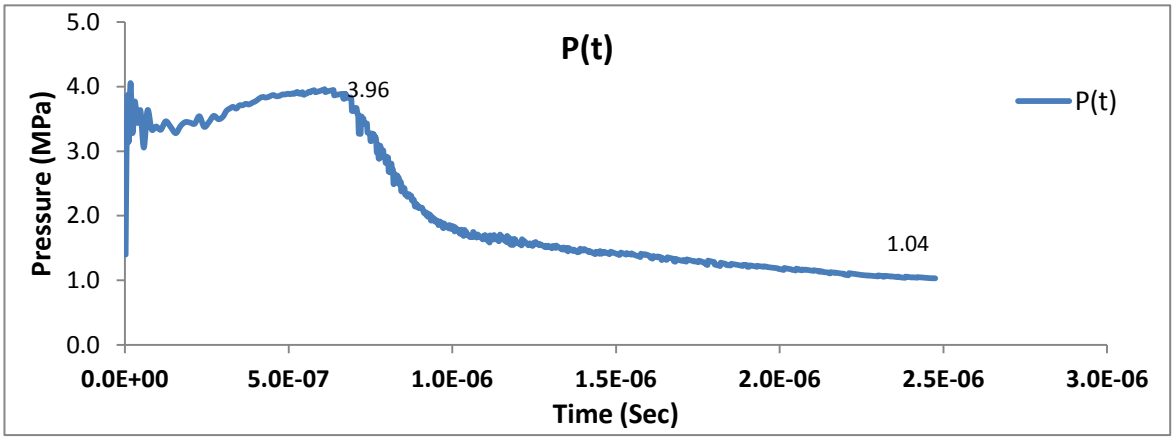


**b) 30 MPa**

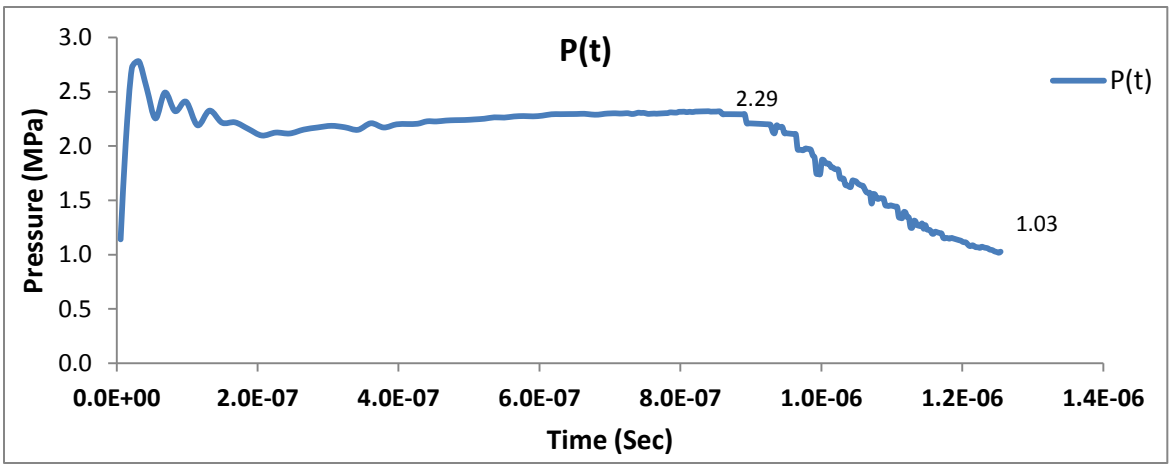


**c) 10 MPa**

Figure (3.2.2) - P (t) curve, 1 mm Case (E), Fixed Elliptic Geometry

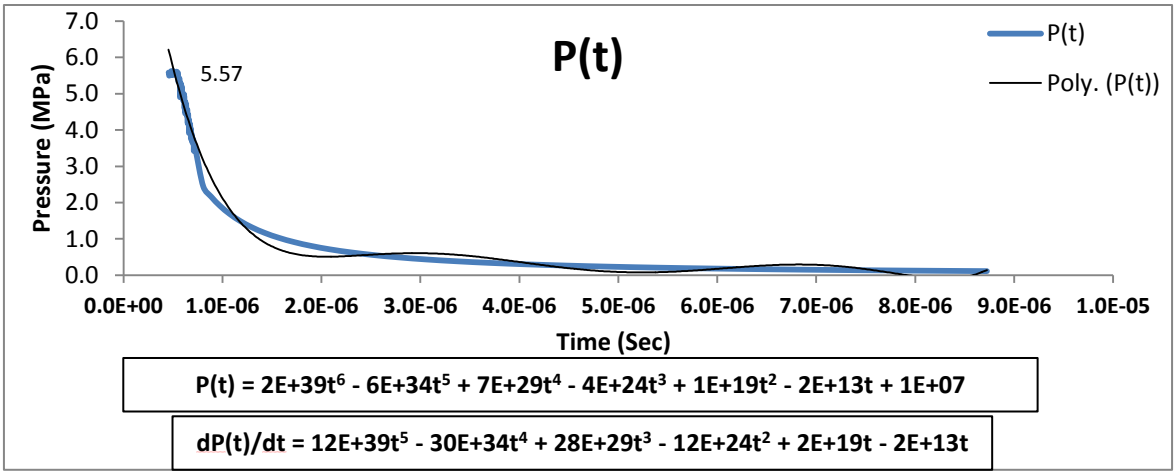


**a) 70 MPa**

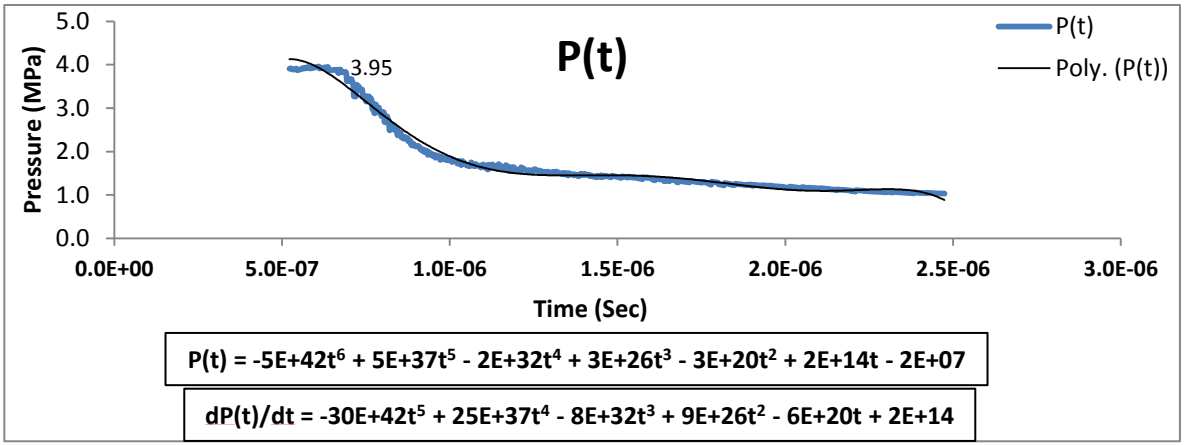


**b) 30 MPa**

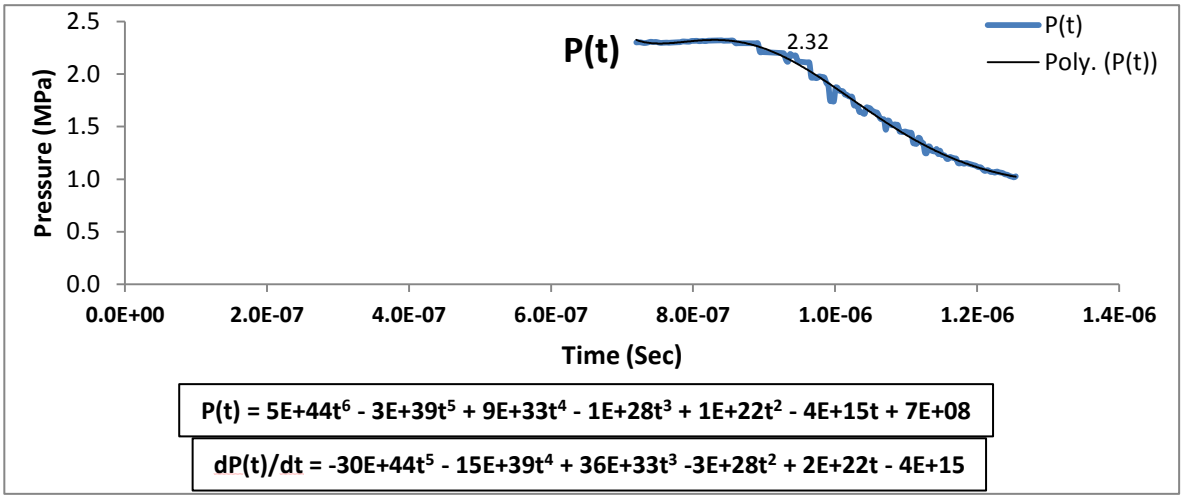


**c) 10 MPa**

Figure (3.2.3) - P (t) & dP(t)/dt, 1 mm Case (E), Fixed Elliptic Geometry

The objective is to extend previous conclusions for circular holes, to elliptic exit geometries. Increasing the area of an elliptic orifice is expected to increase ignition risks, as seen with increases in the diameter of a circular orifice. With both a more dominant diffusion, and a less pronounced expansion, elliptic areas are also expected to have higher ignition probabilities than circular areas.

In figures (3.2.4) - (3.2.7), the hottest point along the gas interface is determined, and then the interface pressure, the hot air, and the cold hydrogen temperatures are recorded to provide input for the ignition model. In figures (3.2.4) - (3.2.7), temperature, interface pressures, as well as pressure versus time curves, and pressure gradient curve fittings, are presented for an elliptic opening, equivalent to a 2mm circular hole.

Figures (3.2.4) - (3.2.7), indicate that temperature peaks are clearly higher as the elliptic area increases, and confirms that increasing the area of an elliptic exit leads to a stronger diffusion of hydrogen. Figures (3.2.5) - (3.2.8), clearly indicate that larger areas have smoother pressure slopes, which validates previous conclusions that larger holes undergo a less pronounced expansion.

In this section, the objective to validate the correlation between the operating pressure, the release area and ignition risks, that higher storage pressures and larger orifice diameters lead to higher ignition risks, is further extended to irregular elliptic exits. Results for elliptic geometries clearly validate that the larger the release area, the more dominant the shock-induced heating and the diffusion of hydrogen, and the less pronounced the expansion, resulting in increased ignition risks for larger holes.

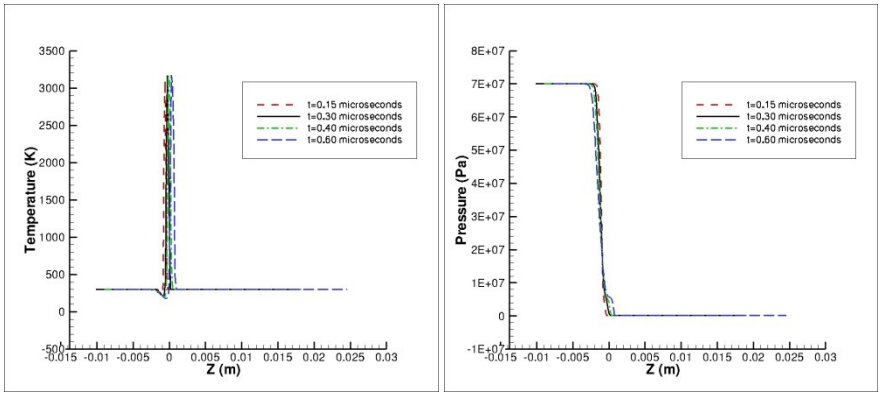


**a) 70 MPa**

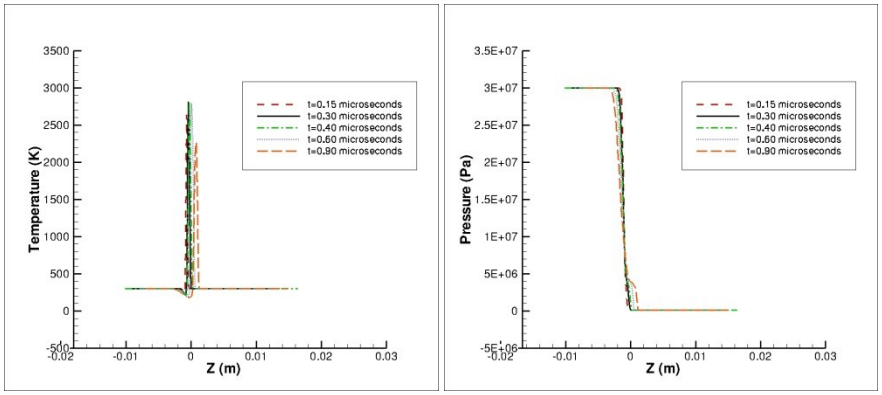


**b) 30 MPa**

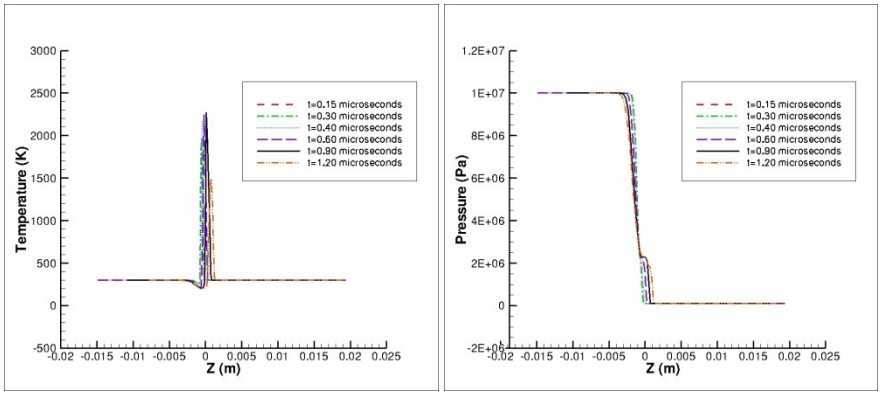


**c) 10 MPa**

Figure (3.2.4) - T (z) (Left), P (z) (Right), 2 mm Case (E), Fixed Elliptic Geometry

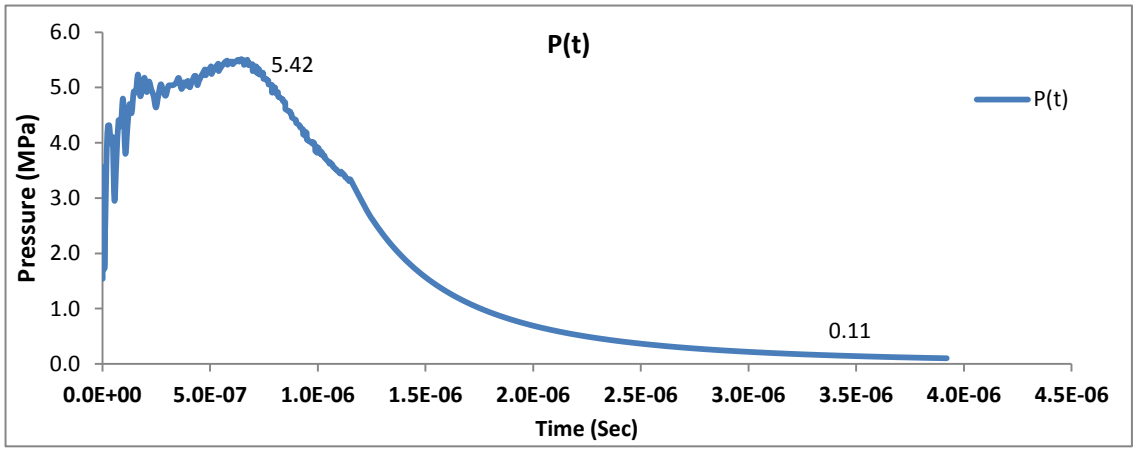


**a) 70 MPa**

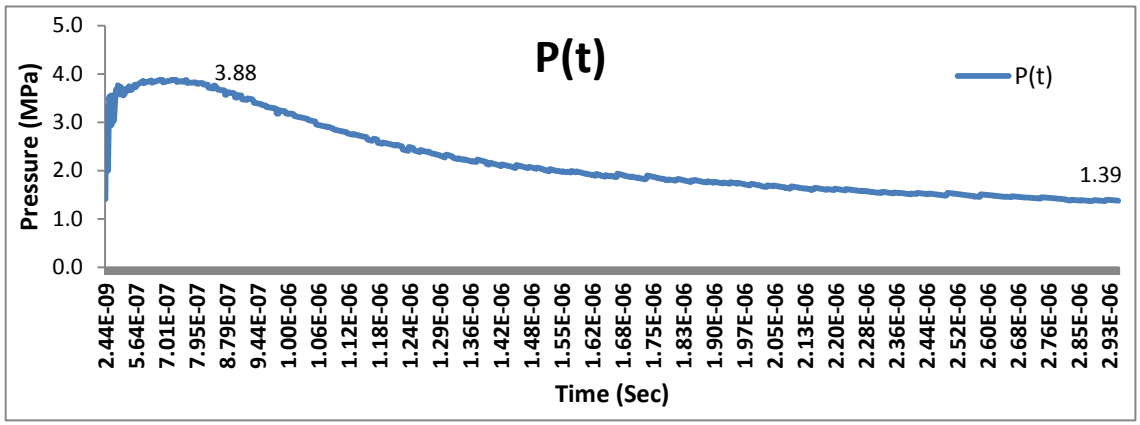


**b) 30 MPa**

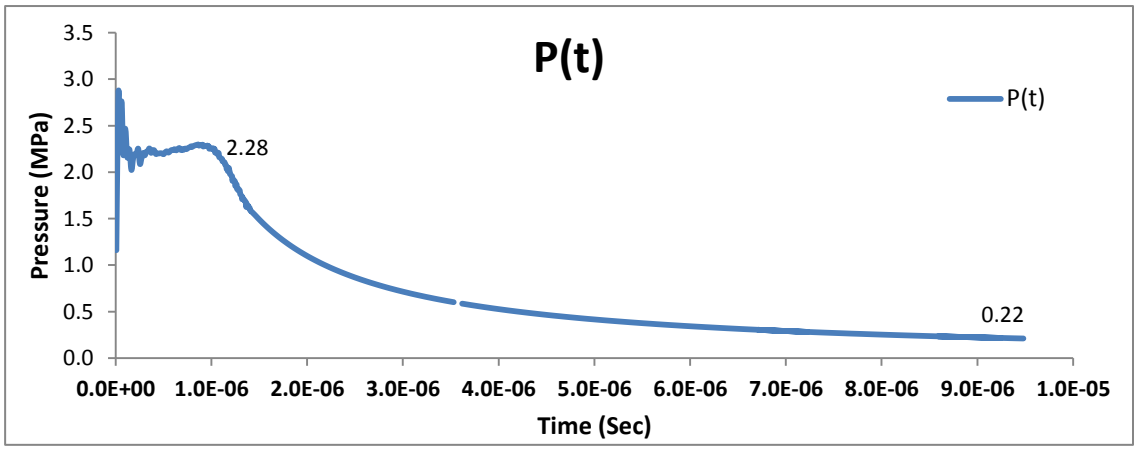


**c) 10 MPa**

Figure (3.2.5) - P (t) curve, 2 mm Case (E), Fixed Elliptic Geometry

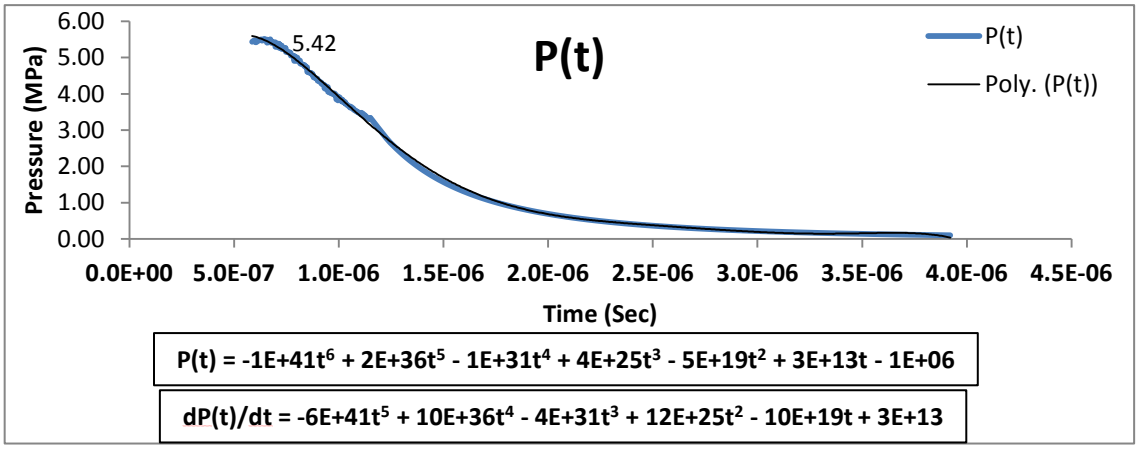


**a) 70 MPa**

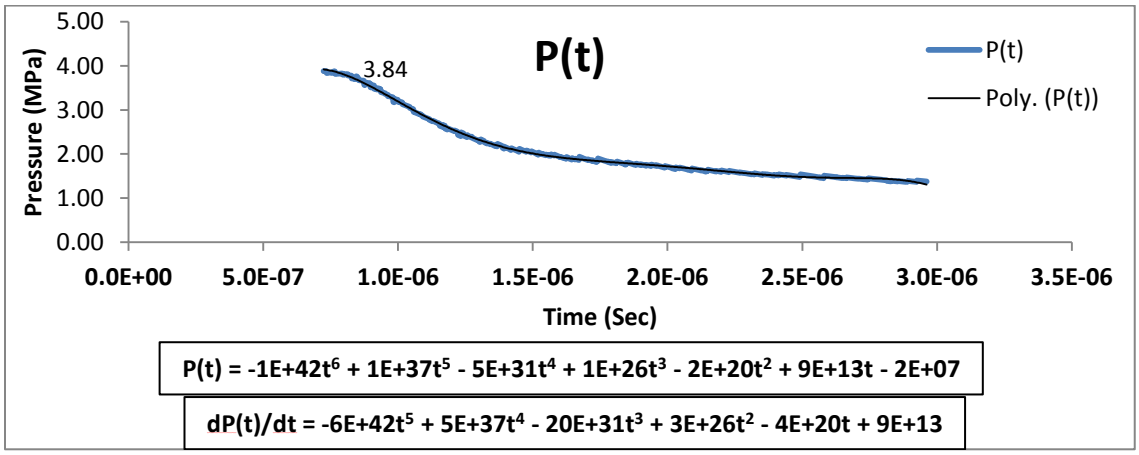


**b) 30 MPa**

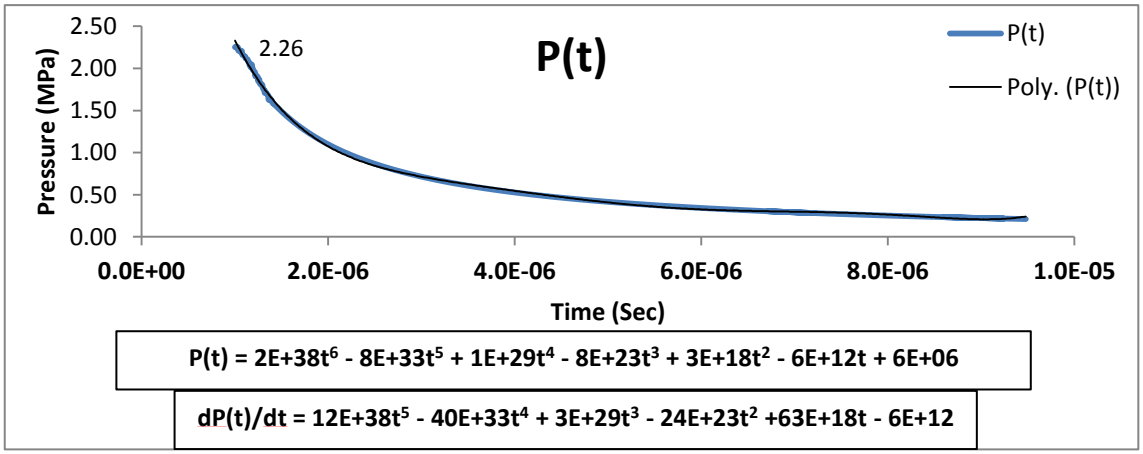


**c) 10 MPa**

Figure (3.2.6) - P (t) & dP(t)/dt , 2 mm Case (E), Fixed Elliptic Geometry

The position and pressure of the contact surface, as well as the temperature peaks, are affected by changing the geometry of the exit, as shown in table (3-2-2). Higher temperature peaks contribute to more dominant diffusive effects, and higher OH fractions.

Table (3-2-2) shows that there's a significant time delay separating the release time from the decay time, for this type of exit geometries. The lag between the time the interface is released from the exit edge, and the time the interface pressure starts to drop, is more visible in elliptic compared to circular geometries, which confirms that elliptic areas experience a more gradual expansion.

| **Fixed Elliptic Release Area** | | | | | |
|---|---|---|---|---|---|
| **1 mm (E)** | **T[High] [K]** | **T[Low] [K]** | **P [MPa]** | | |
| **70 MPa** | 3250 | 185 | 5.53 | **Decay Time [µs]** | **Release Time [µs]** |
| | | | | 0.4 µs | 0.15 µs |
| **30 MPa** | 2900 | 192 | 4.70 | **Decay Time [µs]** | **Release Time [µs]** |
| | | | | 0.55 µs | 0.3 µs |
| **10 MPa** | 2485 | 220 | 2.75 | **Decay Time [µs]** | **Release Time [µs]** |
| | | | | 0.65 µs | 0.4 µs |
| **2 mm (E)** | **T[High] [K]** | **T[Low] [K]** | **P [MPa]** | | |
| **70 MPa** | 3290 | 190 | 5.91 | **Decay Time [µs]** | **Release Time [µs]** |
| | | | | 0.55 µs | 0.3 µs |
| **30 MPa** | 2980 | 200 | 4.87 | **Decay Time [µs]** | **Release Time [µs]** |
| | | | | 0.7 µs | 0.6 µs |
| **10 MPa** | 2570 | 215 | 2.49 | **Decay Time [µs]** | **Release Time [µs]** |
| | | | | 1.1 µs | 0.9 µs |

Table (3-2-2) - Fixed Elliptic Geometry - Input Parameters

### 3.2.2 Ignition Assessment

In table (3-2-3) a summary of the ignition assessment for the elliptic opening case is provided. Table (3-2-3) shows the OH mass fraction maximum and final values, as well as ignition probabilities, with respect to the operating pressure and opening dimension. In table (3-2-3), the maximum OH fraction confirms the increased heating seen in elliptic exits compared to circular exits, and the final value reflects the reduced effect that depressurization has on ignition risks, in this type of fixed exits.

Results also confirm that ignition is most likely to occur for high storage pressures irrespectively of the opening geometry. For 70 MPa reservoir pressures, ignition is most likely to occur, and extremely small holes are required to prevent ignition in this case.

| **Fixed Elliptic Release Area** | | | |
|---|---|---|---|
| **1 mm (E)** | **Y[OH] Max** | **Y[OH] Final Value** | **% Ignition** |
| **70 MPa** | 0.0439 | 0.022 | 100 |
| **30 MPa** | 0.039 | 0.021 | 68 |
| **10 MPa** | 0.035 | 0.02 | 36 |
| **2 mm (E)** | **Y[OH] Max** | **Y[OH] Final Value** | **% Ignition** |
| **70 MPa** | 0.045 | 0.0229 | 100 |
| **30 MPa** | 0.042 | 0.0217 | 72 |
| **10 MPa** | 0.031 | 0.017 | 38 |

Table (3-2-3) - Fixed Elliptic Geometry - Ignition Assessment

The decay slope is slightly steeper for circular areas, however the differences are minor, and the increased ignition probabilities observed for elliptic areas, are mainly due to diffusive effects that trigger faster and stronger chemical reactions.

In figure (3.2.7), the OH mass fraction profile for the 1 mm elliptic opening, similar to the profile observed for the 1 mm circular opening, experiences first a sharp increase, followed by a progressive decay. Figure (3.2.7) shows that the maximum OH mass fraction achieved for elliptic exits is always higher than in circular exits. Figure (3.2.8) compares OH mass fractions, and figure (3.2.9) compares ignition probabilities, for 1 mm elliptic openings at different operating pressures. For the same operating pressure and exit dimensions, elliptic openings have slightly higher ignition probabilities than circular openings.

Figure (3.2.10) shows that expansion is less dominant in larger holes, reflected by smoother OH fraction slopes. Figure (3.2.12) - (3.2.13) validate that as the overall area is increased, diffusive shock properties become more dominant, reflected by higher OH fractions. The comparison shown in figure (3.2.13) for the 1mm and 2mm equivalent elliptic exits supports the previous conclusion that larger holes are more likely to ignite than smaller holes.

Results for fixed elliptic exits confirm that increasing the area of an elliptic orifice increases ignition risks, as seen with increases in the diameter of a circular orifice. Results for fixed elliptic exits also indicate that irregular elliptic exits are more likely to ignite than standard circular holes.

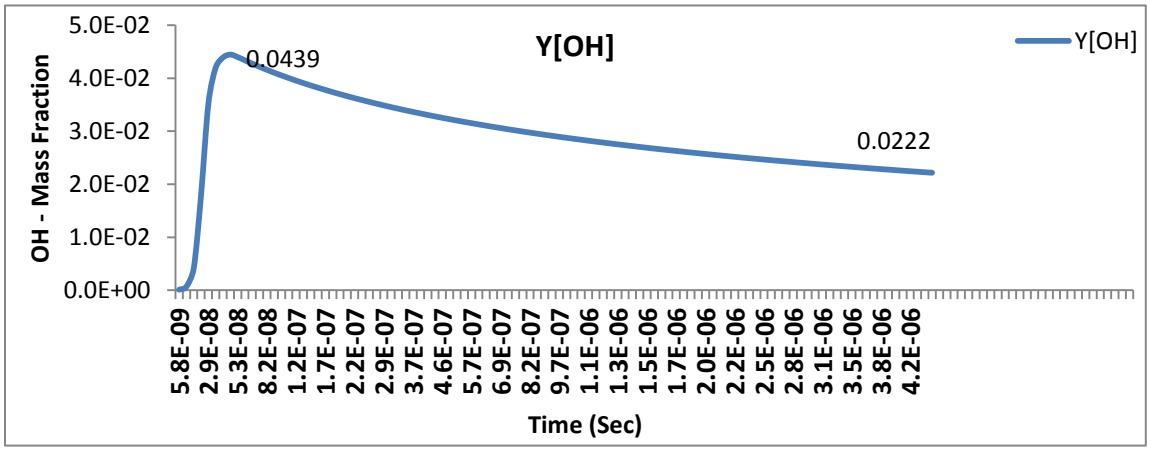


**a) 70 MPa**

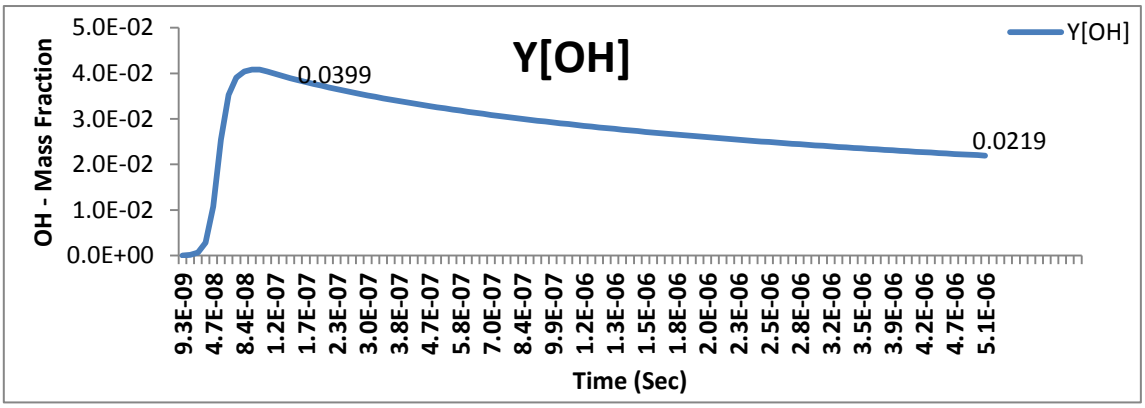


**b) 30 MPa**

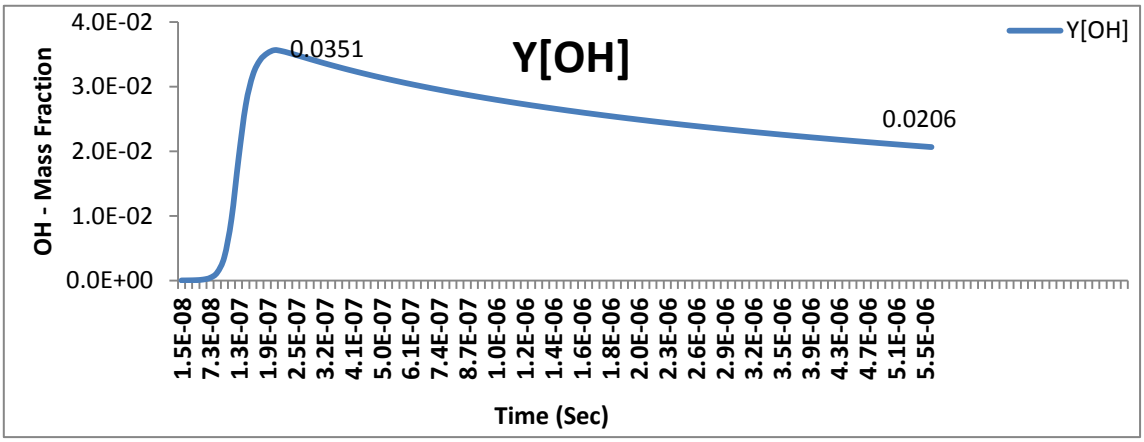


**c) 10 MPa**

Figure (3.2.7) - OH Mass Fraction, 1 mm Case (E), Fixed Elliptic Geometry

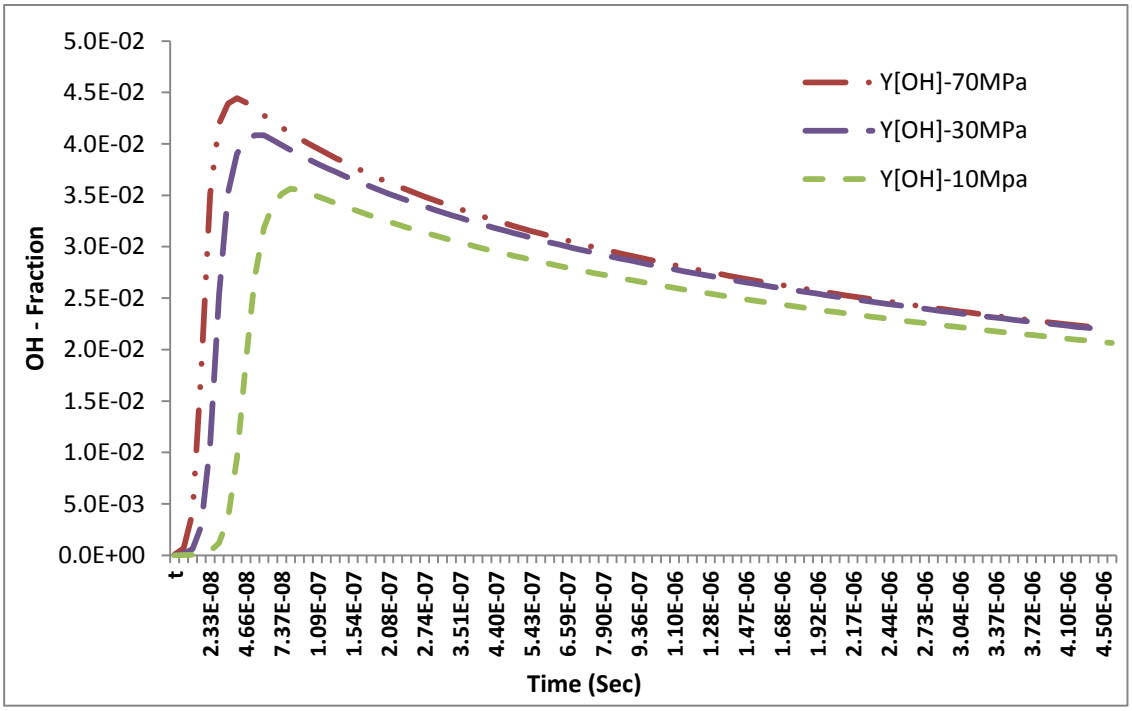


Figure (3.2.8) - OH Mass Fraction, 1 mm Case (E) - 70 MPa, 30 MPa, 10 MPa

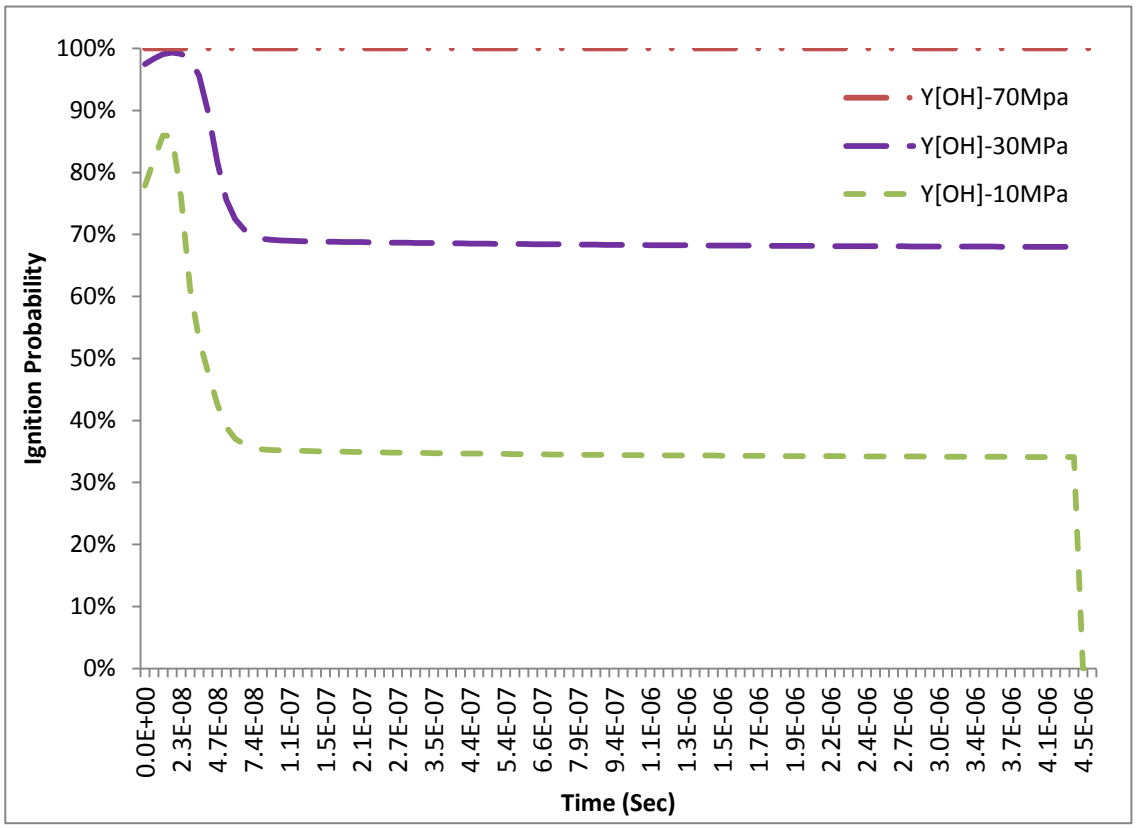


Figure (3.2.9) - Ignition Probability, 1 mm Case (E) - 70 MPa, 30 MPa, 10 MPa

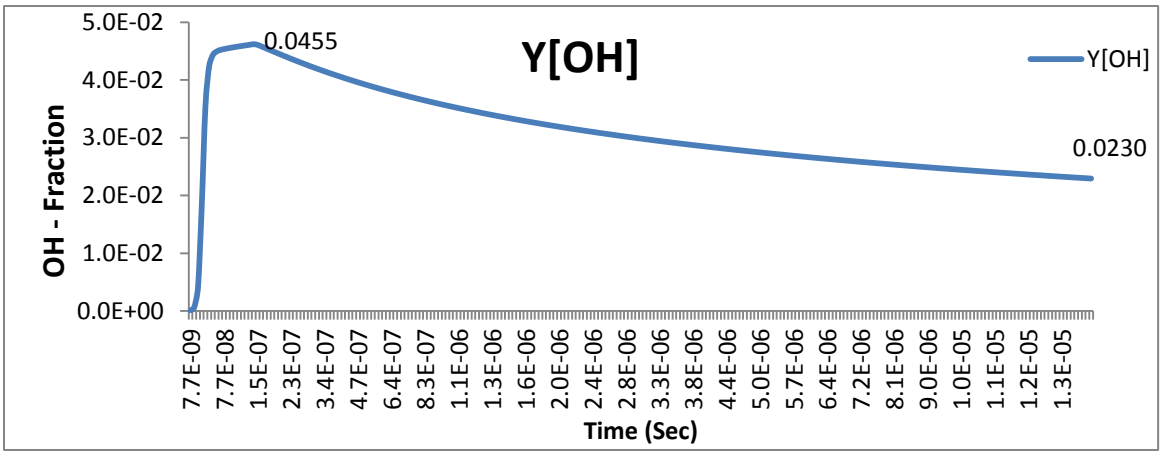


**a) 70 MPa**

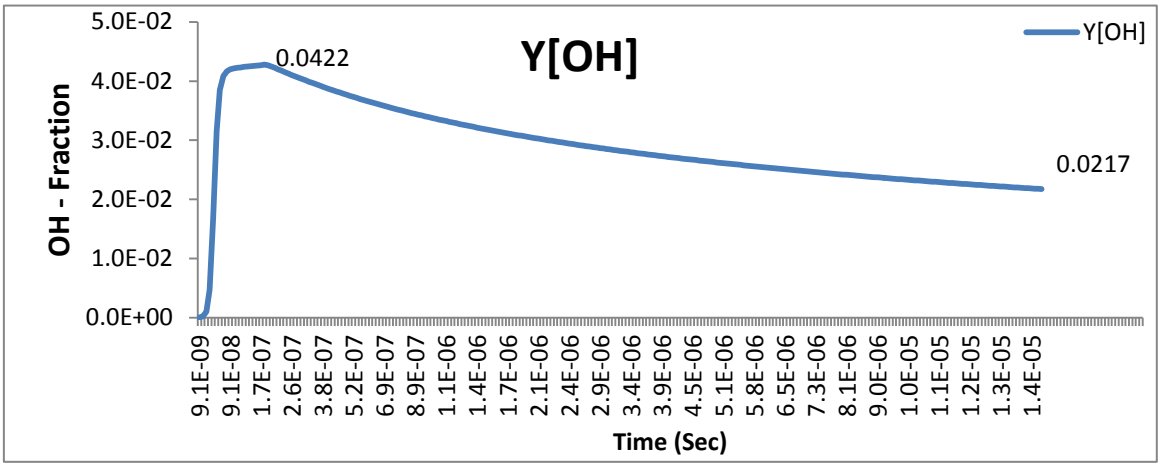


**b) 30 MPa**

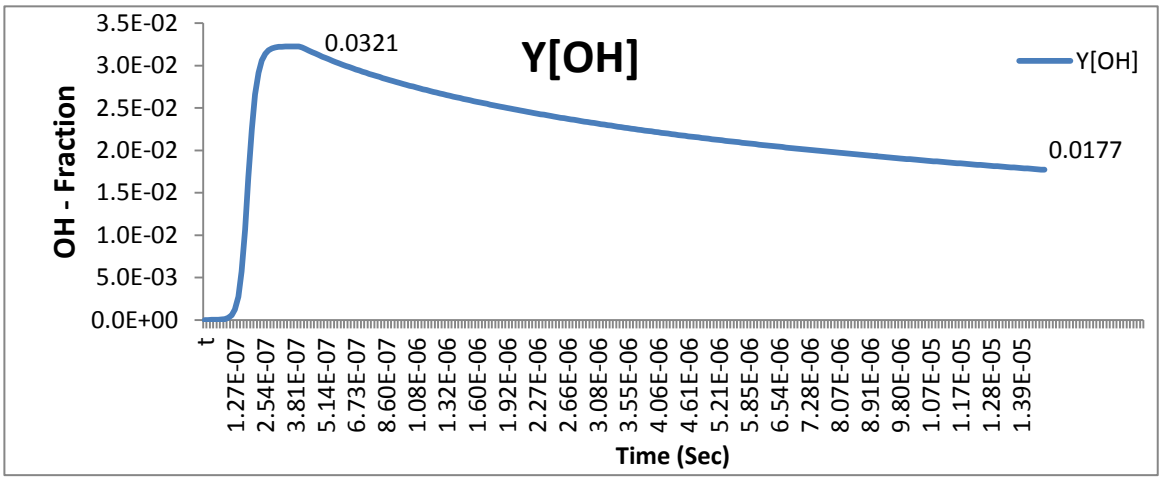


**c) 10 MPa**

Figure (3.2.10) - OH Mass Fraction, 2 mm Case (E), Fixed Elliptic Geometry

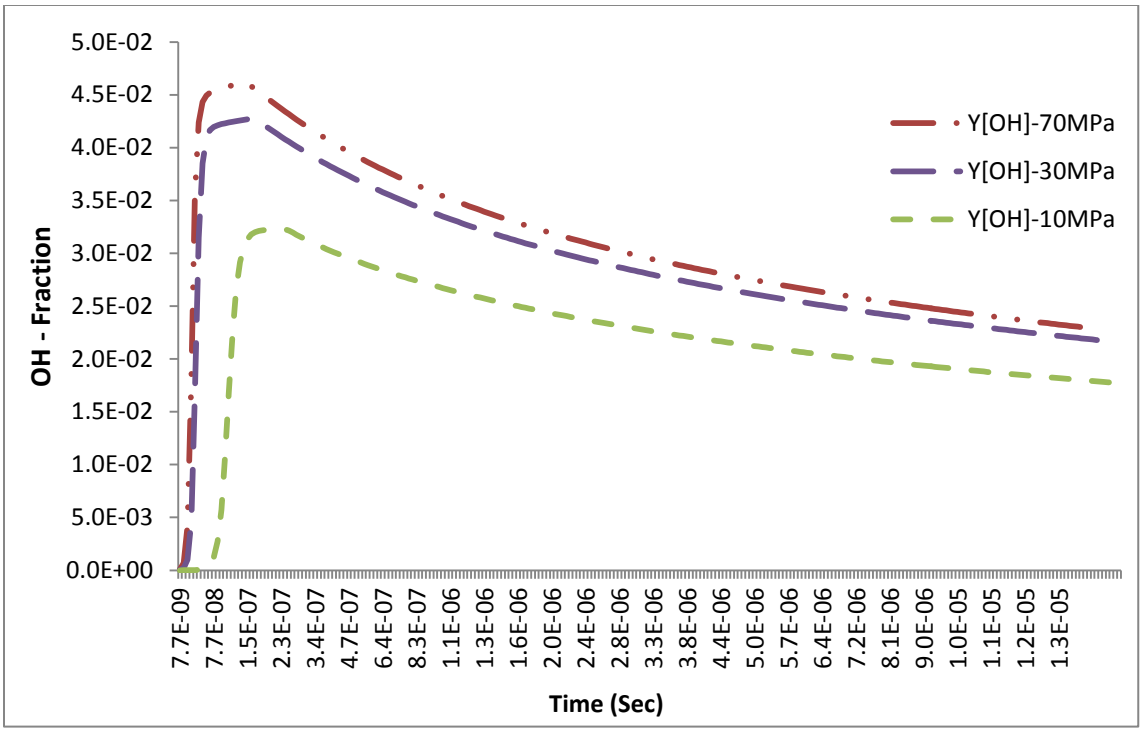


Figure (3.2.11) - OH Mass Fraction, 2 mm Case (E) - 70 MPa, 30 MPa, 10 MPa

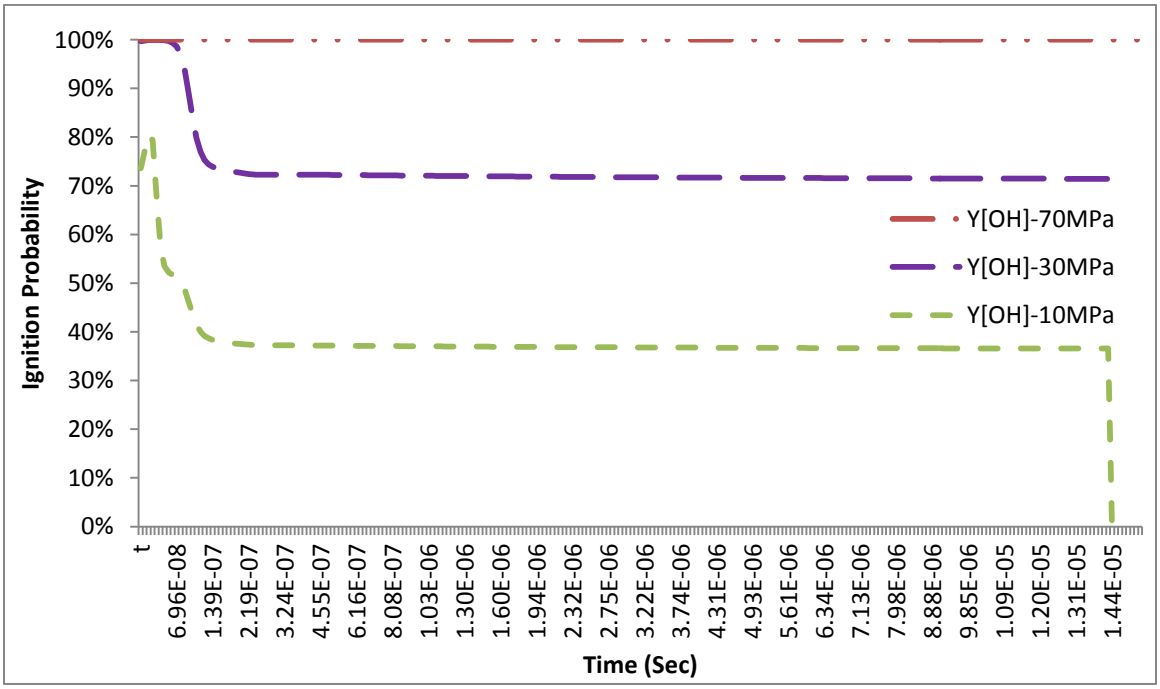


Figure (3.2.12) - Ignition Probability, 2 mm Case (E) - 70 MPa, 30 MPa, 10 MPa

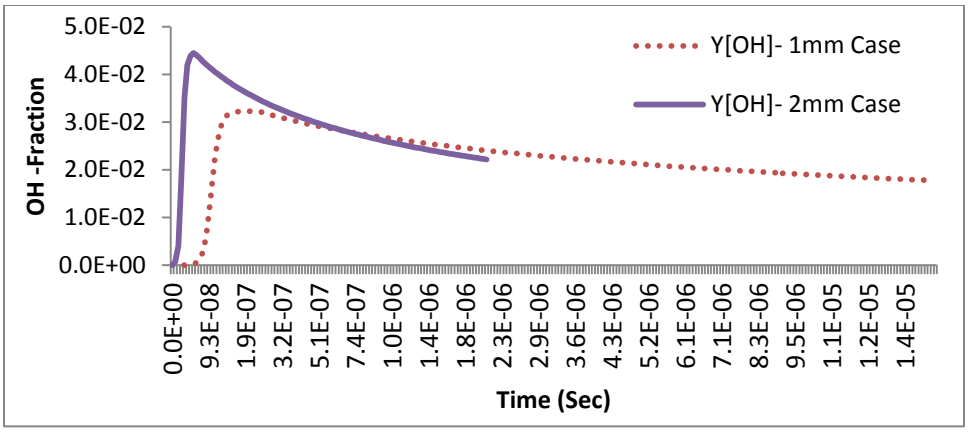


**a) 70 MPa**

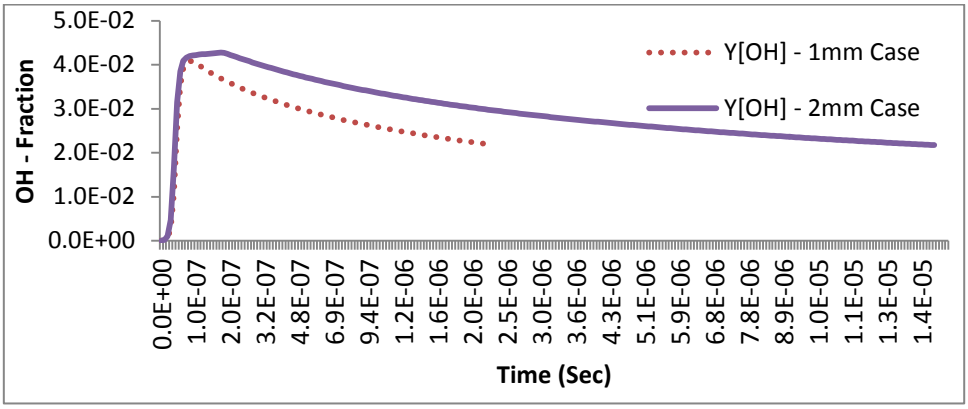


**b) 30 MPa**

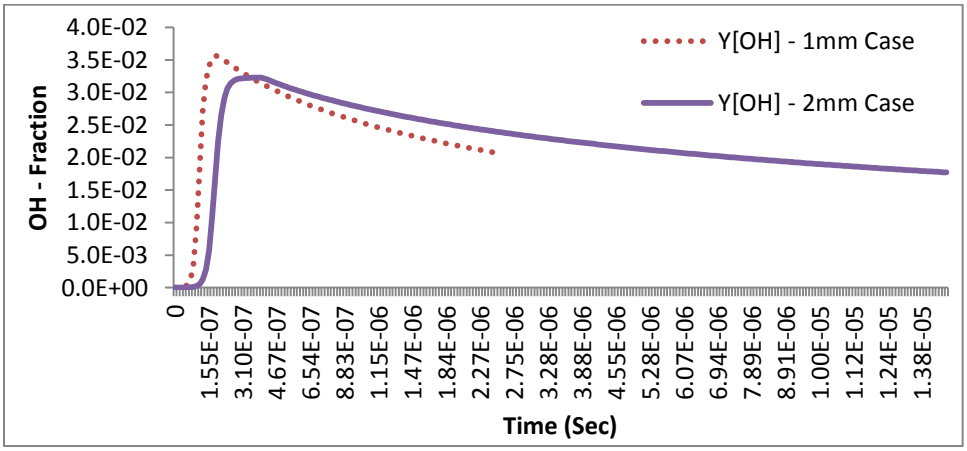


**c) 10 MPa**

Figure (3.2.13) – OH Fraction - 1 mm Case (E), 2 mm Case (E) - Compared

## 3.3 Comparative Analysis - Fixed Release Areas

By maintaining the same overall area, fixed circular and elliptic exit geometries are further compared. In this section, the comparative analysis performed, aims at identifying differences or similarities in the results obtained by varying the shape of the release opening.

### 3.3.1 Flow Parameters

The ignition model relies on the physical flow parameters, namely the hot air temperature behind the shockwave, the cold Hydrogen behind the contact surface, and the pressure behavior at the interface, to describe the diffusion and expansion effects on ignition.

Table (3-3-1) compares the hot air temperature peaks, and shows that the flow achieves higher temperature peaks for elliptic openings, indicating that elliptic exits have a more pronounced diffusion than circular exits. A closer look at the initial lower bound on the cold hydrogen temperature in table (3-3-2) shows that the initial cooling for circular geometries is more dominant, which suggests that expansion is more pronounced in circular rather than elliptic exit geometries.

The hot air temperature provides initial conditions for the shock-induced heating, and the cold hydrogen temperature provides initial conditions for the cooling effect of expansion. The comparison indicates that elliptic exits have a more dominant diffusion, and a slightly less pronounced expansion, and thus are more likely to ignite than standard circular holes.

| Fixed Circular Release Area | | Fixed Elliptic Release Area | |
|---|---|---|---|
| **1 mm** | **T[High] [K]** | **1 mm (E)** | **T[High] [K]** |
| **70 MPa** | 3050 | **70 MPa** | 3250 |
| **30 MPa** | 2732 | **30 MPa** | 2900 |
| **10 MPa** | 2184 | **10 MPa** | 2485 |
| **2 mm** | **T[High] [K]** | **2 mm (E)** | **T[High] [K]** |
| **70 MPa** | 3127 | **70 MPa** | 3290 |
| **30 MPa** | 2750 | **30 MPa** | 2980 |
| **10 MPa** | 2270 | **10 MPa** | 2570 |

Table (3-3-1) - Fixed Elliptic & Circular Geometry Compared - Hot Air Temperature

| Fixed Circular Release Area | | Fixed Elliptic Release Area | |
|---|---|---|---|
| **1 mm** | **T[Low] [K]** | **1 mm (E)** | **T[Low] [K]** |
| **70 MPa** | 180 | **70 MPa** | 190 |
| **30 MPa** | 192 | **30 MPa** | 200 |
| **10 MPa** | 215 | **10 MPa** | 220 |
| **2 mm** | **T[Low] [K]** | **2 mm (E)** | **T[Low] [K]** |
| **70 MPa** | 185 | **70 MPa** | 190 |
| **30 MPa** | 200 | **30 MPa** | 244 |
| **10 MPa** | 235 | **10 MPa** | 252 |

Table (3-3-2) - Fixed Elliptic & Circular Geometry Compared - Cold $H_2$ Temperature

The objective is to validate the increased heating, and the weaker depressurization experienced by elliptic exits, to further extend conclusions regarding ignition likelihood for this type of fixed exits, compared to standard circular holes.

The interface pressure comparison shown in table (3-3-3) is essential to understand the effect of the orifice shape on ignition. Table (3-3-3) compares pressure at the hottest point on the gas interface, for fixed elliptic and circular openings.

Table (3-3-4) provides the required comparative data to understand the effect of the exit geometry on the release time from the exit edge, and the pressure decay time. As shown in table (3-3-4), compared to circular openings, the release time in elliptic openings is less dependent on the storage pressure, and varies significantly by changing the operating pressure and opening dimension.

Table (3-3-4) shows the expansion delay, or the time delay between release from the exit edge and start of expansion, and confirms that circular exit geometries experience a faster depressurization after release. The comparison indicates that irregular elliptic exits are more likely to ignite than standard circular holes.

The conclusion is such that modeling the opening as elliptic, promotes for both a more dominant diffusion and a less pronounced expansion, and leads to increased ignition risks. The next section performs a detailed comparative analysis between fixed circular and elliptic geometries to determine the effect of the opening shape on ignition risks.

| Fixed Circular Release Area | | Fixed Elliptic Release Area | |
|---|---|---|---|
| **1 mm** | **P [MPa]** | **1 mm (E)** | **P [MPa]** |
| **70 MPa** | 4.75 | **70 MPa** | 5.53 |
| **30 MPa** | 4.51 | **30 MPa** | 4.70 |
| **10 MPa** | 2.38 | **10 MPa** | 2.75 |
| **2 mm** | **P [MPa]** | **2 mm (E)** | **P [MPa]** |
| **70 MPa** | 4.77 | **70 MPa** | 5.91 |
| **30 MPa** | 4.39 | **30 MPa** | 4.87 |
| **10 MPa** | 2.27 | **10 MPa** | 2.49 |

Table (3-3-3) - Fixed Elliptic & Circular Geometry Compared - Interface Pressure

| Fixed Circular Release Area | | Fixed Elliptic Release Area | | |
|---|---|---|---|---|
| **1 mm** | **Release Time [µs]** | **1 mm (E)** | | |
| | 0.6 µs | | | |
| **70 MPa** | **Decay Time [µs]** | **70 MPa** | **Decay Time [µs]** | **Release Time [µs]** |
| | 0.65 µs | | 0.4 µs | 0.15 µs |
| **30 MPa** | **Decay Time [µs]** | **30 MPa** | **Decay Time [µs]** | **Release Time [µs]** |
| | 0.7 µs | | 0.55 µs | 0.3 µs |
| **10 MPa** | **Decay Time [µs]** | **10 MPa** | **Decay Time [µs]** | **Release Time [µs]** |
| | 0.8 µs | | 0.65 µs | 0.4 µs |
| **2 mm** | **Release Time [µs]** | **2 mm (E)** | | |
| | 0.6 µs | | | |
| **70 MPa** | **Decay Time [µs]** | **70 MPa** | **Decay Time [µs]** | **Release Time [µs]** |
| | 0.7 µs | | 0.55 µs | 0.3 µs |
| **30 MPa** | **Decay Time [µs]** | **30 MPa** | **Decay Time [µs]** | **Release Time [µs]** |
| | 0.75 µs | | 0.7 µs | 0.6 µs |
| **10 MPa** | **Decay Time [µs]** | **10 MPa** | **Decay Time [µs]** | **Release Time [µs]** |
| | 0.85 µs | | 1.1 µs | 0.9 µs |

Table (3-3-4) - Fixed Elliptic & Circular Geometry Compared - Release & Decay Time

### 3.3.2 Ignition Parameters

Diffusion is slightly more dominant in elliptic exits, reflected by higher maximum OH - mass fraction values and expansion is slightly more pronounced in circular holes, reflected by slightly steeper decay slopes in mass fractions.

Table (3-3-5) compares OH mass fraction maximum and final values, as well as ignition probabilities, and indicates higher ignition probabilities in elliptic exits. Figure (3.3.1) clearly indicates that hydroxides achieve higher mass fraction peaks for elliptic shapes, and confirms that elliptic geometries are more susceptible of igniting.

With both a more dominant diffusion, and a less pronounced expansion, elliptic areas have higher ignition probabilities than circular areas. Results clearly show that elliptic openings, achieve higher hydroxide production peaks than circular openings, and are more likely to ignite.

| **Fixed Circular Release Area** | | | | **Fixed Elliptic Release Area** | | | |
|---|---|---|---|---|---|---|---|
| **1 mm** | **Y[OH] Max** | **Y[OH] Final Value** | **% Ignition** | **1 mm (E)** | **Y[OH] Max** | **Y[OH] Final Value** | **% Ignition** |
| **70 MPa** | 0.042 | 0.0172 | 100 | **70 MPa** | 0.0439 | 0.022 | 100 |
| **30 MPa** | 0.038 | 0.0153 | 62 | **30 MPa** | 0.039 | 0.021 | 70 |
| **10 MPa** | 0.037 | 0.0155 | 32 | **10 MPa** | 0.035 | 0.02 | 38 |
| **2 mm** | **Y[OH] Max** | **Y[OH] Final Value** | **% Ignition** | **2 mm (E)** | **Y[OH] Max** | **Y[OH] Final Value** | **% Ignition** |
| **70 MPa** | 0.043 | 0.0207 | 100 | **70 MPa** | 0.045 | 0.0229 | 100 |
| **30 MPa** | 0.041 | 0.0199 | 70 | **30 MPa** | 0.042 | 0.0217 | 72 |
| **10 MPa** | 0.033 | 0.016 | 38 | **10 MPa** | 0.031 | 0.017 | 38 |

Table (3-3-5) - Fixed Elliptic & Circular Geometry Compared – Ignition

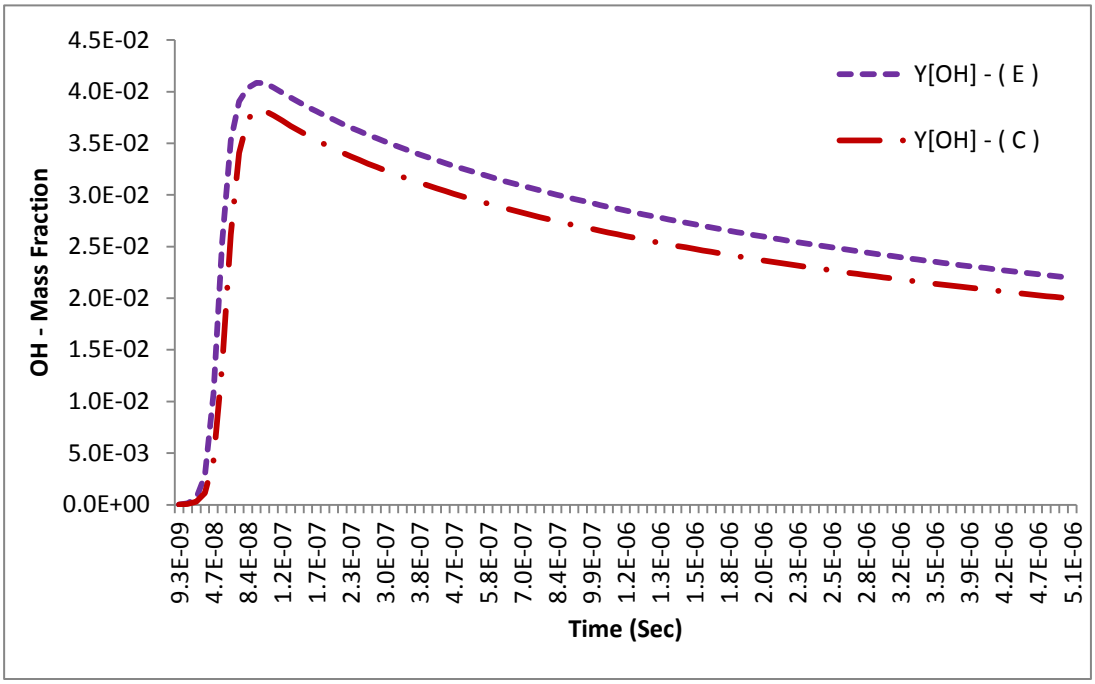


**a) 70 MPa**

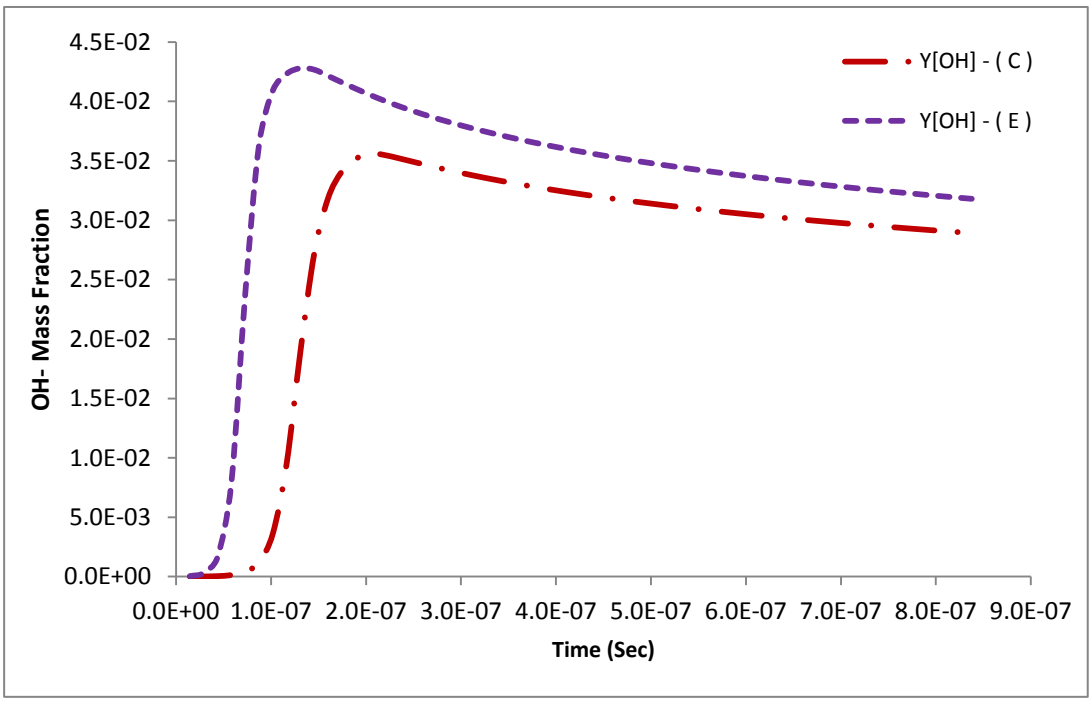


**b) 30 MPa**

Figure (3.3.1) - OH Mass Fraction, 1 mm (E) and 1 mm (C) – Compared

# Chapter 4

# Ignition Analysis for Expanding Circular Release Area

## 4.1 Problem Description

Expanding the orifice during the release significantly affects the flow and the probability of auto-ignition. In this section, we use the methodology presented and validated in the previous chapter to analyze auto-ignition. The geometry is summarized in table (4-1-1), and further compared with circular and elliptic openings, by expanding the geometry from an identical initial diameter, at a rate of 200m/s, or equivalently 0.2 mm/μs. Because the computational mesh moves, Euler equations, as well as the transport equation include the motion of the mesh. The mesh uses the spring method, in which the boundary nodes are moved forcing the interior nodes to move accordingly. Each edge acts like a spring, causing a force that follows Hook's law, to be applied along the boundary edge connected nodes [4].

| Orifice type | Major axis, a (mm) | Minor axis, b (mm) | Area, A (mm2) | Length, L(mm) | Expansion Rate (mm/μs) |
|---|---|---|---|---|---|
| **Circular** | 1 | 1 | 0.79 | 2 | |
| **Elliptic** | 2 | 0.5 | 0.79 | 2 | |
| **Expanding** | 1 | 1 | 0.79 | 2 | 0.2 |
| **Circular** | 2 | 2 | 3.14 | 2 | |
| **Elliptic** | 4 | 1 | 3.14 | 2 | |
| **Expanding** | 2 | 2 | 3.14 | 2 | 0.2 |

Table (4-1-1) - Expanding Circular Geometry

### 4.1.1 Case Study: Expanding Areas

In this section, two cases are studied for expanding circular openings, using the procedure explained in section 3.1. The hottest point at the gas interface is determined, to provide diffusion conditions, and the contact surface pressure is curve-fitted during depressurization, to provide expansion conditions.

As it is essential to determine the hottest point along the interface, figures (4.1.1) - (4.1.3) for 1 mm and 2 mm expanding circular areas, clearly show the temperature and pressure characteristics of the hydrogen-air interface, pertaining to the hottest point. In figure (4.1.1), during the initial diffusion of hydrogen, the hot air temperature reaches a maximum value before expansion starts. Following this peak, temperature sees a gradual decrease during depressurization; similar to what is observed for fixed release geometries. The behavior of temperature at the hottest point in expanding circular exits is such that the hot air temperature is much lower for expanding rather than fixed exit geometries. Figure (4.1.2) displays the pressure-time curve for a 1 mm initial diameter expanding circular geometry, clearly shows that pressure drops sharply and its slope is steeper than for constant area geometries, and confirms that depressurization is faster for expanding cases.

Diffusion is clearly less dominant in expanding exits, reflected by much lower temperature peaks, and expansion is clearly more pronounced reflected by steeper pressure decay slopes. With both a less dominant diffusion, and a more pronounced expansion, expanding geometries are expected to have much lower ignition probabilities than fixed geometries.

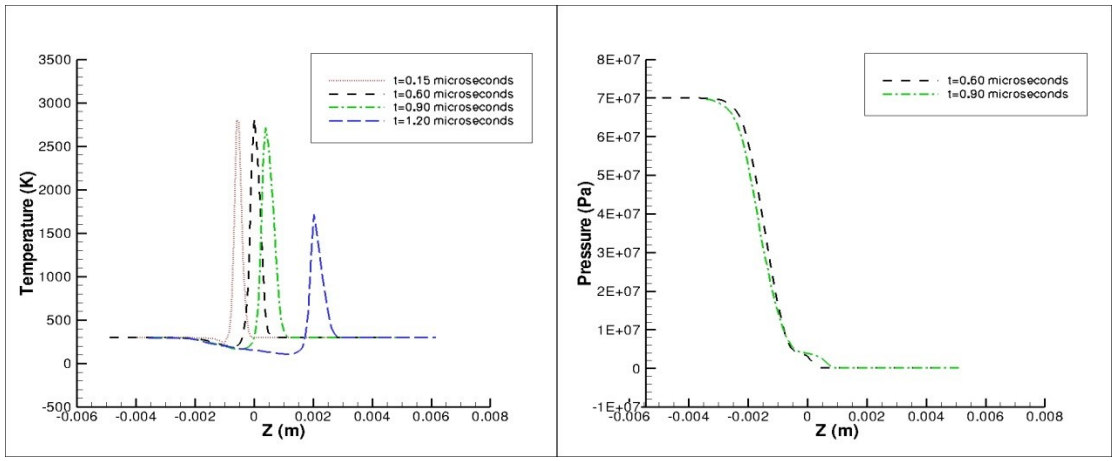


**a) 70 MPa**

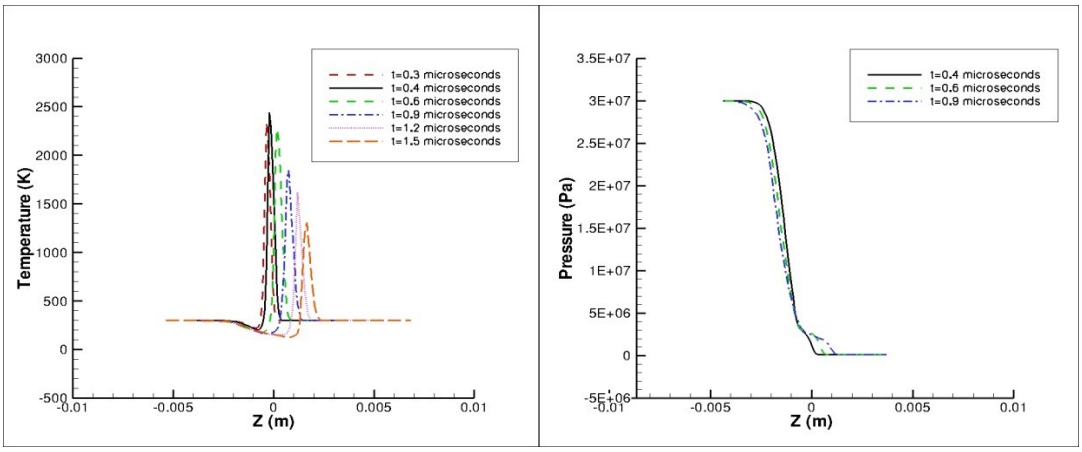


**b) 30 MPa**

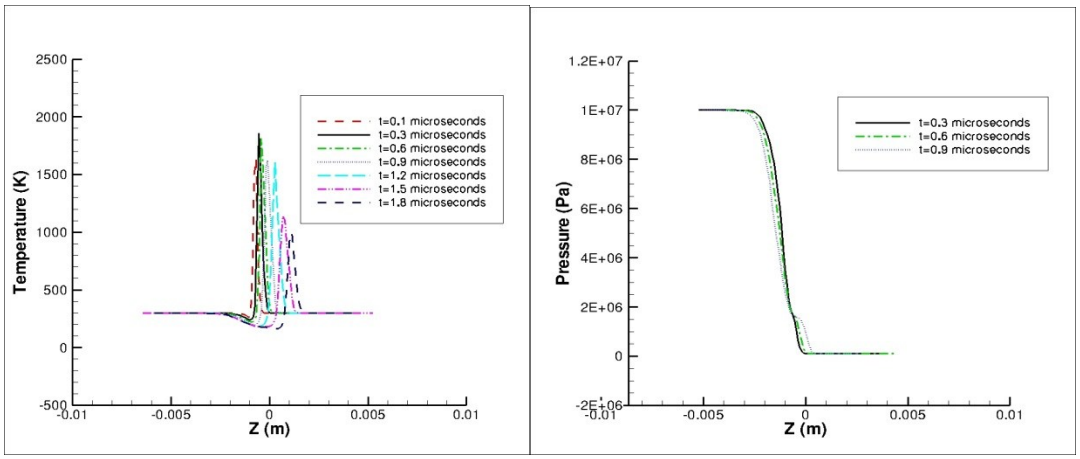


**c) 10 MPa**

Figure (4.1.1) - T (z) (Left), P (z) (Right), 1 mm Case (M), Expanding Circular Geometry

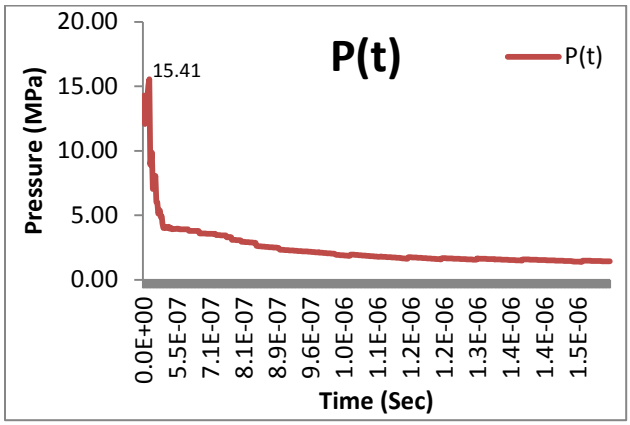


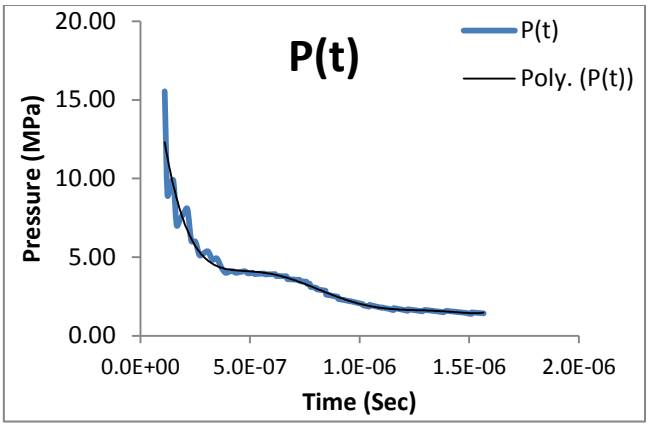


$P(t) = 4E\text{-}14t^6 - 8E\text{-}10t^5 + 6E\text{-}06t^4 - 0.0191t^3 + 31.699t^2 - 23960t + 1E+07$

$dP(t)/dt = 24E\text{-}14t^5 - 40E\text{-}10t^4 + 24E\text{-}06t^3 - 0.057t^2 + 63.398t - 23960$

**a) 70 MPa**

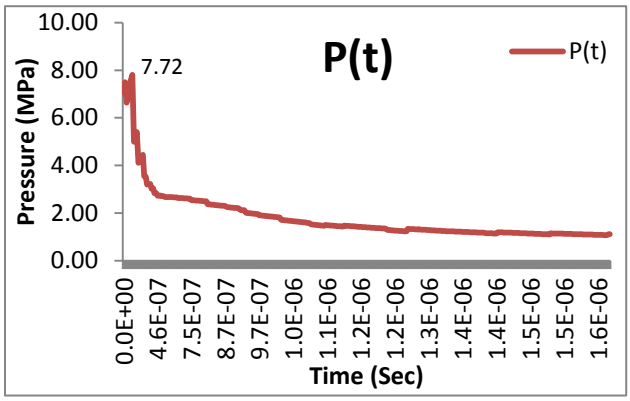


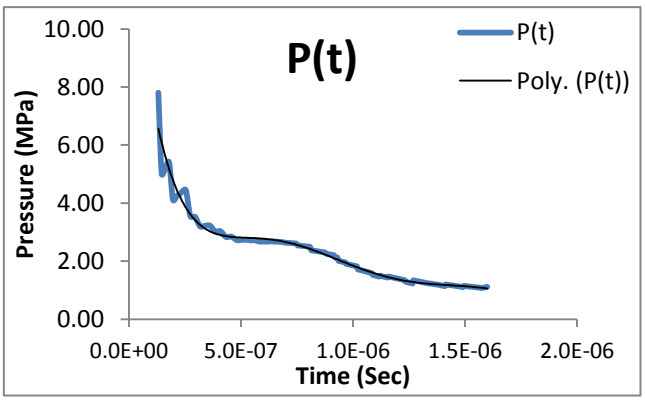


$P(t) = 9E\text{-}14t^6 - 1E\text{-}09t^5 + 7E\text{-}06t^4 - 0.0191t^3 + 24.825t^2 - 15154t + 6E+06$

$dP(t)/dt = 54E\text{-}14t^5 - 5E\text{-}09t^4 + 28E\text{-}06t^3 - 0.057t^2 + 49.65t - 15154$

**b) 30 MPa**

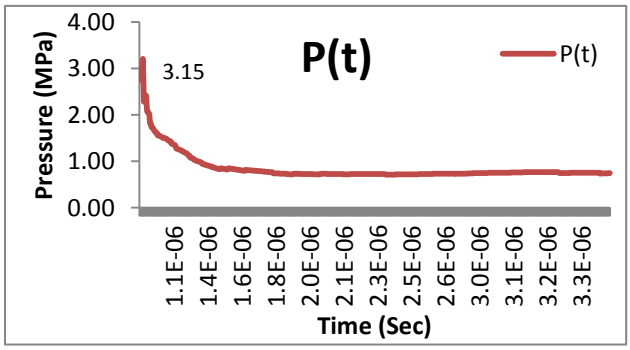


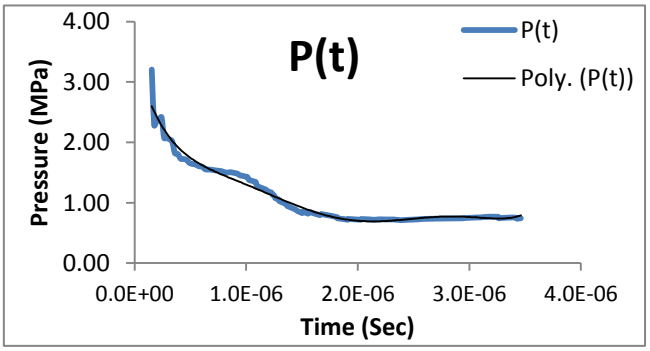


$P(t) = 3E\text{-}11t^6 - 2E\text{-}07t^5 + 0.0003t^4 - 0.2434t^3 + 101.66t^2 - 20469t + 3E+06$

$dP(t)/dt = 18E\text{-}11t^5 - 10E\text{-}07t^4 + 0.0012t^3 - 1.302t^2 + 203.32t - 20469$

**c) 10 MPa**

Figure (4.1.2) - P (t) curve, 1 mm Case (M), Expanding Circular Geometry

The objective is to understand the effect of expanding the area of a circular hole during the simulation on ignition risks, and to validate the conclusion that larger holes always have higher ignition probabilities than smaller openings, because of their stronger diffusion and weaker expansion.

Figure (4.1.4) shows the interface pressure for the 2mm expanding case, and confirms that expanding exits experience a faster depressurization than fixed exits. In figure (4.1.4), polynomial regression is again performed to fit the pressure-time curve, from which the rate of change of pressure with respect to time is derived, and used, as a source term in the ignition model, to account for expansion.

Comparing temperature peaks in figure (4.1.1) and (4.1.3) for 1 mm and 2 mm expanding circular areas, shows that when the storage pressure is reduced, temperature experiences a significant decrease, suggesting that expanding geometries may contribute to reducing ignition risks. In figures (4.1.1.c) and (4.1.3.c) for 10 MPa reservoirs, the increase in initial diameter from 1 mm to 2 mm, leads to a significant increase in temperature peaks. Comparing figures (4.1.1) and (4.1.3) confirms previous conclusions that increasing the initial diameter leads to much higher temperature peaks. Comparing the interface pressure in figures (4.1.2) and (4.1.4), also confirms previous conclusions that smaller holes experience a stronger expansion.

Diffusion in expanding areas is less dominant, reflected by lower temperature peaks, and expansion more pronounced, reflected by steeper pressure decay slopes. With a less dominant diffusion and more pronounced expansion, expanding exits are expected to reduce ignition likelihood.

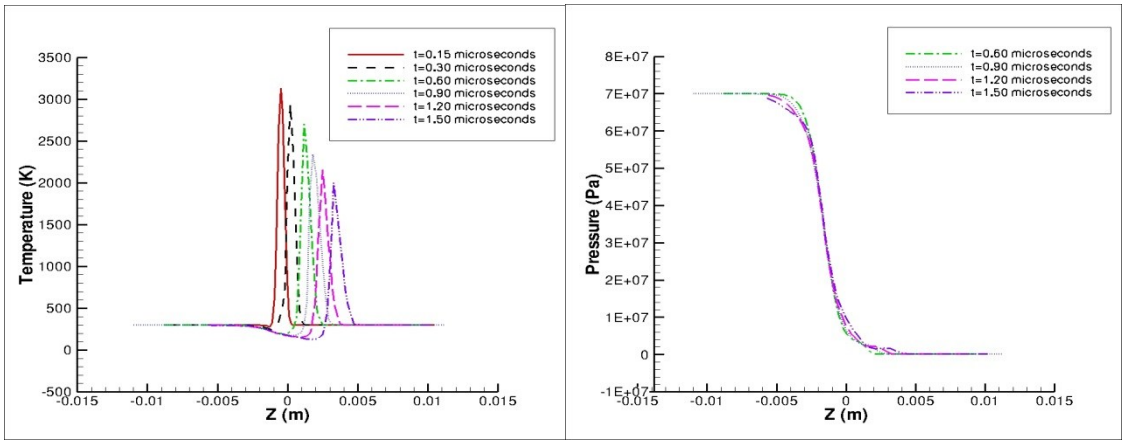


**a) 70 MPa**

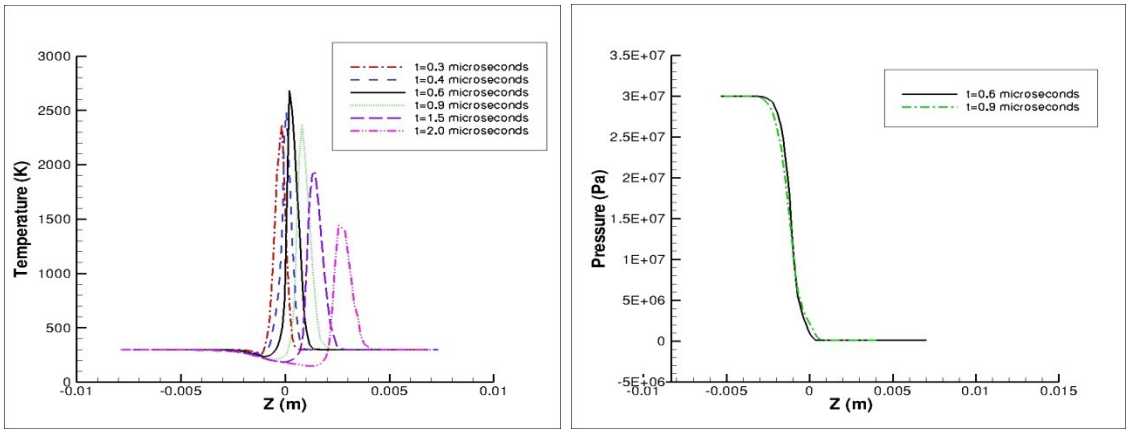


**b) 30 MPa**

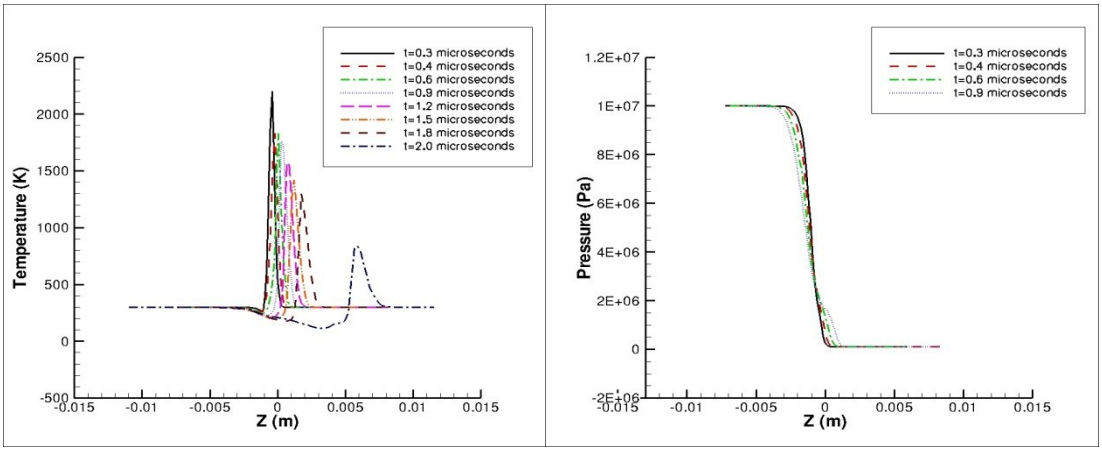


**c) 10 MPa**

Figure (4.1.3) - T (z) (Left), P (z) (Right), 2 mm Case (M), Expanding Circular Geometry

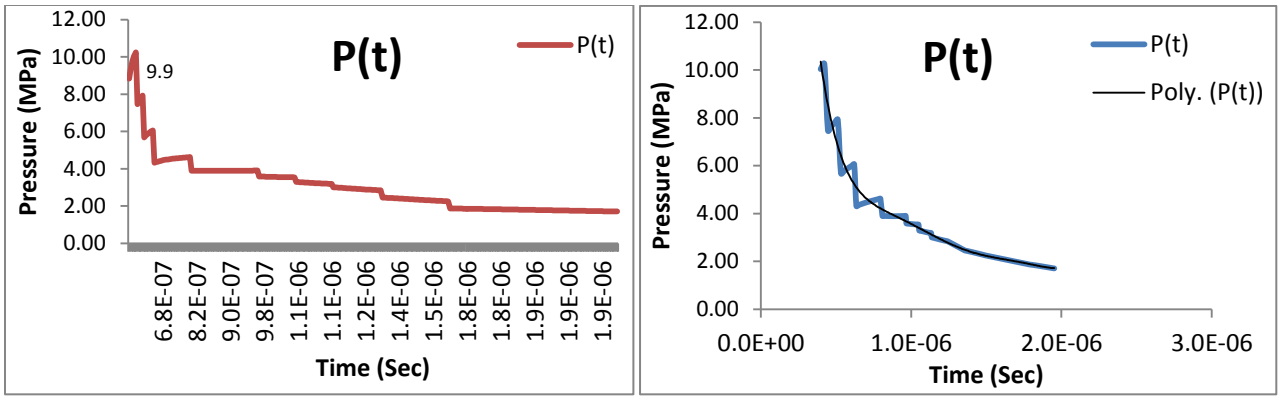


$P(t) = -1E\text{-}12t^6 + 4E\text{-}09t^5 + 5E\text{-}06t^4 - 0.0387t^3 + 54.731t^2 - 30327t + 1E+07$

$dP(t)/dt = -6E\text{-}12t^5 + 20E\text{-}09t^4 + 20E\text{-}06t^3 - 0.1161t^2 + 109.462t - 30327$

**a) 70 MPa**

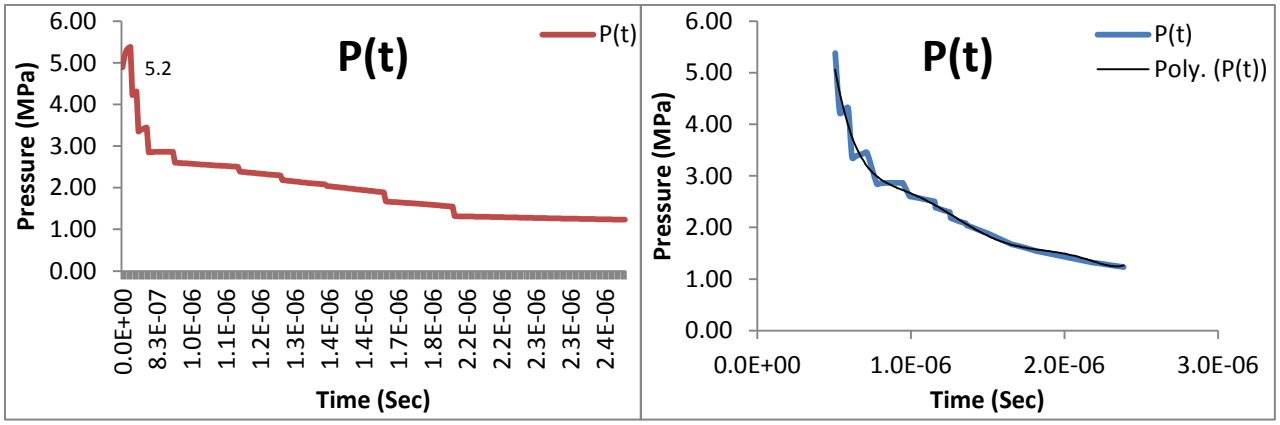


$P(t) = 8E\text{-}10t^6 - 2E\text{-}06t^5 + 0.0025t^4 - 1.3247t^3 + 354.32t^2 - 47893t + 6E+06$

$dP(t)/dt = 48E\text{-}10t^5 - 10E\text{-}06t^4 + 0.01t^3 - 3.9741t^2 + 708.64t - 47893$

**b) 30 MPa**

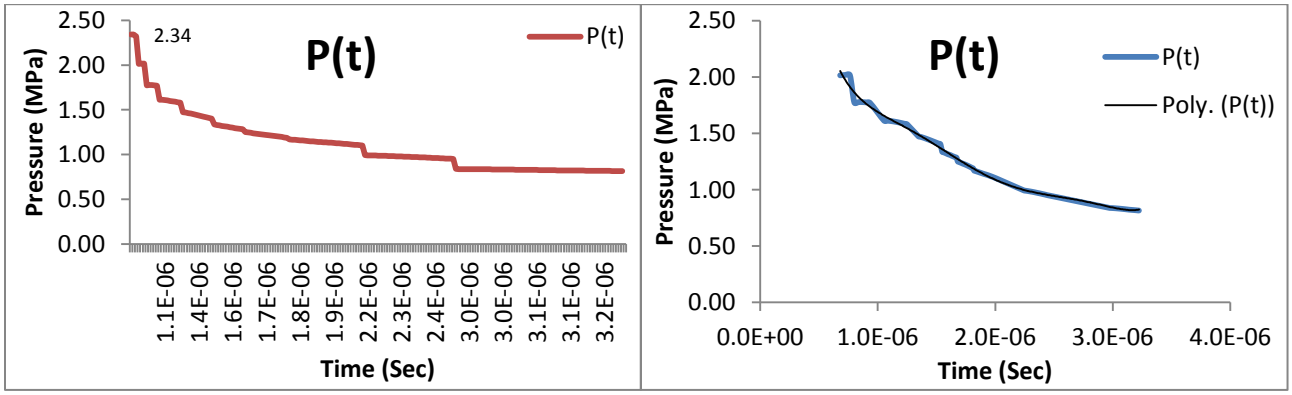


$P(t) = 9E\text{-}09t^6 - 1E\text{-}05t^5 + 0.008t^4 - 2.1648t^3 + 290.77t^2 - 23839t + 2E+06$

$dP(t)/dt = 54E\text{-}09t^5 - 5E\text{-}05t^4 + 0.032t^3 - 6.4944t^2 + 581.54t - 23839$

**c) 10 MPa**

Figure (4.1.4) - P (t) curve, 2 mm Case (M), Expanding Circular Geometry

Table (4-1-2) presents results obtained from an expanding circular release area at a rate of 0.2 mm/μs. The position and pressure of the contact surface, as well as the temperature peaks, are significantly affected by expanding the exit geometry.

Table (4-1-2) shows both the release and decay times for expanding geometries, and indicates that this type of exits experience an instantaneous pressure decay, compared to fixed exits that undergo a more gradual depressurization. Results confirm that expanding geometries have a steeper pressure gradient and a more pronounced expansion, compared to fixed exit geometries.

| **Expanding Circular Release Area** | | | | | |
|---|---|---|---|---|---|
| **1 mm (M)** | **T[High] [K]** | **T[Low] [K]** | **P [MPa]** | | |
| **70 MPa** | 2850 | 175 | 4.6 | **Decay Time [μs]** | **Release Time [μs]** |
| | | | | 0.2 μs | 0.15 μs |
| **30 MPa** | 2350 | 190 | 4.1 | **Decay Time [μs]** | **Release Time [μs]** |
| | | | | 0.35 μs | 0.3 μs |
| **10 MPa** | 1850 | 210 | 1.5 | **Decay Time [μs]** | **Release Time [μs]** |
| | | | | 0.45 μs | 0.4 μs |
| **2 mm (M)** | **T[High] [K]** | **T[Low] [K]** | **P [MPa]** | | |
| **70 MPa** | 3050 | 180 | 4.1 | **Decay Time [μs]** | **Release Time [μs]** |
| | | | | 0.3 μs | 0.15 μs |
| **30 MPa** | 2550 | 195 | 3.6 | **Decay Time [μs]** | **Release Time [μs]** |
| | | | | 0.5 μs | 0.4 μs |
| **10 MPa** | 2050 | 215 | 1.9 | **Decay Time [μs]** | **Release Time [μs]** |
| | | | | 0.7 μs | 0.6 μs |

Table (4-1-2) - Expanding Circular Geometry - Input Parameters

### 4.1.2 Ignition Assessment

Expanding areas achieve lower maximum mass fractions that decay rapidly, reflected by the maximum and final OH mass fractions. In table (4-1-3) a summary of the ignition assessment for the expanding opening cases is provided. Table (4-1-3) shows OH maximum mass fractions, which confirm that expanding exits have a weaker diffusion, as well as OH final mass fractions that confirm that expanding exits experience a faster depressurization than fixed exits.

Figure (4.1.5) shows the OH mass fraction curve, and figure (4.1.6) displays a comparison of the mass fraction behavior for the three pressure cases discussed, for a 1mm initial expanding diameter.

| **Expanding Circular Release Area** | | | |
|---|---|---|---|
| **1 mm (M)** | **Y[OH] Max** | **Y[OH] Final Value** | **% Ignition** |
| **70 MPa** | 0.0389 | 0.0176 | 100 |
| **30 MPa** | 0.0319 | 0.0148 | 60 |
| **10 MPa** | 0.0213 | 0.01487 | 25 |
| **2 mm (M)** | **Y[OH] Max** | **Y[OH] Final Value** | **% Ignition** |
| **70 MPa** | 0.0438 | 0.0275 | 100 |
| **30 MPa** | 0.0376 | 0.029 | 65 |
| **10 MPa** | 0.03 | 0.024 | 30 |

Table (4-1-3) - Expanding Circular Geometry - Ignition Assessment

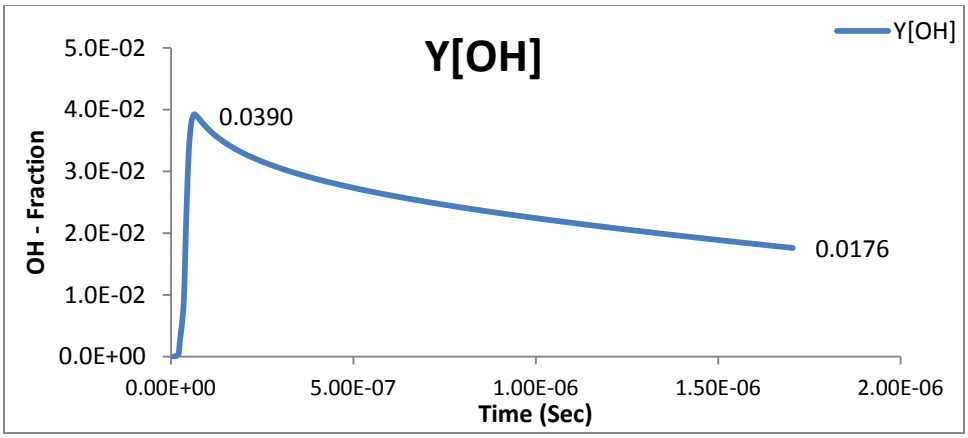


**a) 70 MPa**

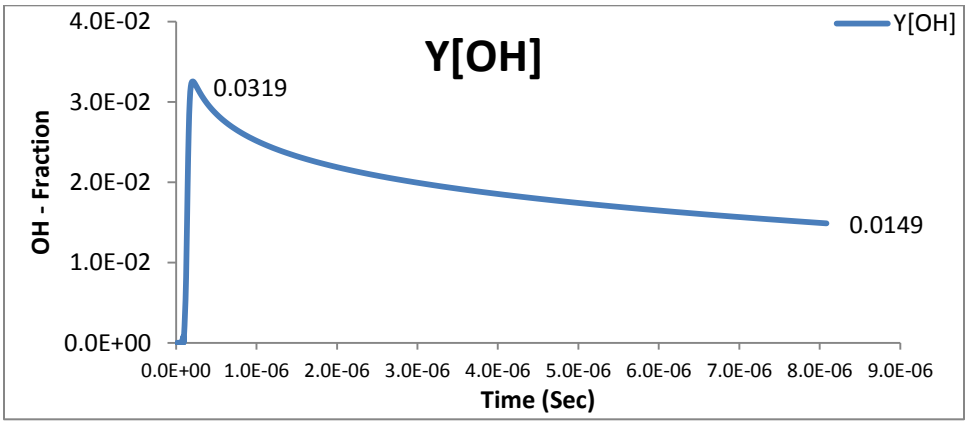


**b) 30 MPa**

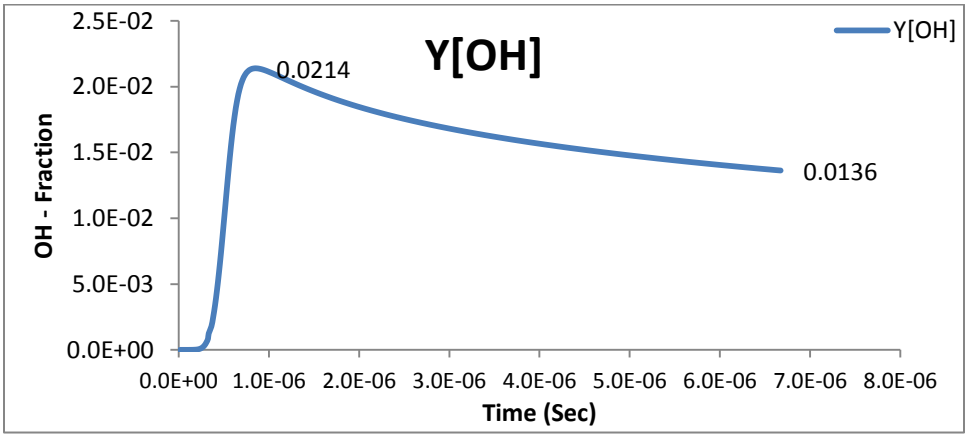


**c) 10 MPa**

Figure (4.1.5) - OH Mass Fraction, 1 mm Case (M), Expanding Circular Geometry

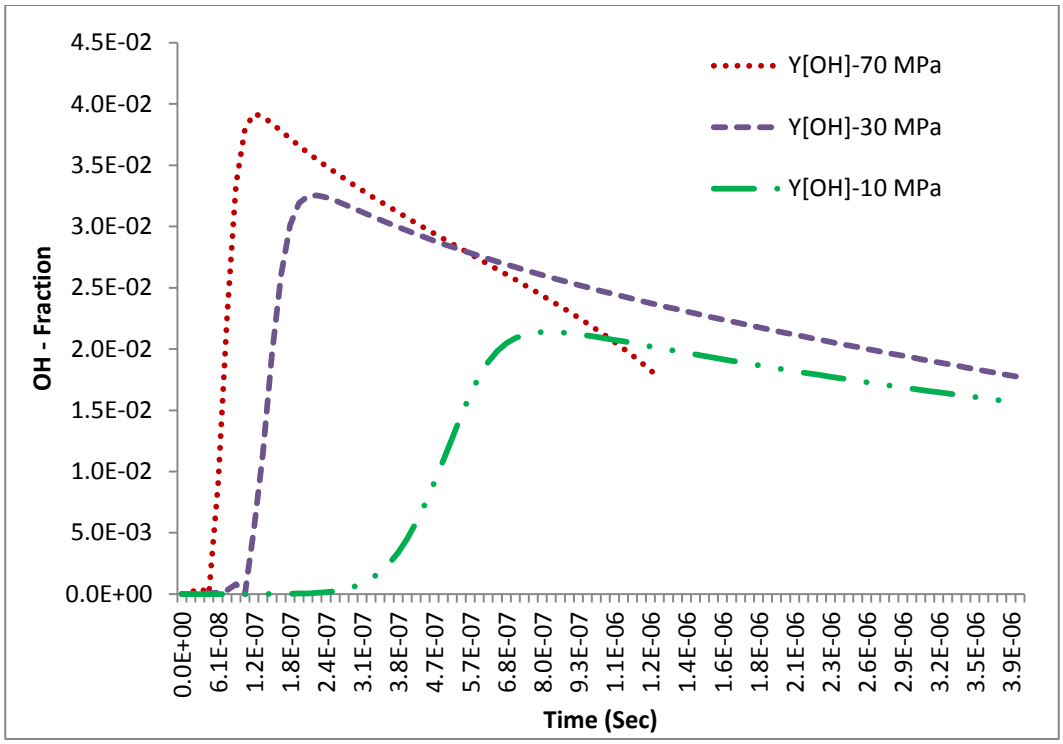


Figure (4.1.6) - OH Mass Fraction, 1 mm Case (M) - 70 MPa, 30 MPa, 10 MPa

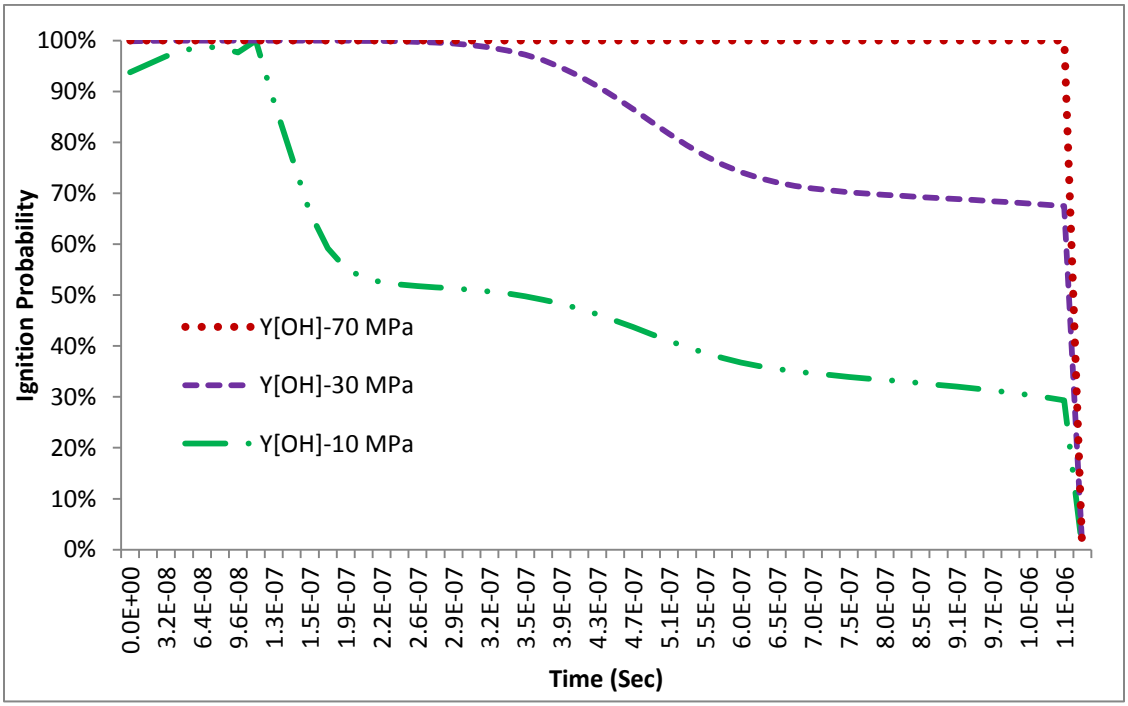


Figure (4.1.7) - Ignition Probability, 1 mm Case (M) - 70 MPa, 30 MPa, 10 MPa

In fact, the effect of depressurization on OH - mass fractions in expanding exits, is such that the initial sharp increase in mass fractions is followed by a much sharper decrease, compared to fixed exits, this behavior is exclusive to expanding areas.

Figure (4.1.5) displays OH mass fractions for an expanding release area of 1 mm initial diameter, and indicates that maximum OH mass fractions achieved are much lower for expanding exits. Figure (4.1.6) compares OH mass fractions for an expanding circular release area of 1 mm initial diameter, for the three different operating pressures, and supports the conclusion of a more pronounced expansion in this type of exits. Expanding exits have a lower maximum OH value, which confirms a less dominant diffusion, and a steeper mass fraction slope, which confirms a more pronounced expansion, and therefore validate the conclusion that much lower ignition risks exist in expanding geometries. Figures (4.1.8) and (4.1.9) display OH mass fractions and ignition probabilities for an expanding exit of 2 mm initial diameter, and validate previous conclusions that for larger operating areas, diffusion is more dominant and expansion is less pronounced. The comparison between the 1mm and the 2mm expanding cases in figure (4.1.11) also confirms that larger holes are clearly more likely to ignite.

Diffusion in expanding areas is less dominant, and expansion is more pronounced, resulting in much lower ignition risks. The probability plot for the 2 mm expanding geometry shown in figure (4.1.9), and the comparison shown in figure (4.1.10) clearly indicate that expanding exits have much lower ignition probabilities. The effect of expanding the area is such that ignition risks can be prevented for this type of exits.

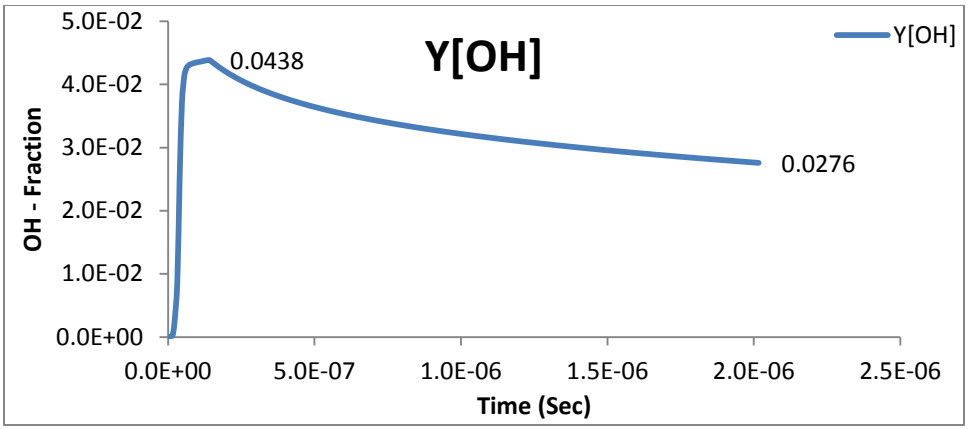


**a) 70 MPa**

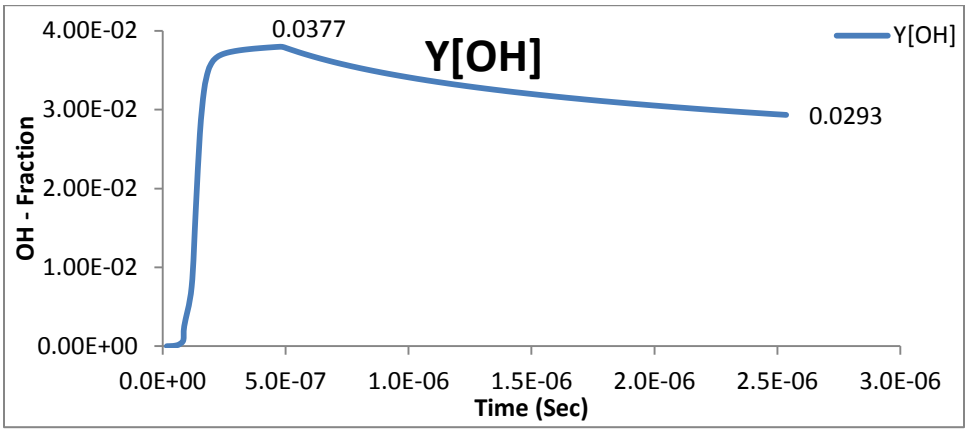


**b) 30 MPa**

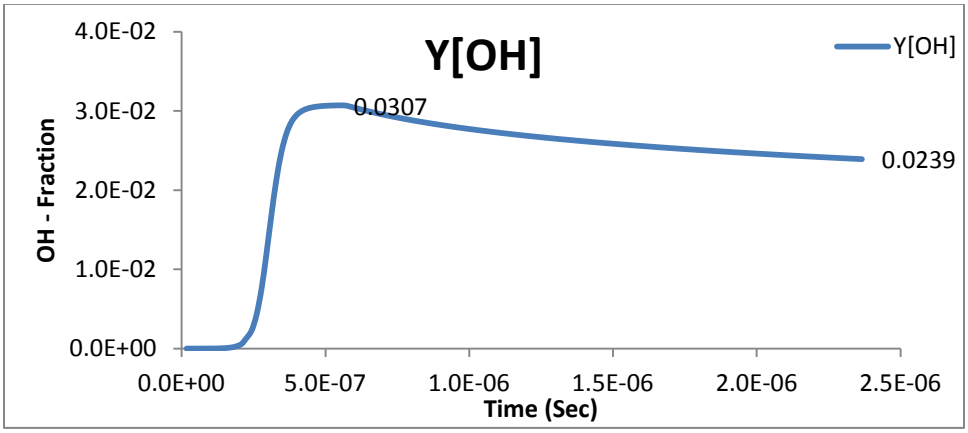


**c) 10 MPa**

Figure (4.1.8) - OH Mass Fraction, 2 mm Case (M), Expanding Circular Geometry

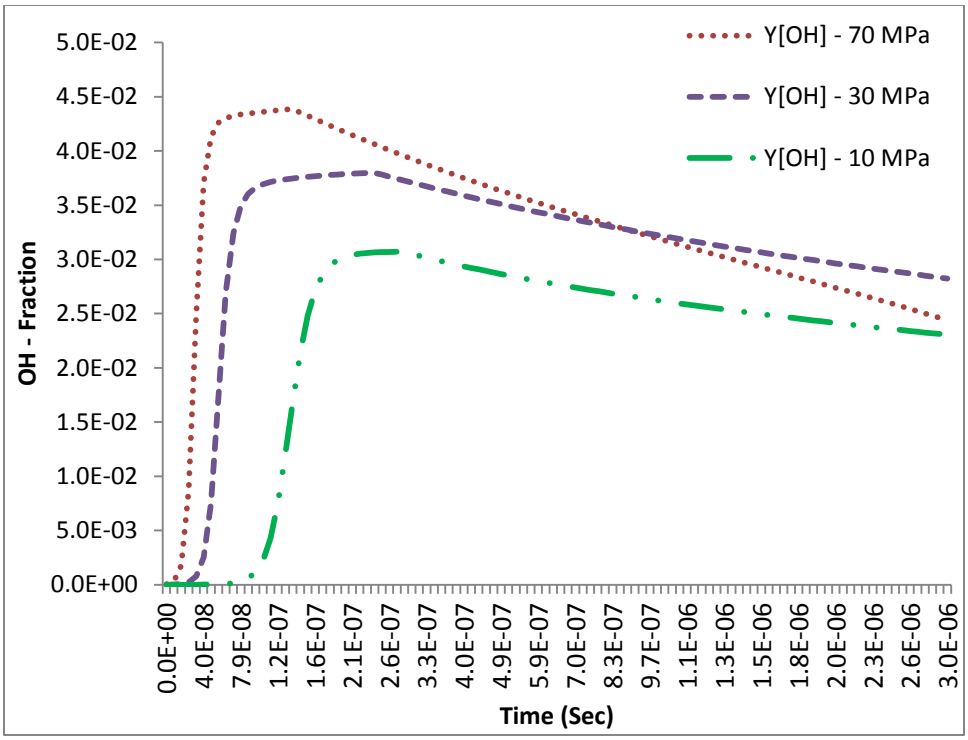


Figure (4.1.9) - OH Mass Fraction, 2 mm Case (M) - 70 MPa, 30 MPa, 10 MPa

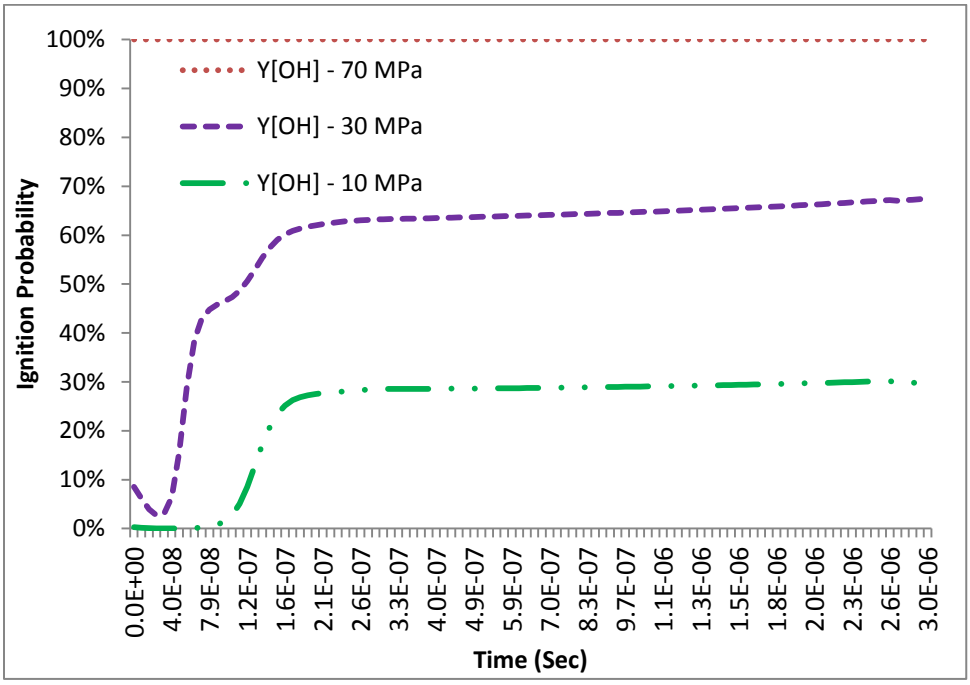


Figure (4.1.10) - Ignition Probability, 2 mm Case (M) - 70 MPa, 30 MPa, 10 MPa

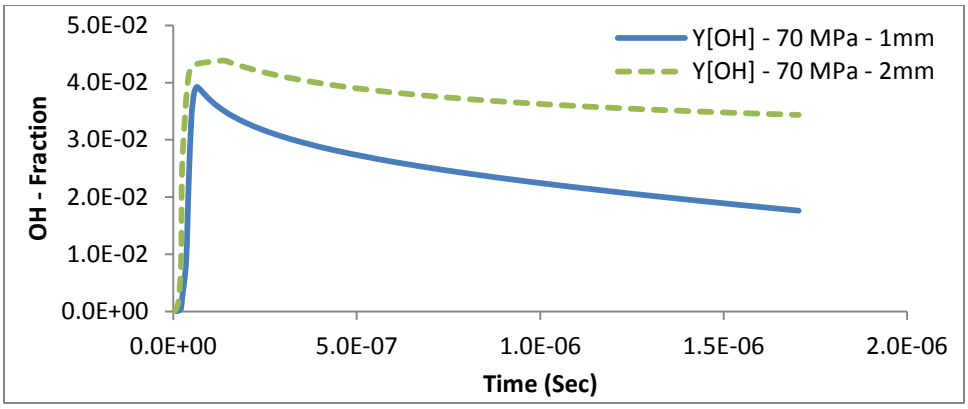


**a) 70 MPa**

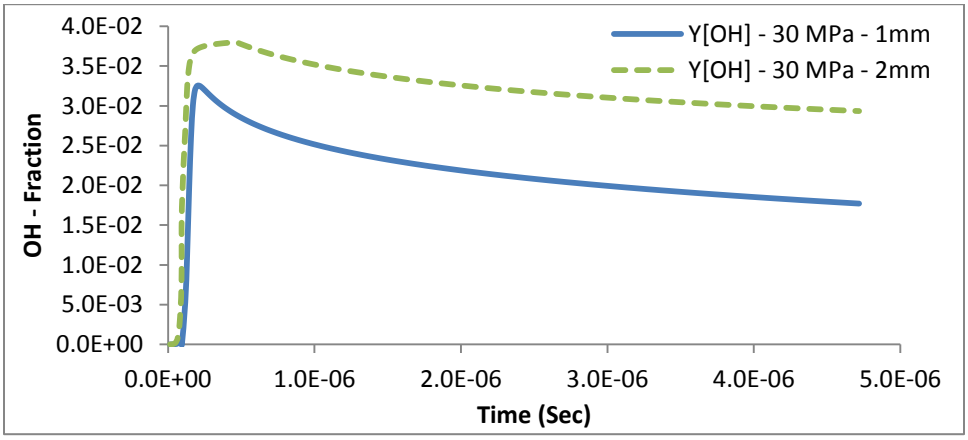


**b) 30 MPa**

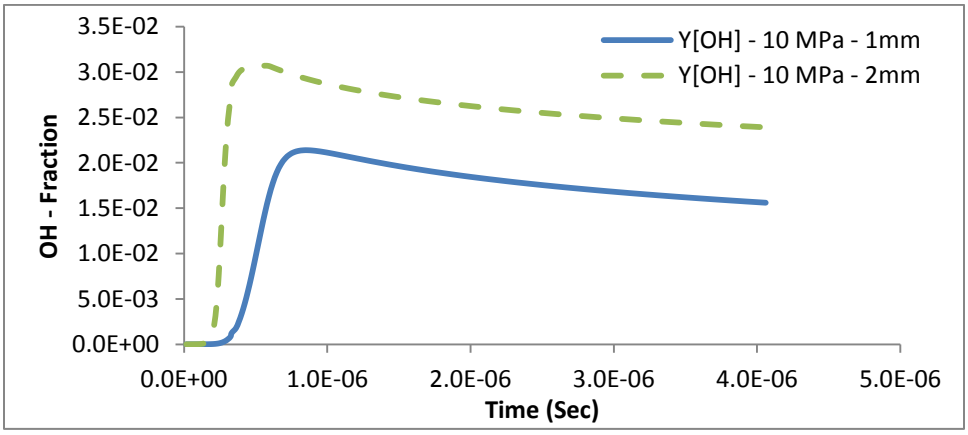


**c) 10 MPa**

Figure (4.1.11) - OH Mass Fraction, 1 mm Case (M) and 2 mm Case (M), Expanding Circular Geometry

## 4.2 Comparative Analysis - Expanding Release Areas

In this section, the comparative analysis performed aims at comparing the flow and auto-ignition behavior obtained from hydrogen release through fixed or expanding geometries circular exits.

### 4.2.1 Flow Parameters

The hot air temperature provides initial conditions for the shock-induced heating and diffusion of hydrogen, and the cold hydrogen temperature, provides initial conditions for the cooling effect of expansion.

Table (4-2-1) compares temperature peaks, and interface pressures for expanding and fixed circular geometries, and shows that the flow achieves much lower temperature peaks for expanding geometries, which suggests much lower ignition risks for this type of exit geometries. Table (4-2-2) shows that the initial cooling effect for expanding geometries, and that Hydrogen in expanding circular geometries is slightly colder.

The temperature profile for the hot air leading the contact surface confirms that expanding areas have a weaker diffusion, and the temperature profile for the cold hydrogen behind the contact surface, suggests that expanding geometries experience a faster depressurization than fixed exits.

| Fixed Circular Release Area | | Expanding Circular Release Area | |
|---|---|---|---|
| **1 mm** | **T[High] [K]** | **1 mm (M)** | **T[High] [K]** |
| **70 MPa** | 3050 | **70 MPa** | 2850 |
| **30 MPa** | 2732 | **30 MPa** | 2350 |
| **10 MPa** | 2184 | **10 MPa** | 1850 |
| **2 mm** | **T[High] [K]** | **2 mm (M)** | **T[High] [K]** |
| **70 MPa** | 3127 | **70 MPa** | 3050 |
| **30 MPa** | 2750 | **30 MPa** | 2550 |
| **10 MPa** | 2270 | **10 MPa** | 2050 |

Table (4-2-1) - Fixed & Expanding Circular Geometry Compared - Hot Air Temperature

| Fixed Circular Release Area | | Expanding Circular Release Area | |
|---|---|---|---|
| **1 mm** | **T[Low] [K]** | **1 mm (M)** | **T[Low] [K]** |
| **70 MPa** | 180 | **70 MPa** | 175 |
| **30 MPa** | 192 | **30 MPa** | 190 |
| **10 MPa** | 215 | **10 MPa** | 210 |
| **2 mm** | **T[Low] [K]** | **2 mm (M)** | **T[Low] [K]** |
| **70 MPa** | 185 | **70 MPa** | 180 |
| **30 MPa** | 200 | **30 MPa** | 195 |
| **10 MPa** | 235 | **10 MPa** | 215 |

Table (4-2-2) - Fixed & Expanding Circular Geometry Compared - Cold $H_2$ Temperature

Both the interface pressure at the hottest point, and the behavior of pressure during expansion, are major factors that reduce ignition risks. The comparison shown in table (4-2-3) is essential to understand the effect that expanding the release area has on ignition, the interface pressure provides initial conditions for the expansion term in the ignition model.

Pressure decays much faster in expanding geometries, and has a steeper pressure gradient, which confirms that expanding exits undergo a stronger expansion, suggesting that ignition can be prevented for this type of exits. The release and decay times allow for a better understanding of the effect of varying the opening diameter during the simulation, on the expansion process. Table (4-2-4) provides the required comparative data to understand the effect of expanding circular geometries on the release and decay times. In fact, the decay time triggers the slowing down of chemical reactions, and clearly confirms that depressurization starts earlier in expanding rather than fixed circular openings.

The conclusion is such that expanding the initial diameter of a standard circular hole during the simulation, promotes for both a less dominant diffusion and a more pronounced expansion, and leads to much lower ignition risks. The next section performs a detailed comparative analysis between fixed and expanding geometries to determine the effect of expanding the geometry on ignition risks.

| Fixed Circular Release Area | | Expanding Circular Release Area | |
|---|---|---|---|
| **1 mm** | **P [MPa]** | **1 mm (M)** | **P [MPa]** |
| **70 MPa** | 4.75 | **70 MPa** | 4.6 |
| **30 MPa** | 4.51 | **30 MPa** | 4.1 |
| **10 MPa** | 2.38 | **10 MPa** | 1.5 |
| **2 mm** | **P [MPa]** | **2 mm (M)** | **P [MPa]** |
| **70 MPa** | 4.77 | **70 MPa** | 4.1 |
| **30 MPa** | 4.39 | **30 MPa** | 3.6 |
| **10 MPa** | 2.27 | **10 MPa** | 1.9 |

Table (4-2-3) - Fixed & Expanding Circular Geometry Compared - Interface Pressure

| Fixed Circular Release Area | | Expanding Circular Release Area | | |
|---|---|---|---|---|
| **1 mm** | **Release Time [µs]** | **1 mm (M)** | | |
| | 0.6 µs | | | |
| **70 MPa** | **Decay Time [µs]** | **70 MPa** | **Decay Time [µs]** | **Release Time [µs]** |
| | 0.65 µs | | 0.2 µs | 0.15 µs |
| **30 MPa** | **Decay Time [µs]** | **30 MPa** | **Decay Time [µs]** | **Release Time [µs]** |
| | 0.7 µs | | 0.35 µs | 0.3 µs |
| **10 MPa** | **Decay Time [µs]** | **10 MPa** | **Decay Time [µs]** | **Release Time [µs]** |
| | 0.9 µs | | 0.45 µs | 0.4 µs |
| **2 mm** | **Release Time [µs]** | **2 mm (M)** | | |
| | 0.6 µs | | | |
| **70 MPa** | **Decay Time [µs]** | **70 MPa** | **Decay Time [µs]** | **Release Time [µs]** |
| | 0.7 µs | | 0.3 µs | 0.15 µs |
| **30 MPa** | **Decay Time [µs]** | **30 MPa** | **Decay Time [µs]** | **Release Time [µs]** |
| | 0.75 µs | | 0.5 µs | 0.4 µs |
| **10 MPa** | **Decay Time [µs]** | **10 MPa** | **Decay Time [µs]** | **Release Time [µs]** |
| | 0.85 s | | 0.7 µs | 0.6 µs |

Table (4-2-4) - Fixed & Expanding Circular Geometry Compared - Release & Decay time

4.2.2 Ignition Parameters

Diffusion is clearly less dominant in expanding exits, reflected by lower maximum OH - mass fraction values and expansion is more pronounced, reflected by steeper OH - mass fraction decay slopes, and final OH - mass fraction values.

Table (4-2-5) compares ignition results obtained for expanding and fixed circular openings. Results show that fixed circular geometries, achieve higher hydroxide production peaks than expanding geometries. Table (4-2-5) also confirms that fixed circular geometries are more likely to ignite than expanding circular geometries. The differences in ignition probabilities, and maximum and final OH – mass fraction values observed in table (4-2-5), support the fact that expanding holes can prevent the occurrence of ignition.

| **Fixed Circular Release Area** | | | | **Expanding Circular Release Area** | | | |
|---|---|---|---|---|---|---|---|
| **1 mm** | **Y[OH] Max** | **Y[OH] Final Value** | **% Ignition** | **1 mm (M)** | **Y[OH] Max** | **Y[OH] Final Value** | **% Ignition** |
| **70 MPa** | 0.042 | 0.0172 | 100 | **70 MPa** | 0.0389 | 0.0176 | 100 |
| **30 MPa** | 0.038 | 0.0153 | 62 | **30 MPa** | 0.0319 | 0.0148 | 60 |
| **10 MPa** | 0.037 | 0.0155 | 32 | **10 MPa** | 0.0213 | 0.01487 | 25 |
| **2 mm** | **Y[OH] Max** | **Y[OH] Final Value** | **% Ignition** | **2 mm (M)** | **Y[OH] Max** | **Y[OH] Final Value** | **% Ignition** |
| **70 MPa** | 0.043 | 0.0207 | 100 | **70 MPa** | 0.0438 | 0.0275 | 100 |
| **30 MPa** | 0.041 | 0.0199 | 70 | **30 MPa** | 0.0376 | 0.029 | 65 |
| **10 MPa** | 0.033 | 0.016 | 38 | **10 MPa** | 0.030 | 0.024 | 30 |

Table (4-2-5) - Fixed & Expanding Circular Geometry Compared - Ignition

All the features of the flow required, to examine ignition risks, and to determine the effect of changing the opening geometry on ignition risks, have been captured. The comparison between elliptic and circular geometries is based on the conservation of overall area, and the comparison between expanding and fixed circular geometries is based on an identical initial diameter at the start of the simulation.

Figure (4.2.1.a) compares OH mass fractions between the three types of exit geometries, for an operating pressure of 70 MPa, and for a 1 mm diameter case. Figure (4.2.1.a) confirms that fixed elliptic geometries are slightly more susceptible of igniting, which suggests that irregular exit geometries are more likely to ignite than standard circular holes. Figures (4.2.1.a) and (4.2.1.b) clearly distinguish ignition risks between the three types of release geometries; expanding exits clearly have lower ignition risks, than fixed exits.

Comparing mass fraction profiles, in figures (4.2.1.a) and Figure (4.2.2.a) for the three types of openings, confirms that expanding geometries experience a faster depressurization that can significantly slow down chemical reactions and OH productions, compared to fixed exit geometries. OH peaks, and ending OH mass fractions, in figures (4.2.1.b) and (4.2.2.b), clearly show that much lower ignition risks are present when the release area is expanding.

Fixed elliptic exits experience the strongest chemical reactions, and the highest OH production rates, which confirms that irregular elliptic geometries are more susceptible to ignite than standard circular holes. Chemical reactions are clearly slowed down for expanding exits, which confirms that expanding holes reduce ignition likelihood.

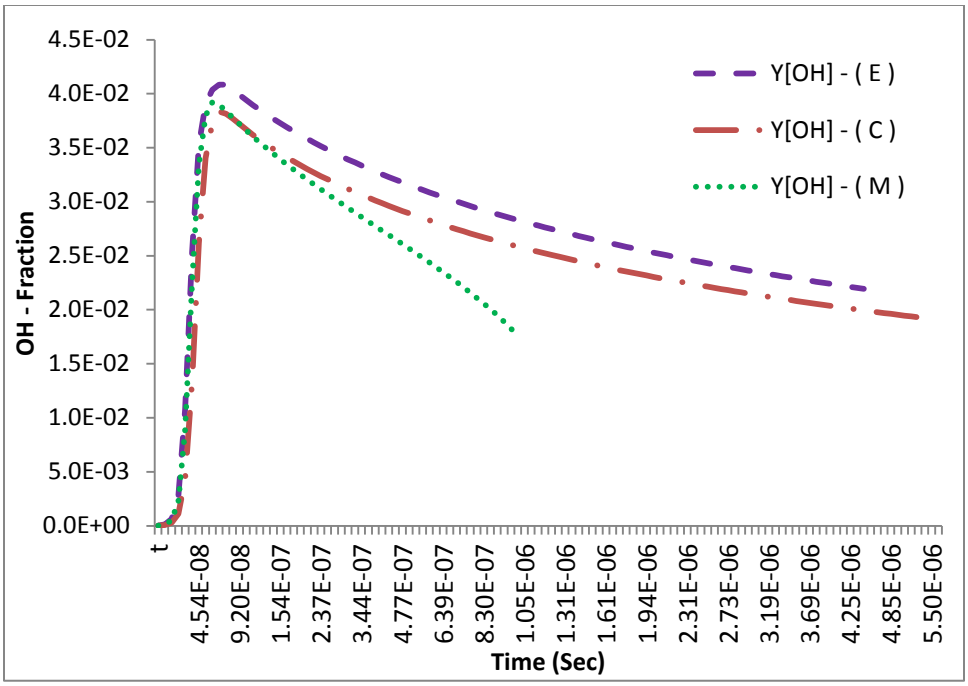


**a) OH - Mass Fraction**

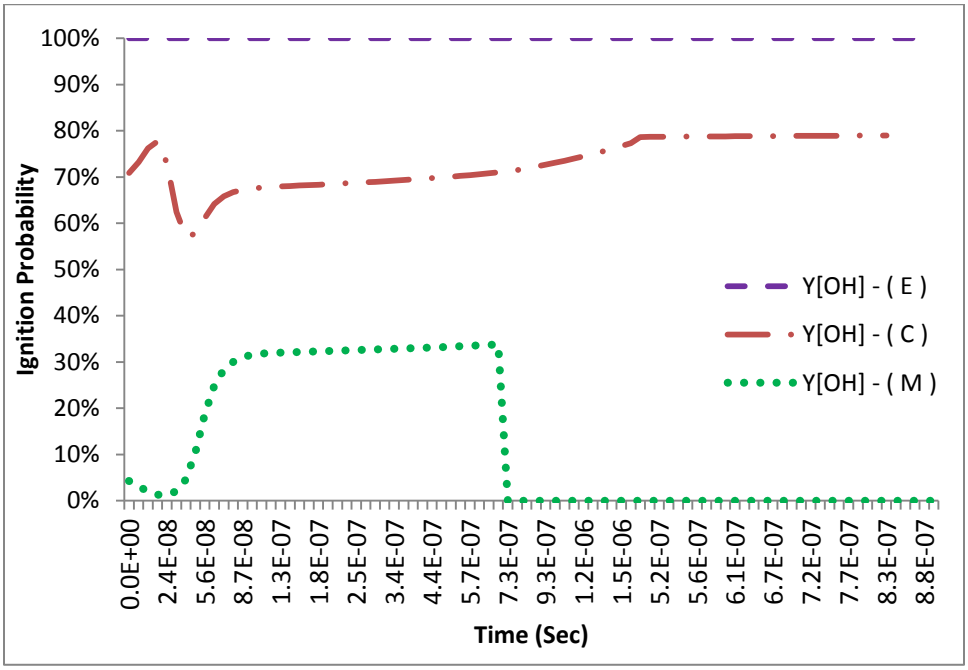


**b) Ignition Probability**

Figure (4.2.1) - OH Mass Fraction, Ignition Probability - 1 mm Case (C) (E) (M) - Compared - 70 MPa

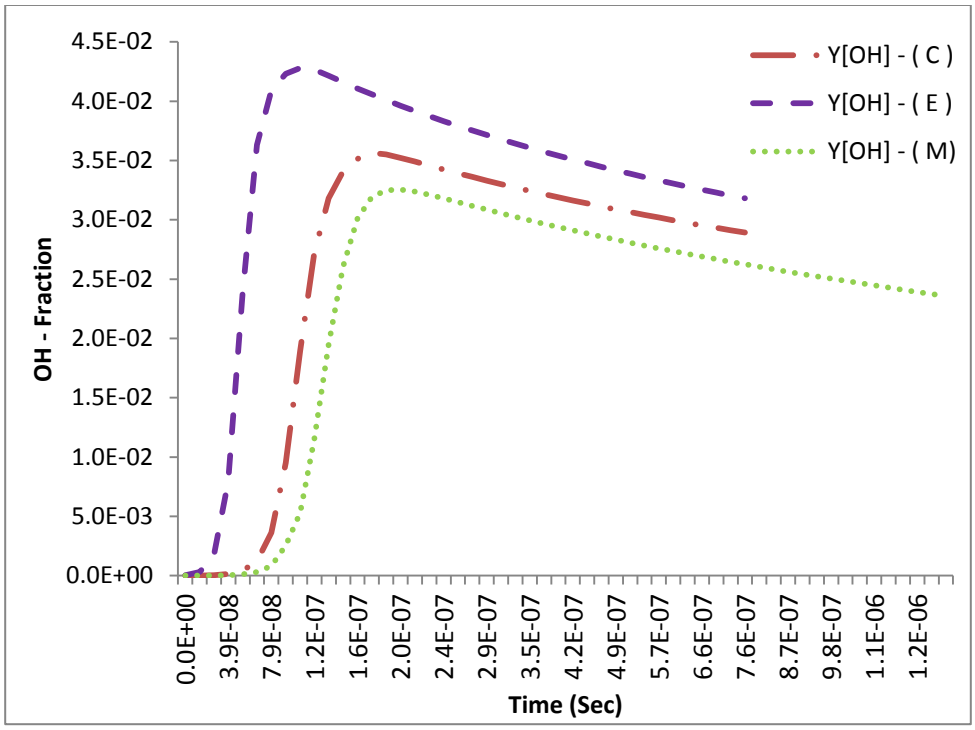


**a) OH - Mass Fraction**

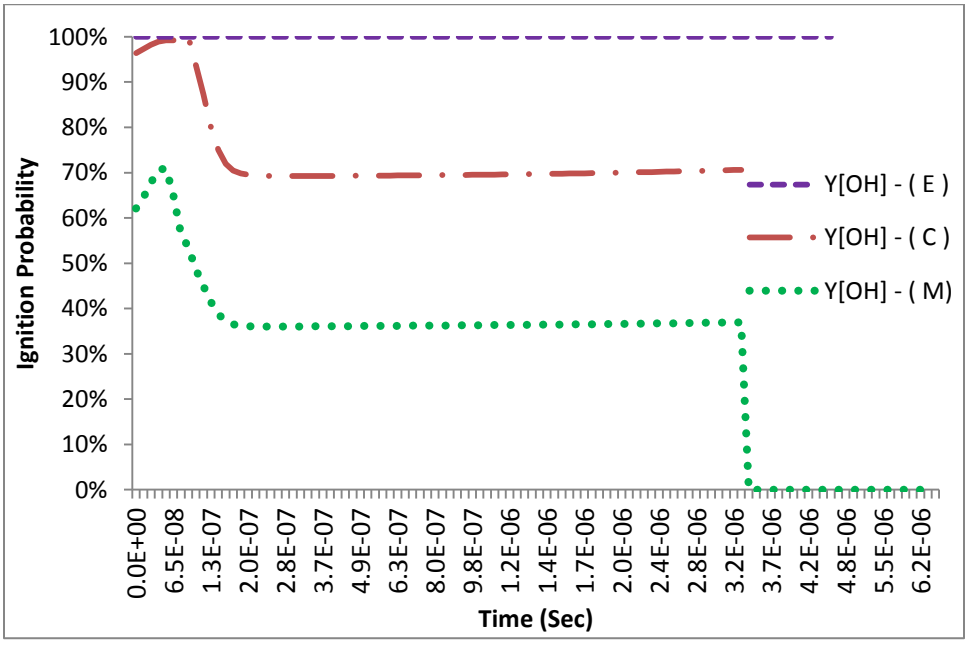


**b) Ignition Probability**

Figure (4.2.2) - OH Mass Fraction, Ignition Probability - 1 mm Case (C) (E) (M) - Compared - 30 MPa

# Chapter 5

# Conclusions and Recommendations

## 5.1 Summary of Validation

The present thesis addresses ignition risks associated with the diffusion-expansion of hydrogen into ambient air, through a series of case studies, covering several types of exit geometries, to describe the properties that affect ignition and to determine when ignition has occurred.

- Table (5.1.1) summarizes ignition results for non-expanding circular geometries, and shows good agreement with results obtained in the work of Radulescu and Maxwell.
- Figure (5.1.1) is from the work of Radulescu and Maxwell, it validates conclusions obtained in this thesis, for standard circular exits: larger hole sizes, require lower storage pressures to prevent ignition, and smaller holes require higher pressures to ignite, and are clearly less likely to ignite.
- Ignition risks relative to critical hole sizes and storage pressures for standard circular holes in figure (5.1.2), and relative to the various geometries studied in figure (5.1.3), validate numerical results and confirm conclusions obtained in this thesis.

Numerical experiments conducted by Radulescu and Maxwell, confirm that smaller holes, through which hydrogen is released, can better prevent ignition. The present thesis explains how the storage pressure, the expansion of the gas, and the hole size contribute to ignition.

| | Pressure [MPa] | | |
|---|---|---|---|
| Diameter [mm] | 70 | 30 | 10 |
| 1 | ✔ | ✖ | ✖ |
| 2 | ✔ | ✔ | ✖ |
| 5 | ✔ | ✔ | ✔ |

| Ignition | |
|---|---|
| Successful | Failed |
| ✔ | ✖ |

Table (5-1-1) - Fixed Circular Geometry - Ignition Assessment – Validation

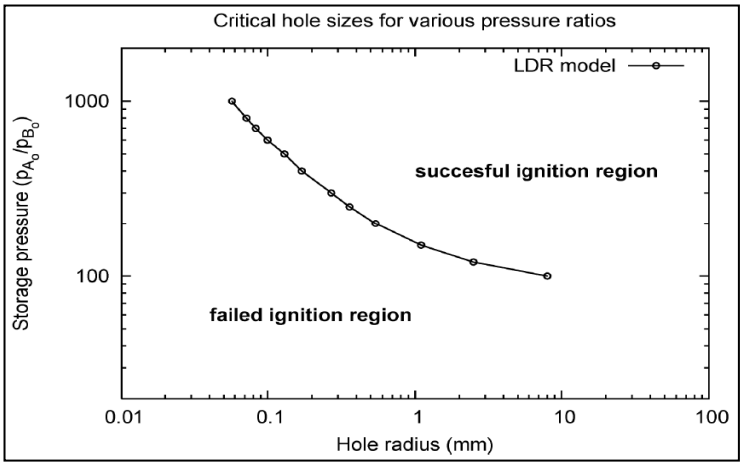


Figure (5.1.1) - Critical Quenching Hole Sizes at Various Storage Pressure - LDR Model [6]

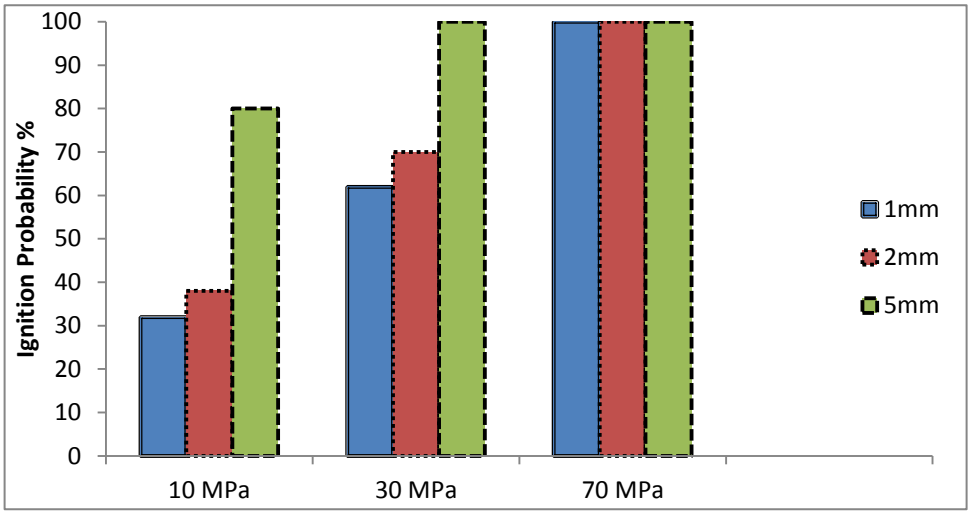


Figure (5.1.2) - Applicability Range - 1mm - 2mm - 5mm Case (C) - Fixed Circular Geometry

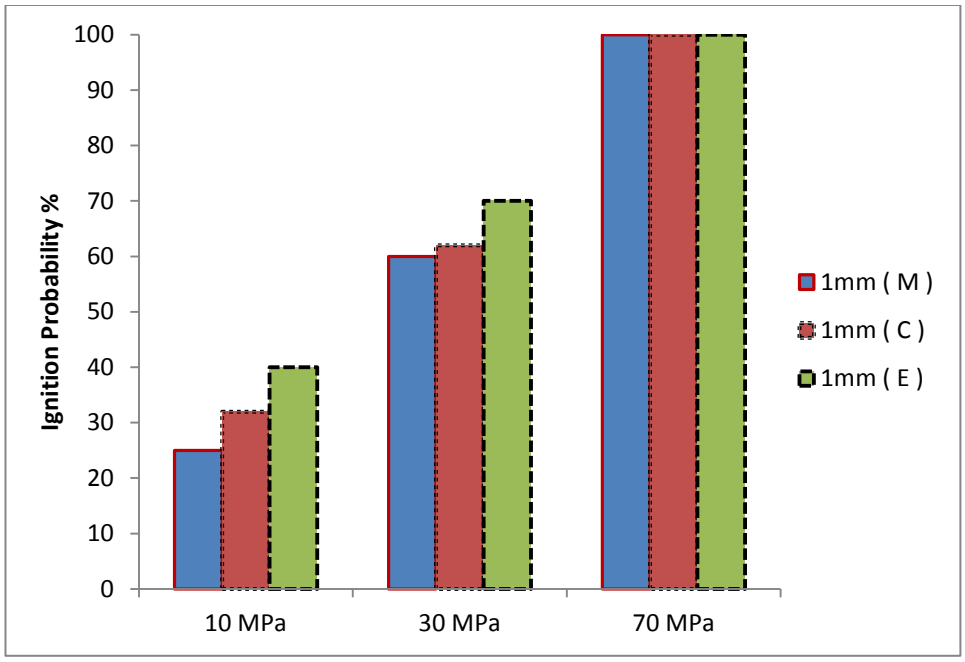


**a) 1 mm Case**

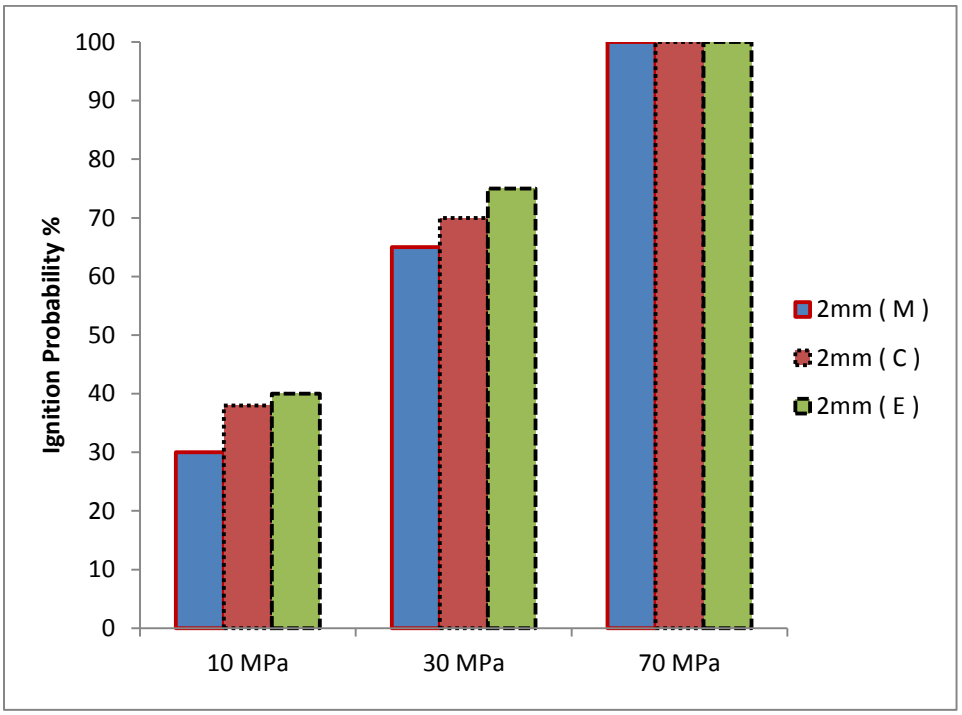


**b) 2 mm Case**

Figure (5.1.3) - Applicability Range - 1 mm Case and 2 mm Case - Expanding - Circular - Elliptic - Compared

## 5.2 Conclusion on Ignition

Auto-ignition of compressed hydrogen releases is a fundamental research area that supports the development of safety codes and standards, for an increased use of compressed hydrogen systems in industry.

A summary of the ignition behavior follows:

I: Standard Geometries - Fixed Release Areas - Circular Exit Geometries

- Smaller holes always have lower ignition probabilities than larger openings, because of their weak diffusion and strong expansion.
- Ignition risks increase as the diameter of the hole increases, smaller holes can better prevent ignition than larger holes.

II: Irregular Geometries - Fixed Release Areas - Elliptic Exit Geometries

- Fixed elliptic exits experience the strongest chemical reactions, and the highest OH production.
- Irregular elliptic geometries are more susceptible to ignite than standard circular holes.

III: Expanding Geometries - Expanding Circular Release Areas - Circular Exit Geometries

- Chemical reactions are greatly slowed down for expanding exits, which are clearly less likely to ignite than fixed geometries.

Because of the statistical nature of auto-ignition, more work is required to fully understand occurrence risks, including experimental testing and validation methods, which will ensure accurate ignition detection.

## 5.3 Contribution

Radulescu et al. [1] have studied auto-ignition of high pressure hydrogen releases, for non-expanding fixed release areas, for different hole diameters and tube lengths. The methodology proposed in this thesis is validated using previous results obtained in the work of Radulescu and Maxwell.

For fixed circular geometries, increasing the opening diameter has shown to increase the shock-induced heating, delay depressurization as hydrogen expands, and increase ignition risks. In this thesis, results of numerical simulations for standard circular exits indicate that smaller holes can prevent ignition, and results for elliptic geometries show that irregular elliptic exits are more likely to ignite than circular exits. Ignition results obtained in this thesis have been compared with results from previous literature, so as to validate the numerical methodology described in this thesis, which is subsequently used to investigate auto-ignition for expanding orifices.

Results of numerical simulations for expanding circular geometries have shown to significantly reduce ignition risks. Although several chemical kinetic models for hydrogen ignition have been proposed, these models have not yet been validated for expanding release problems; thus, another objective of this thesis is to provide a tool that describes auto-ignition in expanding orifices.

The main contributions are summarized as follows: (1) Ignition results for standard circular holes are validated with numerical results in [2] from B. Maxwell. (2) Ignition results for expanding circular holes shows lower ignition risks compared to standard circular holes. (3) A tool that describes auto-ignition in expanding orifices is provided.

## List of References

[1] M.I. Radulescu, C.K. Law, The transient start of supersonic jets, Journal of Fluid Mechanics, 2007, p. 331-369.

[2] B. Maxwell, Ignition limits of rapidly expanding diffusion layers: Application to unsteady hydrogen jets, M. Sc. Thesis, University of Ottawa, Dept. of Mechanical Engineering, 2010.

[3] K. Mohamed, Real Gas Numerical Simulation of Hydrogen Flow, M. Sc. Thesis, Concordia University, Dept. of Mechanical and Industrial Engineering, 2004.

[4] R. Khaksarfard, Numerical Investigation of Hydrogen Sonic Jet with Real Gas Model, Ph.D. Thesis, Concordia University, Dept. of Mechanical and Industrial Engineering, 2011.

[5] J. Li, Z. Zhao, A. Kazakov, F.L. Dryer, An Updated Comprehensive Kinetic Model of Hydrogen Combustion, Department of Mechanical and Aerospace Engineering Princeton University, International Journal of Chemical Kinetics, 2004, p. 566-575.

[6] R. Khaksarfard, M. R. Kameshki, M. Paraschivoiu, Numerical simulation of high pressure release and dispersion of hydrogen into air with real gas model, Shock Waves - An International Journal on Shock Waves, Detonations and Explosions, 2010, p. 205-216.

[7] M. Lamnaouer, Numerical Modeling of the Shock Tube Flow Fields Before and During Ignition Delay Time Experiments at Practical Conditions, Ph.D. Thesis, Dept. of Mechanical Engineering, University of Central Florida, 2010.

[8] D.G. Goodwin, Cantera, 2009. http://code.google.com/p/cantera/, accessed 14.12.11.

[9] A.C. Hindmarsh, P.N. Brown, K.E. Grant, S.L. Lee, C.S. Woodward, ACM Trans. Math Software, 2005, p. 363-396.

[10] B. Maxwell, One-Dimensional Model for Predicting Ignition During an Accidental Release of Pressurized Hydrogen into Air, M. Sc. Thesis, University of Ottawa, Dept. of Mechanical Engineering, 2010.

[11] K. Mohamed, M. Paraschivoiu, Real Gas Simulation of Hydrogen Release from a High-Pressure Chamber, International journal of hydrogen energy, 2005, p. 903-912.

[12] L. Dryer, M. Chaos, Z. Zhao, N. Stein, J. Homer, Spontaneous Ignition of Pressurized Releases of Hydrogen and Natural Gas into Air, Combustion science and technology, 2007, p. 663-694.

[13] S. D. Cohen, A. C. Hindmarsh, CVODE: A Stiff/Nonstiff ODE Solver in C, Computers in Physics 10, 1996, p. 138-143.

[14] M. Bragin, V. Molkov, Physics of spontaneous ignition of high-pressure hydrogen release and transition to jet fire, International Journal of Hydrogen Energy, 2011, p. 2589-2596.

[15] J.X. Wen, B.P. Xu, V.H.Y. Tam, Numerical study on spontaneous ignition of pressurized hydrogen release through a length of tube, Combustion and Flame, 2009, p. 2173-2189.

[16] Y. Liu, F. Tsuboi, N.Sato, H. Higashino, F. Hayashi, A. Gakuin, Direct numerical simulation on hydrogen fuel jetting from high pressure tank, Proceedings of the 20th International Colloquium on the Dynamics of Explosions and Reacting Systems, Montreal, 2005.

[17] V.N. Gamezo, T. Ogawa, E.S Oran, Numerical simulations of flame propagation and DDT in obstracted channels filled with hydrogen-air mixture, The Combustion Institute, The 31st International Symposium on Combustion, 2007, p. 2463-2471.

[18] H.W. Choi, M. Paraschivoiu, Adaptive Domain Decomposition for the Bound Method: Application to the Incompressible Navier-Stokes and Energy Equations in Three Space Dimensions, Computer Methods in Applied Mechanics and Engineering, 2007, p. 1484-1497.

[19] K. Mohamed, M. Paraschivoiu, Real Gas Simulation of Hydrogen Release from a High-Pressure Chamber, International Journal of Hydrogen Energy, 2005, p. 903-912,

[20] V. Molkov, D.V. Makarov, F. Verbecke, H. Schneider, Supra LES of accelerating premixed hydrogen-air flames in the open atmosphere, The International Symposium on Nonequilibrium Processes, Plasma, Combustion, and Atmospheric Phenomena, Russia, 2007.

[21] J. Buckmaster, P. Clavin, A. Linan, M. Matalon, N. Peters, G. Sivashinsky, F.A Williams, Combustion theory and modeling, Proceedings of the Combustion Institute, 2003, p. 1-19.

[22] R.W. Schefer,, W.G. Houf, T.C Williams, B. Bourne, J. Colton, Characterization of high-pressure, underexpanded hydrogen-jet flames, International Journal of Hydrogen Energy, 2006.

[24] G. Mittal, C.J. Sung, R.A. Yetter, International Journal of Chemical Kinetics, p. 516-529, 2005.

[25] Y.A. Çengel, M.A. Boles., Thermodynamics: An Engineering Approach, 4th Edition, McGraw-Hill, 2002.

[26] A.N. Al-Khateeb, J.M. Powers, S. Paolucci., Verified Computations of Laminar Premixed Flame, 45th AIAA Aerospace Science Meeting and Exhibit, Nevada, 2007.

[27] J.D. Anderson, Computational Fluid Dynamics: The Basics with Applications, McGraw-Hill, 1995.

[28] B.P. Xu, L. Hima, J.X. Wen, S. Dembele, V.H.Y. Tam, Numerical study of spontaneous ignition of pressurized hydrogen release into air, International Journal of Hydrogen Energy, 2009.

[29] M. R. Kameshki, Simulation of Hydrogen Jet Exiting a High Pressure Reservoir, M.Sc. Thesis, Concordia University, Dept. of Mechanical and Industrial Engineering, 2007.

[30] Y.L. Liu, J.Y. Zheng, P. Xu, Y.Z. Zhao, H. Dryver, Numerical Simulation on the Diffusion of Hydrogen due to High Pressured Storage Tanks Failure, Journal of Loss Prevention in the Process Industries, 2009, p. 265-270.